5-2019

H2 Control for Improved Stability of Multi-area Electric Power System with High Levels of Inverter-Based Generation

Muthanna Abdulkareem Al-Sarray
University of Arkansas, Fayetteville

H_2 Control for Improved Stability of Multi-area Electric Power System with High Levels of Inverter-Based Generation

A dissertation submitted in partial fulfillment
of the requirements for the degree of
Doctor of Philosophy in Electrical Engineering

by

Muthanna Abdulkareem Hasan Al-Sarray
Mustansiriya University
Bachelor of Science in Electrical Engineering, 2006
University of Technology
Master of Science in Electrical Engineering, 2009

May 2019
University of Arkansas

This thesis is approved for recommendation to the Graduate Council.

Roy A. McCann, Ph.D.
Dissertation Director

Juan Balda, Ph.D.
Committee Member

Simon Ang, Ph.D.
Committee Member

Edward A. Pohl, Ph.D.
Committee Member

Abstract

Increased generation capacity from non-dispatchable energy resources such as wind and solar has created challenges to ensuring the reliable delivery of electric power. This research develops a systematic three-step method of assessing the reliability of electric power systems under a variety of different possible fault conditions to ensure that overall system stability is preserved in a manner the meets regulatory requirements. The first step is a risk-based reliability method (RBRM) that accounts for the probability of a line outage versus the severity of impact. This allows system planners to judiciously allocate expenses for reliability improvements based on the greatest economic benefit. The second approach is the synchrophasor validation method (SVM) which allows system planners and analysis to develop accurate models of electric power system behavior. This improves the decision making capability for implementing new system designs and equipment choices. The third new area is the development of norm-based wide-area control methods that optimize system stability and reliability based on the statistical characteristics found in the first two steps. This norm-based approach includes calculating optimal values for parameters of flexible ac transmission system (FACTS) devices and high voltage direct current (HVDC) links in order to have results within the regulatory requirements of the North American Electric Reliability Corporation (NERC). Power flow and frequency criteria are used to verify conformance with the regulations. These criteria are evaluated under N-1-1 conditions in two reduced order models to demonstrate the ability of the norm-based wide-area controller to maintain performance of these systems within acceptable ranges. The obtained simulation results confirm the benefits of the proposed technique in meeting regulatory requirements under conditions of N-1-1 contingencies in electric power systems with large amounts of renewable energy resources.

Acknowledgments

This research was funded in part by the National Science Foundation Industry/University Cooperative Research Center on Grid-connected Advanced Power Electronics Systems (GRAPES) and the Foundations for Engineering Education for Distributed Energy Resources (FEEDER).

I would like to acknowledge the assistance from Southwest Power Pool (SPP) in power flow and transient stability analysis and to Oklahoma Gas and Electric (OG&E) in providing PMU data in conducting this research.

I also gratefully express my appreciation for the Higher Committee for Educational Development (HCED) in Iraq for giving me the opportunity to study in the U.S.A and reach this level of knowledge and support for me during my doctorate studies.

Dedication

First and foremost, I would like to thank God, Allah, for giving me the strength, courage, and knowledge to pursue this research study. This journey initially seemed long and arduous. But He made it short and enjoyable. Without Him this would have been impossible.

I dedicate my dissertation to my parents for their prayers and patience, for my wife who encouraged and supported me to pursue my dreams and finish this long and complex project, and for my kids, Mohammed, Murtadha, and Mirna, who color my life and give me strength to achieve my goals.

I would like to express my appreciation to my advisor Dr. Roy A. McCann for his continued support and guidance throughout my PhD study. I would also like to thank the rest of my thesis committee for their support.

Special thanks to thank my siblings for being there for me and for all they have done for me throughout the entire doctorate program and all of you have been my best cheerleaders. I would like to thank my friends who have supported me throughout the process for their continued support and encouragement.

Table of Contents

List of Figures

List of Tables

1 Introduction

1.1 Background and Motivation

Increasing energy demand brings many challenges for ensuring the reliability of electricity delivery infrastructure around the globe. One factor is increased capacity from variable wind and solar generation that may result in transmission line congestion. A second factor, especially in North America, is meeting recent NERC TPL-001-4 standards [1] for analyzing multiple contingency cases for reliability studies and maintaining frequency and power changes within limits of NERC BAL-003-1 standard [2]. Presently, N-1 analysis is analyzed continuously during system operation to ensure that generators will maintain synchronism after any single fault that might occur on the system. N-1-1 contingency analysis is significantly more challenging in terms of evaluating transient stability characteristics.

For the N-1-1 disturbances, this first contingency event is then followed by the loss of a second element [3]. This type of analysis ultimately is used to assist in sustaining economic activity and quality of life through reliable electric power delivery. If the resulting analysis indicates an unacceptably high likelihood of a major power disturbance, then further system modifications and upgrades may be justified such as installing new transmission lines, designing new exciter controls, implementing more aggressive demand response agreements, installing power electronic based equipment such as Flexible AC Transmission Systems (FACTS), or adopting High Voltage DC (HVDC) links within or between different areas [4]. This work brings N-1-1 contingency analysis to the spotlight in dynamic security assessment (DSA) that will produce improved methods for system planners in designing reliable electric power systems.

These types of developments require more preceding steps to identify locations that may suffer high load conditions or lose synchronism after N-1-1 contingency events. Several efforts have tried to predict the contingency events in power systems under dynamic conditions to anticipate corrective actions that allow networks to withstand these events without outages while also allowing for electricity market transactions. Probabilistic studies are considered as one promising method to achieve a predictive capability to assist operators in control rooms via probabilistic calculations. For instance, the concept of using probabilistic approaches for dynamic power system stability studies was introduced in [5] and [6]. A cumulant-based probabilistic power flow (PPF) and a hybrid algorithm in [7] and [8] were utilized to correlate various input of random variables. In [9]-[12], computing of probabilistic evolution for power systems was performed by assigning an initial probability distribution for the system building on uncertain parameters.

Moreover, [13]-[18] showed that different factors with hidden failures affect reliability and security of power systems and these factors present in relays, transducers and circuit breaker trip mechanisms. Probability of failure and frequency of failure were used to evaluate the operation of composite electric power systems from an economic perspective in [19, 20]. The results of optimal load flow analysis and load curtailment were employed when the system was unable to meet the load amount. Aleatory (deteriorating components and repair processes) and epistemic (limiting actual parameter values for probabilistic factors) were used in [19], [21]-[23] to evaluate reliability with a probabilistic Monte Carlo simulation. All these analyses give clear evidence that probabilistic approaches could help in obtaining the likelihood of failures for the second event in a N-1-1 contingency sequence.

Many researchers continue to develop new methods based on power systems models representing electrical systems that no longer physically exist. For example, the widely used IEEE

68-bus benchmark model was originally developed for the New England regional transmission grid in the 1960's. Since then, there has been rapid expansion in renewable energy resources, changes in load characteristics and increased use of static VAR compensators and other types of FACTS equipment. Therefore, there is a need to have better methods for deriving and calibrating electric power system models. In many cases, reduced order models are preferred during initial investigations of power system stability analysis. These simplified power system models should capture the same stability characteristics as the overall larger system. This helps planners and policy makers to have an overview of their systems and optimize utilization of renewable resources. Reduced models of large-scale power systems facilitate testing different operating situations, such as line congestion, thermal limits, negative locational marginal pricing, wind curtailment, etc., and give results close if those issues were tested in the actual physical system. Therefore, extraction of benchmark models of large power systems should meet requirements of the NERC standards and result in models with smaller errors if their measurements match with real ones of original power systems [24, 25].

Various methods have been employed to derive reduced models for analysis purposes, such as Ward Reduction, Kron Reduction Approach, Dimo Method, and Zhukov Method, after extracting them from large-scale networks [26]. Ward Reduction Method divides large power systems into two systems: an internal system and an external system. The buses are divided into three types: internal, boundary, and external buses [27, 28]. For example, both the Standard and Extended Ward Equivalent methods in [29] are applied on transmission systems in the Netherlands to produce a 65-bus benchmark model after reducing the external system to specified boundary nodes. Researchers in [30] have developed a decomposition and coordination algorithm based on the Ward Equivalent process to optimize reactive power flows. The Ward reduction method in

[31] is used with a modified load shedding algorithm to evaluate the reliability of the Southern China grid after reducing to 22 buses. In [32], this reduction process is applied to the IEEE 118-bus system to produce a 35-bus reduced model for optimal power flow purposes. From that research, a Ward reduction technique was used due to simplicity and accuracy, in addition to keeping the studied area as the internal system with full details [27]-[32]. Therefore, this technique is selected in this research after some modifications in its procedure to derive a new model that retains the full details of the studied area.

High levels of wind turbine generation result in critical and complicated risks of inter-area oscillations. Wide-area control (WAC) designs, via involvement of advanced wide-area measurement (WAM) technologies such as phasor measurement units (PMU), can effectively reduce power flow oscillations in multi-area electrical systems. Optimal WAC methods for improving transient stability could enhance the power transfer capability of transmission networks and avoid dangerous cases, such as load or generator disconnection or cascading blackouts after a sequence of disturbances [33]-[35]. This work suggests a WAC approach based on a modified H_2 control method, one of to dampen frequency oscillation and power flow excursions through adjusting variables in both HVDC ties and FACTS devices with particular attention to Static Synchronous Series Compensators (SSSC).

This research examines methods based on two specific case studies that are modeled after existing transmission networks in order to demonstrate a realistic level of improved stability by adopting the proposed methods. The first system is a new reduced benchmark model from a large-scale system in North America. This reduced benchmark model consists of 456 buses and is used in validating a novel reduction technique developed in this dissertation. This system is further reduced to a three- area 21 buses model to run the proposed H_2 control method. The second system

is a Load Frequency Control (LFC) model of the Iraqi electrical network. Both systems have or are in the process of installing wind or solar generation stations to increase the use of renewable energy. Also, HVDC links and SSSC devices have been placed in the targeted systems to emphasize their roles in improving reliability and stability.

1.2 Objectives

The goal of this dissertation is to create a new algorithm that detects instabilities in transmission systems after having N-1-1 disturbances and design a control method that maximizes the reliability and stability boundaries when accounting for inverter-based generation. These algorithms are developed in terms of the flow chart shown in Fig. 1.1.

First, utilization of probabilistic techniques in creating a risk-based reliability method to determine potential outage of lines in transmission systems through considering two main variables: age of line and post first-fault load flow with consideration of line overload following a second fault. This method also provides appropriate locations to place HVDCs and SSSCs.

Second, there is a need to have a power model with high levels of wind generation from realistic networks that have not been previously analyzed. A novel reduction method is developed in this research through three parts: a reduction part that consists of four sub-parts; a validation state that also consists of two sub-parts; and an error reduction part. All of these parts with their substeps produced a new reduced model with high levels of wind transferred surplus energy to remote areas. Results of this method guarantee that the reduced technique could be generalized on various systems to build reduced models to mimic large-scale systems with low error.

Third, a H_2 control framework as a new WAC technique is applied on power systems with LFC models. The new method assumes load variation and renewable generation as disturbance inputs to the H_2 controller after consideration of communication time-delays. The parameters of

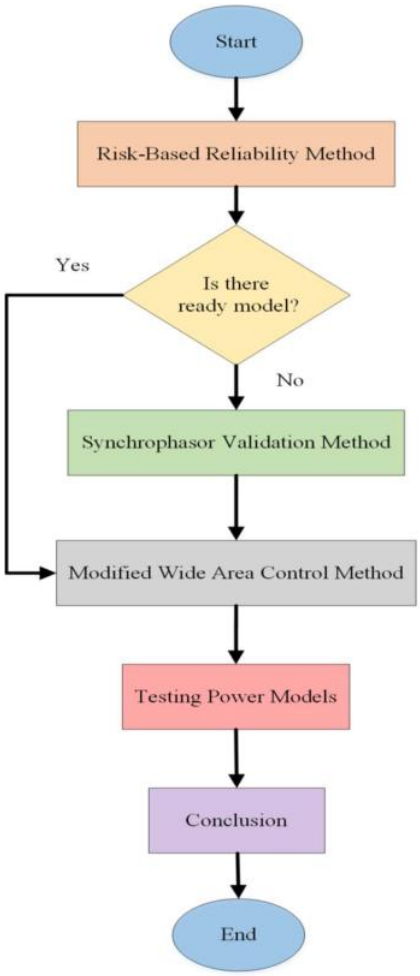

Fig. 1.1. The proposed method for improved power system planning to achieve increased reliability with renewable energy.

inverter-based generation equipment are obtained in the proposed control method in order to find optimal values with minimum frequency and power deviations and low cost. This step is examined with the LFC model of the reduced North American and Iraqi multi-area systems.

The final aspect of this dissertation is investigating the H_2 control framework under the conditions of N-1-1 disturbances due to losing load and tripping two transmission lines. These changes by employing the H_2 controller and HVDC links, or SSSC devices with their optimal parameters, show results that meet the requirements of NERC standards compared to the original uncompensated responses that violate the regulatory standards.

1.3 Dissertation Outline

The outline of the dissertation is given as follows: Chapter Two focuses on studying contingency analysis and N-1-1 disturbances. Also, previous research into probability in power systems is reviewed and a new risk-based reliability method is presented. An application of the reliability method to the IEEE 68-bus benchmark system is provided with calculation of optimal parameter values that allow for more effectively distinguishing the severity of a second disturbance. Chapter Three discusses building a novel method to reduce large-scale power systems to reduced models for research and planning purposes. Chapter Four shows the proposed control method and how it can be configured in LFC models with different types of inputs and outputs. Also, installing of HVDC and SSSC equipment is studied in this chapter. The Chapter Five and Chapter Six present the application of the new control method to the reduced North American and the Iraqi national electrical system for N-1-1 contingency analysis. Results are compared with a conventional controller in order to show the benefits of the new method. The major contributions of this dissertation are summarized in addition to some future research topics in Chapter Seven.

2 Modified Reliability Method

2.1 Contingency Analysis

Electric power systems are complex networks whose operational modes require complicated processes to provide consumers with uninterrupted sources of electricity. For meeting regulatory requirements in electricity grid operations, electric utility providers try to maintain their systems to withstand abnormal conditions due to fault conditions and various types of anomalous conditions that might occur. Preventive steps are prepared in advance by operators and planners to keep power systems at acceptable levels of frequency and voltage being delivered to consumers [36, 37]. All of these plans and procedures are analyzed under a power system security umbrella, which is the ability of the power system to remain secure without serious consequences to different types of contingencies [38].

Power systems have five defined operating conditions during pre- and post-fault circumstances. These are (i) normal, (ii) alert, (iii) restorative, (iv) emergency and (v) in-extremis are shown in Fig. 2.1. These classifications are dependent on voltage, frequency, and overload limit criteria. In the normal operating states, the system functions in a secure manner where voltage and frequency are within the acceptable ranges and all equipment are not overloaded. In addition, any loss of a single piece of equipment will not violate operational constraints of the system. Alert conditions reflect that the system that could experience a type of disturbance that may cause some elements to become overloaded. However, this condition could lead to a more severe state such as an emergency or in-extremis condition prior to returning to the normal state. The emergency state reflects that a power system has low voltage or overloaded equipment that are in violation of power constraints (and possibly for only a short-term period). However, this state could deteriorate into

the in-extremis state if remedial actions do not occur, otherwise with protective actions then the system can revert to an alert state.

During an in-extremis state some consumers will lose their power partially or power systems might be in a total blackout condition due to lack of fast and desired response to clear or treat large disturbances. In this situation, the system will need to progress through a restorative state in order to rebuild the electrical networks after total or partial [39]-[41] blackout. Analytical studies in power system security consider all possible disturbances that would result in circuit breaker operations due to overload conditions or inadequate voltage levels at buses. This type of analysis is generally referred to as Contingency Analysis.

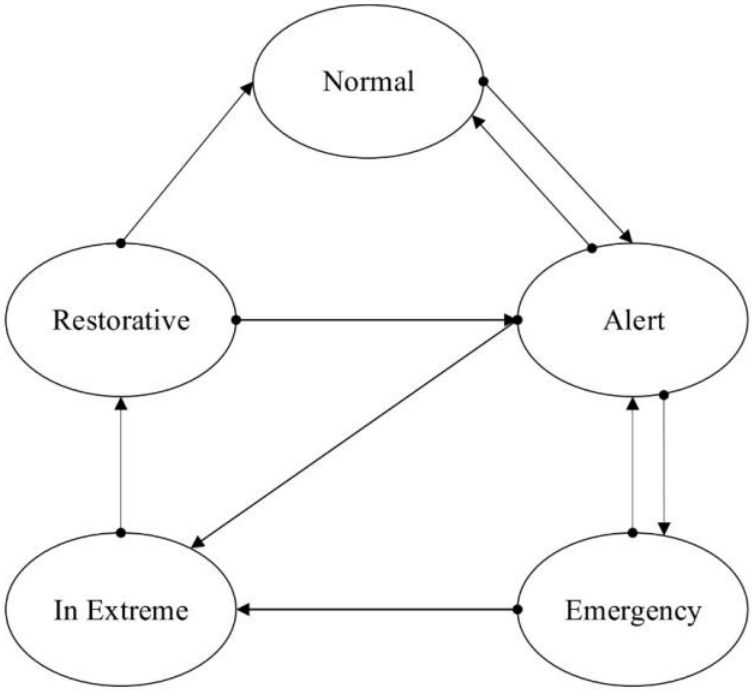

Fig. 2.1. Operating states for electrical power systems [39]-[41].

The reliability of delivering electricity to customers without interruptions and within acceptable levels of frequency and voltage regulation is an essential aspect of operating a bulk electric power system. It is also required to provide power delivery while withstanding possible

disturbances and equipment failures. Preparing for abnormal situations and investigating the resulting load flow on transmission lines and bus voltages after disturbances is used to evaluate the security of electric power systems. Assessment of transient stability for possible contingencies on transmission lines is a significant aspect of power system security planning [19]. Contingency Analysis (CA) is a part of power system security analysis and also impacts power market studies, security assessment, and electricity market transaction management. A typical CA consists of various models such as single-component outage (one line or one generator outage), multiple-component outage (two lines outage, one line and one generator outage, etc.), and sequential outage (one outage after another) [42]. Evaluation of voltage levels, transmission capacities, and generator power limits is completed for each contingency to determine whether the system is secure [43].

2.2 N-2 or N-1-1 Contingency Analysis

Contingency analysis in power systems is important for operators, owners, planners, and policy makers in the electrical energy sector. Various remedial actions, such as transmission switching and other corrective actions are considered to reduce consequences of disturbances, increase reliability and stability levels, and provide economic benefits [44]. Obtainment of all these aspects is included in regulatory requirements from federal agencies such as the National Electric Reliability Corporation (NERC) and the Federal Energy Regulatory Commission (FERC). When considering N-1 constraints, a power system should continue in normal operation conditions after any single element failure, such as an outage of a transmission line. However, NERC sets regulations to ensure that operators will maintain contingency plans for further possible conditions, such as N-2 or N-1-1 (two elements fail within a short time-frame) contingencies [45]. A N-2 contingency event is defined as when a sequence of cascading outages in transmission system occurs within 1 second.

In contrast with N-2 contingencies, a N-1-1 contingency event could be defined as cascading faults occurring with a time interval longer than one second. More specifically, N-1-1 contingency analysis is defined based on NERC guidelines where there is a loss of one element, followed by adjustments to the electric power systems (either automatic or operator initiated). This first contingency event is then followed by the loss of a second element [3]. This type of analysis ultimately is used to assist in sustaining economic activity and quality of life through reliable electric power delivery. If the resulting analysis indicates an unacceptable likelihood of a major power disturbance, then further system modifications and upgrades may be justified such as installing new transmission lines, designing new exciter controls, implementing more aggressive demand response agreements, installing power electronic based equipment such as Flexible AC Transmission Systems (FACTS), or adopting High Voltage DC (HVDC) links within or between different areas.

Identification of critical N-2 or N-1-1 contingencies is a computationally challenging problem, especially with complex and large-scale networks, and a large amount of research has been conducted on his topic. Risk-based planning methods are one group of alternatives to evaluate electric power systems [46, 47]. For example, in [7] and [8] a cumulant-based Probabilistic Power Flow (PPF) and a hybrid algorithm are employed to correlate the parametric input of random variables. The concept of using probabilistic approaches for dynamic power system stability studies was introduced in [5] and [6]. Those methods could help operators in control rooms via probabilistic calculations to make a decision for situations involving security levels and market transactions. Computing the probabilistic evolution of power systems is performed by assigning an initial probability distribution for the system through dealing with the uncertainty of power systems parameters is described in [9]-[12]. Uncertain barriers in power calculations may be integrated and

approximated by using probabilistic methods to evaluate the transient stability for multi-machine power systems, and the evaluation methods provide remedial actions for electric utilities to avoid voltage collapse and frequency instability [48].

Moreover, [13]-[18] shows the importance of accounting for factors that affect the reliability and security of power systems. Those factors include protection systems having hidden failures present in relays, transducers and circuit breaker trip mechanisms. Probability of failure and frequency of failure were used to evaluate the operation of composite electric power systems from an economic perspective in [19, 20]. The results of optimal load flow analysis and load curtailment were employed when the system was unable to meet the load amount. Aleatory (failing components and repairing processes randomly) and epistemic (limiting actual parameter values for probabilistic factors) were used in [21]-[23] to evaluate reliability with a probabilistic Monte Carlo simulation. In [49, 50] an approach utilizing steady-state load flow to analyze the reliability of power systems included uncertainties in wind power was introduced. The probabilistic analysis in [51] illustrated that increasing the number of surge arresters, and aging of cables, and lines were factors that influenced reliability. The researchers in [52] used weather forecast factors such as humidity, wind speed, temperature, and their effects during maintenance periods as parameters that impact power system equipment failure rates. However, this work presents a new method to emphasize the critical cases under N-1-1 contingencies with different aspects.

2.3 Risk Based Reliability Method (RBRM)

In this dissertation, a new method is proposed for calculating the reliability of a power system depending on a combination of variables such as transmission line ageing and power-flow. The age of the various transmission lines, the load flow under normal conditions, and load flow under post-first disturbance conditions, are used to develop the suggested approach. A probabilistic

method is used to select a transmission line based on likelihood of a contingency and calculate the load flow for it under normal and post-fault conditions. These factors lead to developing a Risk-Based Reliability Method (RBRM). A RBRM that uses a ratio between the reliability of a system under the first faulty condition to the reliability of system under normal conditions to obtain the final probability of occurrence the N-1-1 contingency event as shown in Fig. 2.2.

In this figure, the age of the transmission lines is assumed as a proxy for probability of failure in order to obtain a reliability measure for each case. A hypothesized age estimation is done in order to complete the reliability calculations. The values for line age are given in seconds in order to relate standard electrical SI units, but in the actual practice the line's age T_a is given in thousands of hours. To get T_a in seconds, the age of each line is reduced after ignoring the first ten years from all lines. Then the rest of the line's age is converted to hours after multiplying the rest by 8760, which is equal to 365 days multiplied by 24 hours. For obtaining the line's age in seconds, T_r is selected arbitrarily to reduce T_a to seconds through [19];

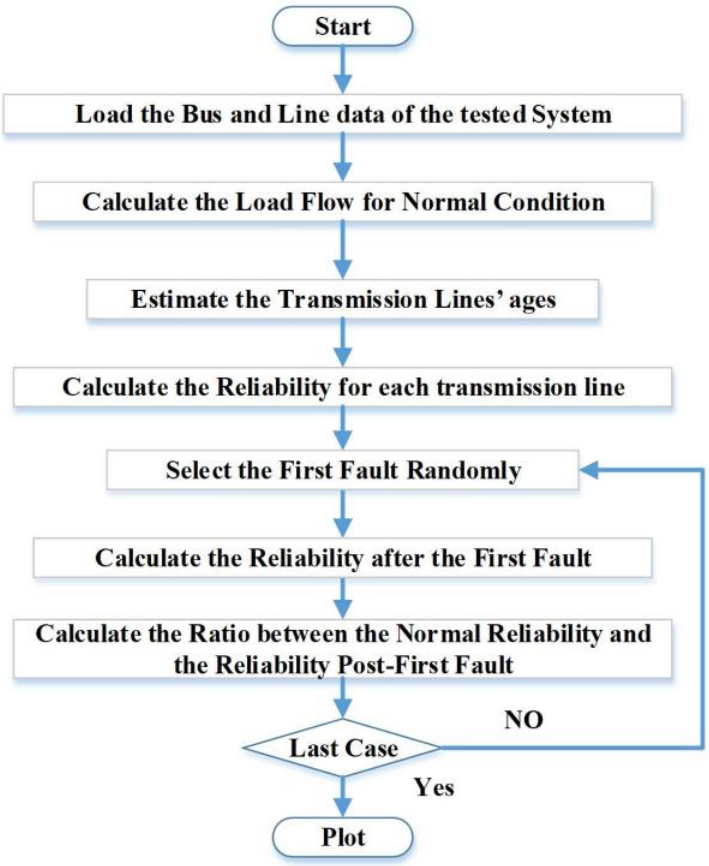

Fig. 2.2. Flow chart of the proposed probability method.

$$T_i = T_a/T_r, \tag{2.1}$$

After obtaining the line's age, the load flow that passes through the line for the non-fault case is calculated and used along with the line age to determine the probability of a failure occurring on that line. These factors are used for the i^{th} line can be given in [19],[53]-[56]

$$\eta_{1i} = \alpha_0 e^{-\alpha_1 * S_{1i}}, \tag{2.2}$$

where η_{1i} is a characteristic life parameter under the normal case, α_0 and α_1 are the coefficients in the life-stress relationship parameters (scale parameters of the distribution function). S_{1i} is the load flow in the normal condition at line i. α_0 and α_1 are calculated relying on the ratio between values of load flows for lines i and j in the normal condition after comparing them with the maximum

value in that case. Calculations of α_0 and α_1 are dependent on assumptions that all lines have the same conductor, and a line with low load flow would have high reliability and vice-versa. These values can be adjusted to evaluate the behavior of the power system to possible design changes, such as replacing or upgrading transmission lines[19]. Using η_{1i} and T_i, the reliability of i^{th} line under normal statues can be given as in [19],[53]-[56]

$$R_{1i} = e^{-(T_i/\eta_{1i})^{\beta}}, \tag{2.3}$$

where R_{1i} is the reliability of line *i* at the normal condition and T_i is the age of line *i,* while β is the shape parameter. After the first reliability calculations, the same steps would be utilized to calculate the same variables but under different conditions. Via the load flow after the first event, α_0 and α_1, new calculations would be shown in [19],[53]-[56]

$$\eta_{2i} = \alpha_0 e^{-\alpha_1 * S_2 i}, \tag{2.4}$$

where η_{2i} is a characteristic life parameter under the post-first fault case and S_{2i} is the load flow in the post-first fault condition at line *i.*

$$\tau_i = \eta_{2i} \sqrt[\beta]{(-\log(R_{1i}))}, \tag{2.5}$$

where τ_i is the time that line *i* can carry load flow S_{2i}. Equation (2.4) shows the approach to calculation of τ_i when the line carries the different current after disturbances with taking in account that α_0 and α_1 are constant. τ_i would be higher than T_i because τ_i comes from T_i plus the time of the post-first fault's current. After getting τ_i, the reliability of line after the first fault can be obtained by using τ_i and T_f and given in [19],[53]-[56]

$$R_{2i} = e^{-((T_i+\tau_i+T_f)/\eta_{2i})^{\beta}}, \tag{2.6}$$

where R_{2i} is the reliability of line i after the first fault and T_f is the time of the first fault. From previous steps, the reliability of each line could be modified in the formula

$$R_{21} = R_{2i}/R_{1i}, \tag{2.7}$$

where R_{21i} is the final reliability of line i given by the first fault of the system. By using this analysis, the prediction of an N-1-1 contingency event can be obtained by using an inverse relationship between reliability and probability ($R = 1 - P_r$)[19].

Calculation of the severity index (SE) for the double contingency depends on each generators' weight and generator phase angles and is given by

$$SE = \frac{W_1(t+1)\,\delta_1(t+1) + W_2(t+1)\,\delta_2(t+1) + \cdots + W_m(t+1)\,\delta_m(t+1)}{W_1(t)\,\delta_1(1) + W_2(t)\,\delta_2(1) + \ldots + W_m(t)\,\delta_m(t)}, \tag{2.8}$$

where, $W_m(t)$ is the weighting factor of the generator m for the normal condition. $W_m(t+1)$ is the weighting factor of the generator m after the second fault. $\delta_m(t)$ is the phase angle of the generator m for the normal condition. $\delta_m(t+1)$ is the phase angle of the generator m after the second fault and

$$W_m(t+1) = \frac{P_m(t+1)}{\sum_{m=1} P_m(t)} \tag{2.9}$$

where $P_m(t)$ is the real power of generator m for the normal case. $P_m(t+1)$ is the real power of generator m after the second fault. The level of transient stability of the system is checked by observing the maximum value that each generator rotor angle changes from the pre-fault condition. This is the $\|\delta(t)\|_\infty$ norm of the vector of machine rotor angles [4, 19, 58]. This approach is developed for contingencies on transmission networks and applied to transient stability analysis of an IEEE 68-bus, 16-machine, 5-area benchmark system [57].

2.4 IEEE 68 Bus System

A sequence of random N-1-1 contingency events were simulated for the 68-Bus, 16-machine, 5-area (geographical regions) system [57]. This is an IEEE transient stability benchmark system. It is based upon a reduced-order equivalent model of the interconnected New England test system (NETS) and New York power system (NYPS). A one-line diagram of the benchmark system is shown in Fig. 2.3. The frequency of the system is nominally 60Hz and the base power is 100 MVA. Transmission lines, generators and exciter data used in this simulation are given in [57].

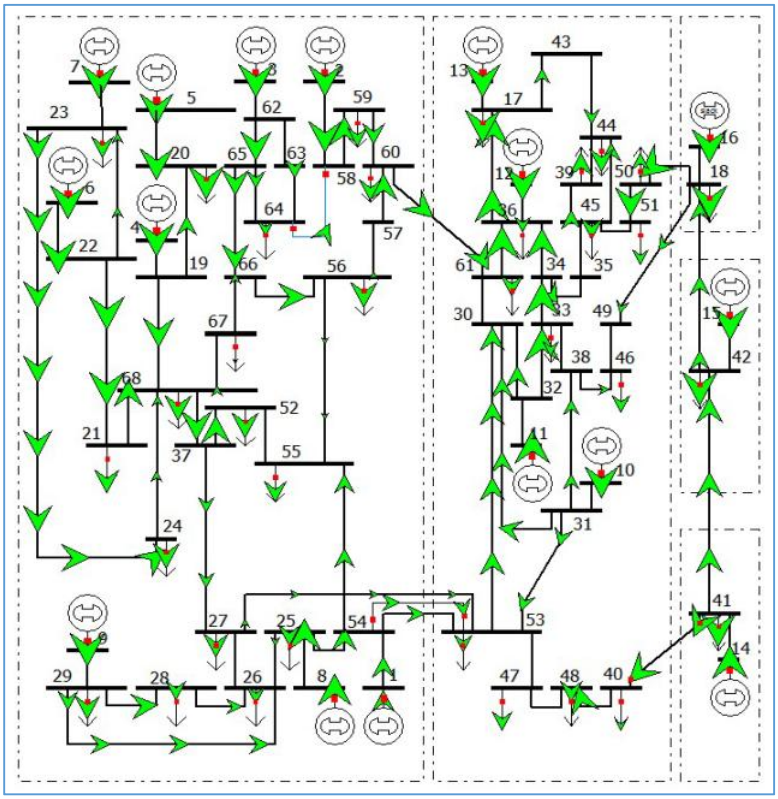

Fig. 2.3. One-line diagram of IEEE 68-bus system [57, 71].

Multiple contingencies in power systems may possibly occur that have the potential for resulting in a partial or regional blackout. Many parameters are used to estimate or predict and evaluate the dynamic stability of power systems such as rotor angle, speed of synchronous

generators, bus voltage, etc. Modeling the dynamic components and their controls is necessary for power system planning studies [58, 59]. The analysis of power system behaviors during transients resulting from fault conditions used in this research is based on the following equations [57]:

Generator Modeling:

$$\frac{d\delta_i}{dt} = \omega_B\,(\omega_i - \omega_s) = \omega_B S_{mi}, \tag{2.10}$$

$$2H\,\frac{dS_{mi}}{dt} = \,(T_{mi} - T_{ei}) - D_I S_{mi}, \tag{2.11}$$

where T_{ei} consists of different components, which are given by:

$$T_{ei} = EF + ED + EC + EH + EQ, \tag{2.12}$$

and,

$$EF = E'_{di} I_{di}\,\frac{(X''_{qi} - X_{lsi})}{(X'_{qi} - X_{lsi})}, \tag{2.13}$$

$$ED = E'_{qi} I_{qi}\,\frac{(X''_{di} - X_{lsi})}{(X'_{di} - X_{lsi})}, \tag{2.14}$$

$$EC = I_{di} I_{qi}\,\left(X''_{di} - X''_{qi}\right), \tag{2.15}$$

$$EH = \psi_{1d}\, I_{qi}\,\frac{(X'_{di} - X''_{di})}{(X'_{di} - X_{lsi})}\,, \tag{2.16}$$

$$EQ = \psi_{2qi} I_{di}\,\frac{(X'_{qi} - X''_{qi})}{(X'_{qi} - X_{lsi})}\,, \tag{2.17}$$

and,

$$I_{qi} + I_{di} = (1/(R_{ai+j}\,X''_{di}))(E_1 + E_2 - V_{qi} + jWFD), \tag{2.18}$$

where,

$$E_1 = E'_{qi}\,\frac{(X''_{di} - X_{lsi})}{(X'_{di} - X_{lsi})}\,, \tag{2.19}$$

$$E_2 = \psi_{1di}\,\frac{(X'_{di} - X''_{di})}{(X'_{di} - X_{lsi})}, \tag{2.20}$$

$$WFD = (EF - \psi_{2qi}\frac{(X'_{qi}-X''_{qi})}{(X'_{qi}-X_{lsi})} - V_{di} + E'_{dci}), \tag{2.21}$$

and,

$$T_{ci}\frac{E'_{dci}}{dt} = I_{qi}\left(X''_{di} - X''_{qi}\right) - E'_{dci}, \tag{2.22}$$

$$T'_{q0i}\frac{dE'_{dt}}{dt} = \ -E'_{di} + \mathrm{XQE}, \tag{2.23}$$

where,

$$XQE = \left(\mathrm{X_{qi}} - \mathrm{X'_{qi}}\right)(-\mathrm{I_{qi}} + \mathrm{XQ}\left(\left(\mathrm{X'_{qi}} - \mathrm{X_{lsi}}\right)\mathrm{I_{qi}} - \mathrm{E'_{di}} - \psi_{2\mathrm{qi}}\right)), \tag{2.24}$$

and,

$$XQ = \frac{(X'_{qi}-X''_{qi})}{(X'_{qi}-X_{lsi})^2}, \tag{2.25}$$

$$T'_{d0i}\frac{dE'_{dt}}{dt} = E_{fdi}\ - E'_{qi} + XDE, \tag{2.26}$$

where,

$$XDE\ = (X_{di} - X'_{di})(I_{di} + XD\left(\psi_{1d}\ - \left(X'_{qi} - X_{lsi}\right)I_{di} - E'_{qi}\right)), \tag{2.27}$$

where,

$$XD = \frac{(X'_{di}-X''_{di})}{(X'_{di}-X_{lsi})^2}, \tag{2.28}$$

$$T''_{d0i}\frac{d\psi_{1di}}{dt} = E'_{qi} + (X'_{di} - X_{lsi})I_{di} - \psi_{1d}\ , \tag{2.29}$$

$$T''_{q0i}\frac{d\psi_{2qi}}{dt} = -E'_{di} + \left(X'_{qi} - X_{lsi}\right)I_{qi} - \psi_{2qi}. \tag{2.30}$$

The excitation systems have automatic voltage regulators (AVRs):

$$T_E\frac{dE_{fd}}{dt} = V_r - \left(K_E E_{fd} + E_{fd}A_{ex}e^{A_{ex}E_{fd}}\right), \tag{2.31}$$

where,

$$T_r \frac{dV_r}{dt} = V_t - V_r; \;\; T_F \frac{dV_F}{dt} = E_{fd} - V_F, \tag{2.32}$$

and,

$$T_A \frac{dV_A}{dt} = K_A \left(V_{ref} + V_s - V_r - \frac{K_f}{T_F} \left[E_{fd} - V_f \right] \right) - V_A, \tag{2.33}$$

$$E_{fd} = K_A \left(V_{ref} + V_s - V_r \right). \tag{2.34}$$

Power system stabilizer:

$$V_S = K_{pss} \frac{sT_w(1+sT_{11})(1+sT_{21})}{(1+sT_w)(1+sT_{22})(1+sT_{21})} S_m \, . \tag{2.35}$$

Load network:

$$I_{Qi} + jI_{Di} = \left(I_{qi} + jI_{di} \right) e^{j\delta i}, \tag{2.36}$$

$$V_{gi} = V_{Qi} + jV_{Di} = \left(V_{qi} + jV_{di} \right) e^{j\delta i}, \tag{2.37}$$

$$V = Z_{Aug} I, \tag{2.38}$$

where,

$$Z_{Aug} = (Y_{Aug})^{-1}. \tag{2.39}$$

Variable i refers to the i^{th} generator; δ is the rotor angle in radians; ω_B is the rotor base angular speed in radians per second; H is the inertia constant in seconds; T_{d0}' and T_{d0}'' are the d-axis open circuit transient and sub-transient time constants, respectively; T_{q0}' and T_{q0}'' are the q-axis open circuit transient and sub-transient time constants, respectively; and T_c is the time constant for the amortisseur rotor coil (which is usually taken as 0.01 seconds). The other variables are in per unit (pu): ω: rotor angular velocity; ω_s: synchronous angular velocity; S_{mi}: slip; Tm is the mechanical torque; T_e: electrical torque; D: machine rotor damping; E_q': transient electromotive force (emf) of field flux linkages; E_d': transient emf of flux linkage in q-axis damper coil; ψ_{1d} and

ψ_{2q}: sub-transient emfs of d-axis and q-axis damper coils, respectively; E_{fd}: field excitation voltage; E_{dc}': transient emf across the dummy rotor coil; I_d and I_q: d-axis and q-axis components of the stator current, respectively; Vd and Vq: d-axis and q-axis components of the stator terminal voltage, respectively; X_d, X_d' and X_d'': synchronous, transient and sub-transient reactance, respectively, along the d-axis; X_q, X_q' and X_q'': synchronous, transient and sub-transient reactance, respectively, along the q-axis; R_a: armature resistance and X_{ls}: armature leakage reactance [4, 19, 57, 58]. In this work, a three-phase fault is assumed to be the cause both of the contingencies in N-1-1 sequence mode and the age of each line is scaled for simplification of the calculations. This resulting scaling is summarized in Table 1.

Table 1. The age of some lines in seconds

Line No.	Bus from-Bus to	T_i (Sec)
1	27-53	190
22	47-48	901
45	39-45	552
54	22-23	206
63	17-36	536

To simulate the N-1-1 contingencies in the IEEE 68 bus system, the first fault occurs at time 5 seconds and the time clearing for this disturbance is assumed to be a standard 2 electrical cycles (33 ms) setting. After 2.0 seconds from clearing the first fault the second contingency occurs. There are five types of line impedances used in simulating the fault sequence for transient analysis purposes of the N-1-1 contingency sequence: 1- normal impedance; 2- first fault impedance; 3- post first-fault impedance; 4- second impedance; and 5- post-second fault impedance. Each impedance

has a matrix of values depending on the configuration of the system during and after the disturbance. For illustration of N-1-1 contingency analysis, two instances of several sequences that were simulated in order to compute of the severity indices. As an example, the first case shown in Fig. 2.4 represents a double contingency that occurs on transmission lines 18-49 and 28-26, while Fig. 2.5 shows the N-1-1 contingency occurs on transmission lines 30-32 and 25-26 and both cases experience faults at 5 seconds and 7 seconds, respectively [58].

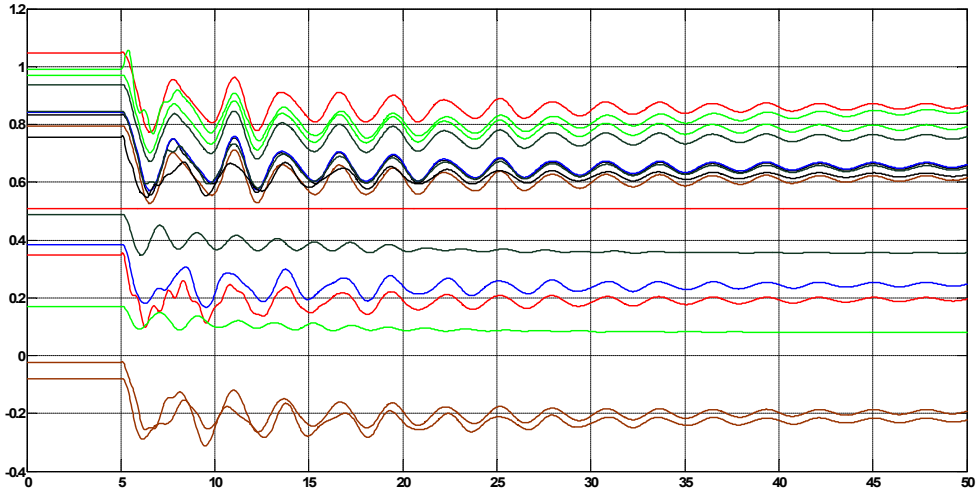

Fig. 2.4. Transient response for phase angles of generators for case #1.

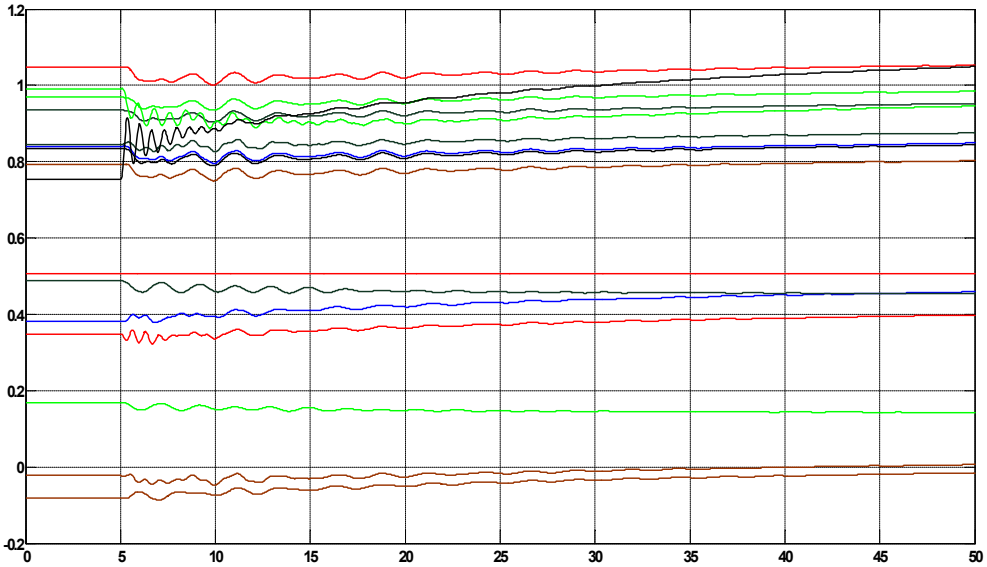

Fig. 2.5. Transient response for phase angles of generators for case #2.

In Fig. 2.4, the disturbances produce low power oscillations and the system recovers along time of the simulation and the cause for this behavior is the positions of outage lines and amount of power flow in tripped lines after disturbances do not affect generators of the system largely. In Fig. 2.5, the disturbances change the phase angle of generators due to varying paths of power flow due to outage of transmission lines. The tripped lines make significant variations in impedance values between load points and generators. Therefore, phase angles for some generators would be shifted. After applying the N-1-1 contingencies on the 68-bus benchmark model in [17], the severity index (SE) is calculated for showing the severe cases of double contingencies as in (2.8) [19, 21]. The *SE* for all possible N-1-1 contingencies for line outages in the 68-bus system are illustrated in Fig. 2.6.

These cases are sorted depending on (x, y, z) coordinates, where the x-axis is the number of line, which has the first fault, the y-axis is the number of line which has the second fault, and z-axis is the value of *SE*. Each case in the figure has a different value of *SE* that depends upon the load flow and maximum rotor angle deflection. Cases that have high *SE* are visually emphasized in Fig. 2.6 to draw attention to those N-1-1 contingencies that required corrective actions to increase the reliability and stability of power system. Depending on these cases and their computed reliability, system planners and operators can mitigate the N-1-1 effects by upgrading their networks with proper components [4, 19]. The results of the *SE*'s calculation will be combined with the following results of RBRM to predict the most severe cases in order to increase reliability.

Studying the reliability of power systems is essential in helping reliability coordinators and system planners to decide upon remedial actions in critical situations. The proposed Risk-Based Reliability Method (RBRM) is utilized to evaluate the system reliability after a first fault and to predict the probability of an N-1-1 event. It is displayed that RBRM enhances the ability to

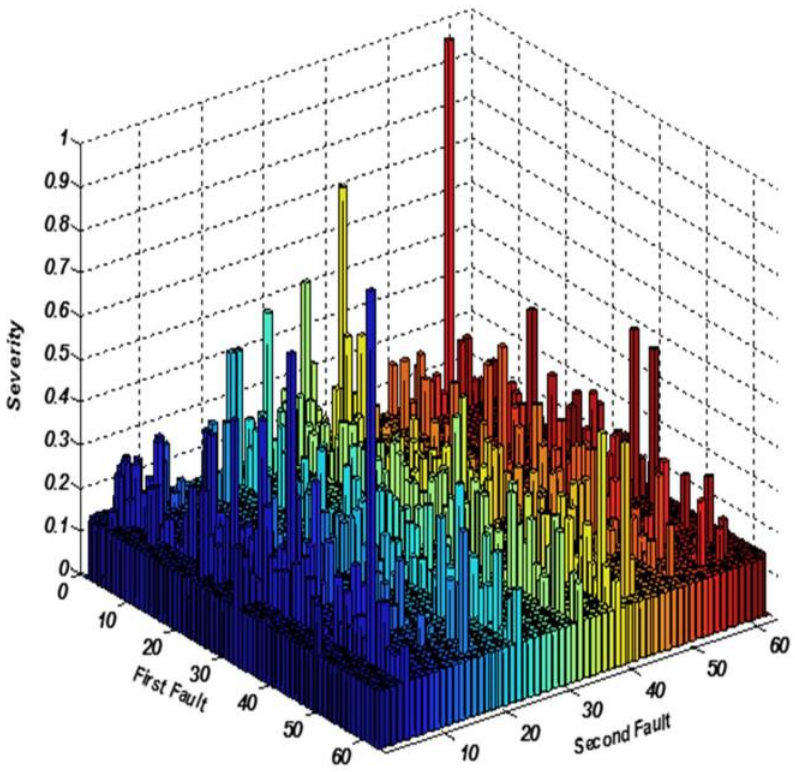

Fig. 2.6. Severity index (SE) for IEEE 68 bus system under N-1-1 contingencies[19, 58].

distinguish between the severities of various N-1-1 contingencies. The results of the research indicate that RBRM would improve the ability of reliability coordinators to identify weak elements in a power system and thereby provide a guide to transmission planners in prioritizing system upgrades.

RBRM is applied to evaluate the reliability and predict which line will be most likely to have the second fault through applying equations (2.1) to (2.7). Selection of the values of α_0 and α_1 is done after choosing a specific line and using its load flow with a specific value of β via equations (2.3), (2.5), and (2.6). This process is accomplished through adopting two values of load flow, which are normal and post-first fault conditions, for each line in the systems. Values of load flow under the two conditions have been employed for different moments (T_i and τ_i). By applying (2.2) , the values of α_0 and α_1 are obtained when a transmission line is under normal load condition

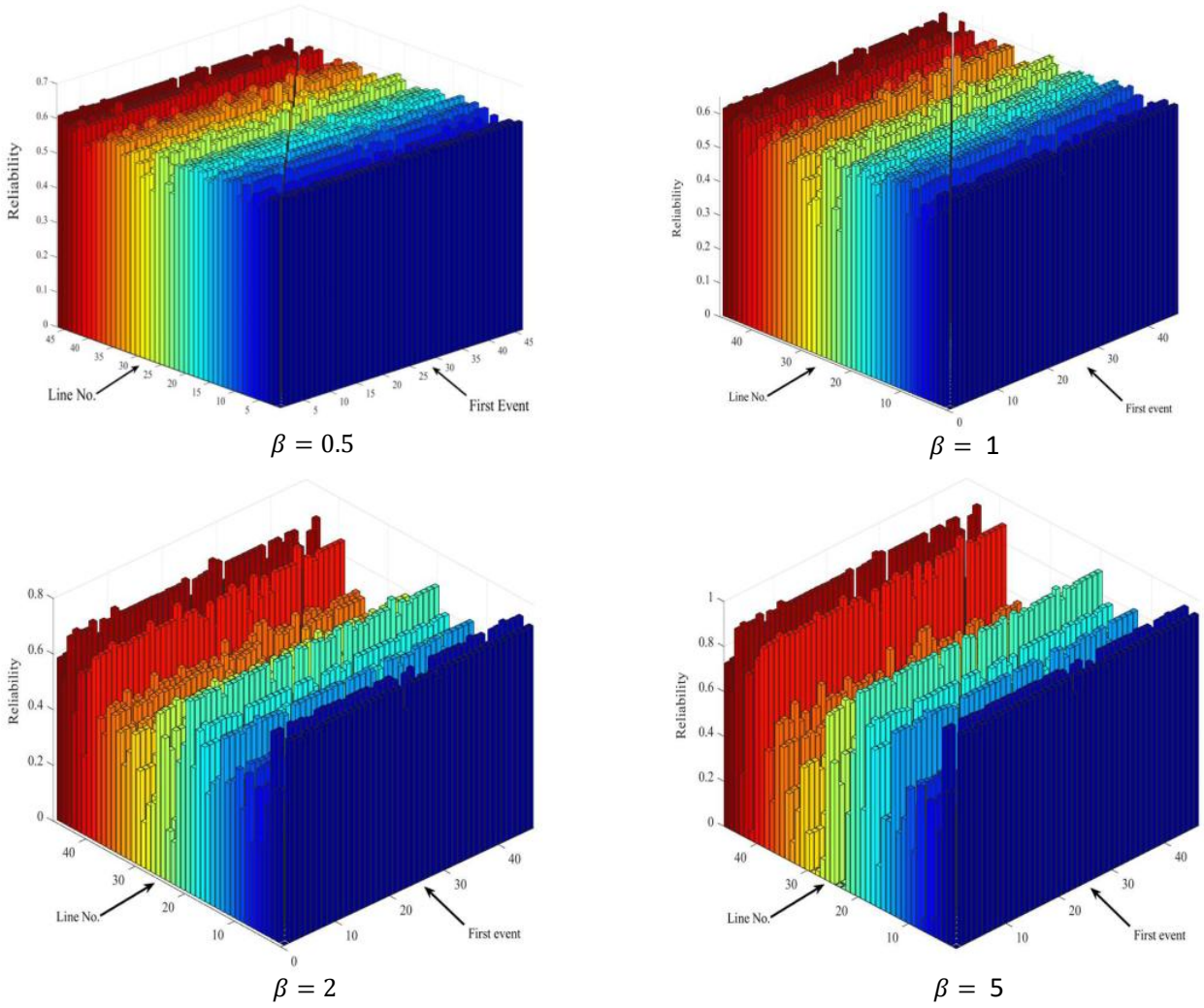

Fig. 2.7. Reliability of IEEE 68 bus system when $\boldsymbol{\beta}$ *=0.5, 1, 2, 5 [19].*

and maximum power flow could pass through it. To analyze the RBRM of the system, β is varied from 0.5 to 5 [19, 60]. This range provides ability to observe cases that have the worst impacts on the overall system reliability and these changes are shown obviously in Fig. 2.7. In this figure, the *y*-axis represents first fault case, the *x*-axis represents the transmission line number, the *z*-axis is the value of the reliability of the (x^{th}, y^{th}) associated transmission line and fault case. As illustrated in Fig. 2.7, reliability for some cases is affected by three factors which are the amount of load flow, age of lines, and β. Increased power rating leads to distinguish normal cases having

high values of reliability and abnormal cases having low reliability due to the value of currents for both conditions [19].

The high value of active power flows in this system under normal conditions would not exceed 0.5pu, while the active power passes under abnormal conditions may exceed 1pu. This is interpreted as the line *i* carries high load flow (apparent power) passing through it; the reliability of it would be low compared with lines that have low power flow. That is because of the natural exponential function producing the reliability evaluation through impacting with the amount of power flow and age of line. The impacts of the value of α_0 and α_1 come from their roles in calculating the characteristic life parameter ($\boldsymbol{\eta}$) as indicated in (2.2) and (2.4). Also, when a generator loses synchronism due to severe disturbances, the power flow would be increased in some of the remaining lines, thereby generating cases of lowered reliability for those lines most impacted by increased power flow (i.e., reduced thermal margins). On the other hand, having contingency cases with small values of probability distribution function of RBRM, due to the value of the shape parameter β, makes recognizing the lines that have low reliability (high failure probability) more complex[19].

First of all, β is set to be 0.5 and the final probability for the second disturbance is obtained for 2070 cases in 2.6 hours via (2.3), (2.5), (2.6), and (2.7) . Then the value of β has been varied to be equal to 1, 2, and 5 in 2.6, 2.6, and 2.4 hours, respectively, shown in Fig. 2.7. when β is equal to 1, the reliability of different cases almost has same values of cases in the calculation of reliability with β =0.5 and that makes difficult to distinguish which line would be likely to have a next fault. Moreover, the investigated cases with β =2 or 5, the probability distribution function of RBRM is changed and it is easy to identify lines have low reliability, high failure probability [19].

Selection of the optimal value of β could play a favorable role in distinguishing cases with high reliability. The value of reliability would be increased or decreased relying on the ratio of time over $\boldsymbol{\eta}$ powered by β. When β is equal to 0.5, the reliability of different cases almost have the same values and that leads to difficulty in finding the line that would be likely to have a next fault while when β is equal to 2, the different values of reliability between lines can be recognized easily. Increasing β to be equal to 2 or 5 will help in highlighting which cases would have high or low reliability. However, when β is set 5, as shown in Fig. 2.7, several cases would be considered having low reliability due to increasing values of exponential to power 5 and that leads to minimize the obtained reliability even when $\boldsymbol{\eta}$ has small differences. Therefore, selection of β in the range between 2 and 3 would be the optimal value to find cases with lower reliability.

3 New Benchmark Wind Model

3.1 New Benchmark Wind Model

Due to clean environment policies, lower capital costs and electricity production tax credits (PTC), the growth of wind source use in the United States and other countries may tend to increase the risk levels of the operational characteristics and dynamics of electric power systems. It also impacts their reliability and stability [61]-[63]. The installation of new wind generation and the expansion of transmission systems encourages researchers to think of having smaller power models that have the same characteristics of larger systems, which are difficult to access due to security aspects and to analyze the existence of new components and their influences under various situations. These system models that represent realistic conditions help planners and policy makers to have an overview of their systems and optimize utilization of renewable resources. Small models of large-scale power systems facilitate testing different power issues, such as line congestion, thermal limits, negative locational marginal pricing, wind curtailment, etc., and provide accurate results to those issues that are tested in real power systems. Therefore, extraction of benchmark models of large power systems should meet the requirements of the NERC standards and result in models with smaller errors if their measurements are examined with real ones from the original power systems [24-25].

Several methods are employed to build small power models for analyzing purposes, such as Ward Reduction Technique, Kron Reduction Approach, Dimo Method, and Zhukov Method, after extracting them from large-scale networks [26]. Ward Reduction Method divides large power systems into two systems, internal system and external system. The buses are divided into three types, internal, boundary, and external buses [27-28]. For instance, both the standard and extended

Ward equivalent methods in [29] are applied on transmission systems from the Netherlands to produce a model with 65-bus test system after reducing the external system to boundary nodes. [30] develops a decomposition and coordination algorithm based on the Ward equivalent process to optimize reactive power flow. Ward reduction method in [31] is used with a modified load shedding algorithm to evaluate the reliability of the Southern China grid after reducing to a power system with 22 buses. In [32], a reduction process is applied on IEEE 118-bus system to produce the 35-bus reduced model for optimal power flow purposes. From previous research, Ward Reduction Technique is used widely due to simplicity and accuracy, which are in existent in the reduced models in the internal system, with full details [27]-[32]. Therefore, this technique is selected in this work, after some modifications in its procedure, to accompany with a new model that has the full details of the studied area.

3.2 Novel Reduction Method

Synchrophasor technology is adopted in many power grids due to producing both big amounts of data and high accuracy. Both are sought for reliability and stability purposes [64-65]. Several papers depend on phasor measurement units (PMUs) data to examine and validate their works. For instance, [66] utilizes PMU data to validate and calibrate measurements of power models with measured models of real power systems. In addition to use of the Ward equivalent method in [67], is used to reduce New-England system with constant *PQ* loads and benefited from PMU data from analyzing the new model. The results in [64] highlight both the accuracy of the model, obtained after comparing data measured by PMUs and simulation measurements, and cause of errors in frequency and phase angle measurements. In [68], researchers develop a method to complete the measurements of large power systems depending on a number of PMUs installed in those systems. For previous works, PMU technology is employed to validate and calibrate power

models. In this work, PMU data from a real system is provided to validate the new model after reduction and calibrate its measurements to minimize significant errors if they are present.

This work focuses on building models with high wind generation and calibrating simulation results with PMUs measurements, which are the main contributions. In addition to previous contributions, the response of breakers in transmission systems under variable generation and abnormal events is presented in this research. A novel reduced model method in this research has extracted new models from real power systems, including several wind or solar generation, through a specific process. The specific process for reducing large-scale power system includes: the reduction part that consists of the Ward equivalent technique with modified steps; the validation part that compares simulation results of reduced model with real measurements data with preliminary relative errors; and the error correction part that adjust some parameters in the small model to obtain small values of errors. The accuracy of this method in the resulting reduced system model gives system planners a realistic opportunity to study transmission systems with non-dispatchable resources under various conditions.

This dissertation develops the Synchrophasor Validation Method (SVM) as a new reduction procedure consisting of three parts to create accurate models from large-scale power systems. Each part in SVM has specific steps to reduce time of simulations and obtain high accuracy. This research uses a Ward Equivalent Technique, PMU measurements data provided by a transmission operator, and a network simulator such as PowerWorld apply the new proposed method. A large-scale power system studied in this work is comprised of 15,310 buses, 19931 lines, 2204 generators, and 69 areas through various voltage levels and the operational model to run in PowerWorld environment, which included all the mentioned data and is provided by Network6 company. The Network6 grid includes large amounts of surplus wind generation

capacity carried by transmission systems to demand buses in remote areas. The approach is divided into the following three main parts, which are;

3.2.1 Reduction Part

Ward Reduction Technique in this part comes with some modifications and these changes centralize the selection of specific electric components of the studied area from other areas. First, Ward Reduction Method divides any studied system into two areas, an internal system and external system. The buses are partitioned to internal (I), boundary (B), and external buses (E), as shown in Fig. 3.1. The bus admittance matrix (Y) for large scale systems can be written as [28]

$$Y = \begin{bmatrix} Y_{EE} & Y_{EB} & 0 \\ Y_{BE} & Y_{BB}^{E} + Y_{BB}^{I} & Y_{BI} \\ 0 & Y_{IB} & Y_{II} \end{bmatrix}, \tag{3.1}$$

where Y_{EE} and Y_{II} are the bus admittances inside external and internal systems, respectively, Y_{EB}, Y_{BE}, Y_{IB}, and Y_{BI} are the bus admittances connect the boundary buses with external and internal buses, Y_{BB}^{E} and Y_{BB}^{I} are the bus admittances for all lines between boundaries and external and internal buses, respectively.

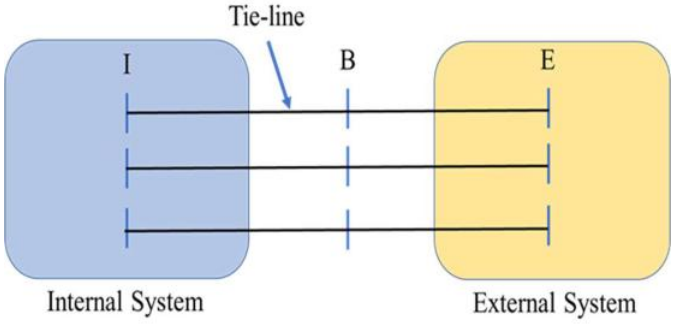

Fig. 3.1. Studied system before the Ward reduction method [28].

In the reduction method, the external system would be equivalenced while the internal system that is kept as is without changes. From buses sight, the boundary and external buses would be reduced to the following form,

$$Y_{EB}^{EQ} = \begin{bmatrix} Y_{EE} & Y_{EB} \\ Y_{BE} & Y_{BB}^{E} \end{bmatrix}, \tag{3.2}$$

The lines connecting the boundary buses with the internal system that would not be influenced by the equivalencing process while lines that connect boundary buses with the external system would be reformed [28], as shown in Fig. 3.2. Equation (3.1) can be written in different form if the voltage or current for both internal and external systems are considered [69];

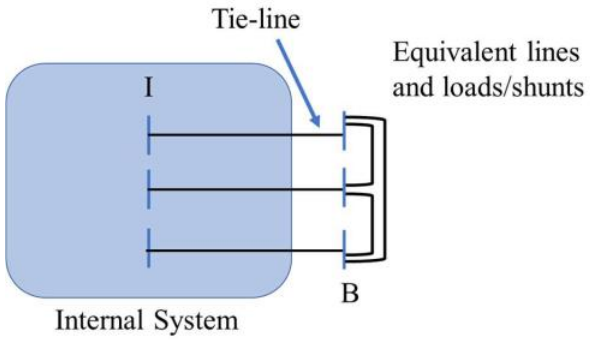

Fig. 3.2. The internal system with the Ward equivalent connections [30].

$$I = YV, \tag{3.3}$$

$$\begin{bmatrix} I_I \\ I_E \end{bmatrix} = \begin{bmatrix} Y_{II} & Y_{IE} \\ Y_{EI} & Y_{EE} \end{bmatrix} \times \begin{bmatrix} V_I \\ V_E \end{bmatrix}, \tag{3.4}$$

where I_I and I_E are the injection currents at internal and external buses respectively, V_I and V_E are voltage at internal and external buses respectively. Eliminating the external system reforms the equation (3.4) into

$$I_I = \left(Y_{II} - Y_{IE}{Y_{EE}}^{-1}Y_{EI}\right) \times V_I + Y_{IE}{Y_{EE}}^{-1}I_E \tag{3.5}$$

where $Y_{IE}{Y_{EE}}^{-1}Y_{EI}$ part leads to new equivalent branches, equivalent power lines, connected boundary buses while $Y_{IE}{Y_{EE}}^{-1}I_E$ part provides the equivalent currents at boundary buses [69].

In this research, internal and external systems are selected depending on locations of both wind generation and load areas in the Network6. This selection is required to classify buses into

internal, boundary, and external buses. Also, availability of buses and lines in PMU measurements data is another criterion to choose components for both reduction and validation purposes. In this work, the modification brought by SVM to the Ward reduction technique are explained in following steps:

3.2.1.1 Area Reduction

The first step is selecting geographical areas where wind generation are located in Network6. Also, areas of load buses are chosen to add to the internal system for achieving the balance between generation and demand. The Area2, which is a part of Network6 consisting of surplus generation, is selected to be as a generating area while areas in the east of Network6 are opted to be load areas for the new power model. Areas that have transmission systems linked the generating and load buses are considered to be in the internal system of the Ward reduction technique to complete power paths. Boundary buses are chosen in this work relying on having either generating components or considerable value of loads and both are needed for completing power balance in the new power model. After these processes, the first task with Ward technique is completed with the new internal system including only the targeted of generating, transmitting, and demand areas.

3.2.1.2 Transmission Reduction

The second task of using the Ward technique is selection of main transmission levels, which are 345 and 138kV in this work, for the new power model and eliminate the other transmission levels. The chosen transmission levels represent essential paths to transfer generating power from wind generation and other generating plants to load areas. Some expectations are taken place in the process of removing because some transmission levels, such as 500, 230, and 161kV infrastructures, should be kept in the internal system because they complete paths for

transferring power without overloading 345 and 138kV lines. By the end of this step, the internal system would have a transmission system with a reduced number of lines that are sufficient to transfer power in the original system and most lines in the new system are similar to lines in the original system. However, there are some new branches, not presented in the initial system, and those lines come from connecting boundary buses together building on the Ward equivalent method to complete power paths in the new power system ([28], [67], [70]).

3.2.1.3 Substation Reduction

The third step of the proposed work focuses on reducing number of buses in the small power model. The selection of desired buses is relying on some criteria like generating units, demand nodes, connecting buses, and off-line status in the original files provided by Network6. For more clarification, most of generating plants, are either wind generation or other types of power plants in Area2, and are chosen to be within the new system to produce the power required to have power flow like in the original model. Moreover, the connecting buses are kept in the internal system of the third application of Ward method because they are parts of power routes between generating and load buses and maintaining them gives the small model more realistic situations. The other criterion of selection is the status of the buses and lines in the original operational model provided by Network6 company. Some of buses in the studied areas of the original files are eliminated in the new model because they are off-line and there is no benefit to keep them unless those buses with their lines would be in future plans. The last criterion are demand buses, especially with high amount of load, are chosen in the new model to fulfill the cycle between the generation and demand. The new model by this step would have almost all its main components to run normally comparable with the operational files.

3.2.1.4 Internal Reduction

Generally, substations are comprised of different buses at various voltage levels and those buses may have generators, transformers, shunt capacitors or a reactor depending on the type of substation. The final step in this part, internal reduction, focuses on reducing the number of components in substations by the Ward technique. Internal reduction means eliminating or shifting some electrical components to different locations in substations in the new system. All previous parts and steps of the proposed method are described in Fig. 3.3. In this figure, i_A is the number of area, i_L is the number of line, i_S is the number of substation, i_C is the number of component.

Some criteria are utilized in this step to decrease the complexity of the new model. For instance, amount of load <5 MVA, small shunt capacitor or reactor are ignored due to the low impacts they have on the model performance. However, this process will be adjusted in the third part of this novel method to reduce the relative error. Also, generators or loads in low levels are moved to high voltage buses, especially if the maximum values of generators or demand points are too small, compared to the capacity of lines or transformers linked those components to substations. Therefore, moving those components reduces the size of substations and then the size of the new model. Some substation components with low voltage levels, especially transformers connect generators and loads to main buses, are kept in the new model to give planners and researchers the ability to analyze transformers behavior during studies. After this step, 456-bus simplified wind equivalent test system, WTS456, is completed.

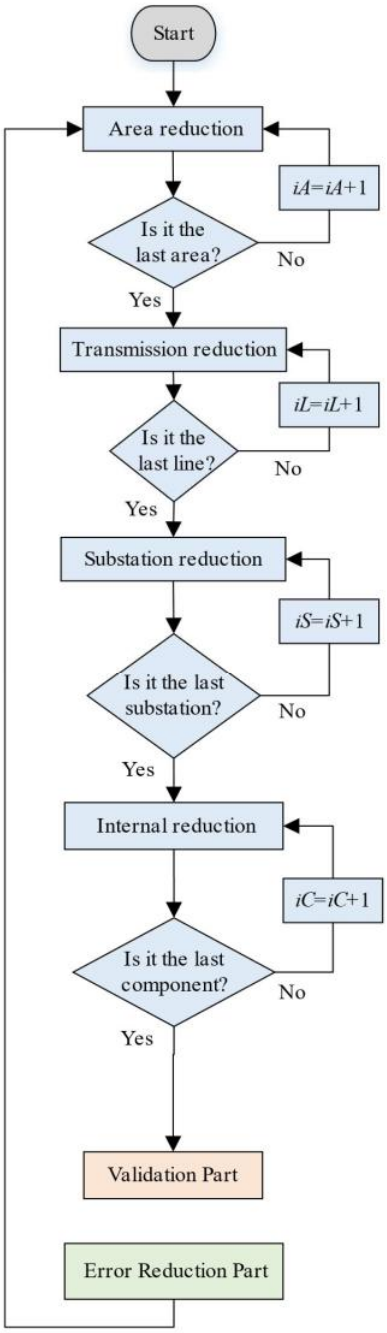

Fig. 3.3. Flow chart of reduction part of the proposed method.

3.2.2 WTS456 Model

The new model consists of 56 buses, 98 generators, 785 lines, and 15 areas is built as an example of applying first part of SVM. The WTS456 model has a transmission system with

different voltage levels and is made up of various substations with high levels of wind generation for mimicking Network6 with a low level of complexity. The reduction benchmark model produced by SVM, WTS456, is shown in Fig. 3.4 where the main transmission voltage systems, 500 and 345kV are presented. In this figure, bold horizontal lines are buses, thin lines are transmission lines linked to buses, circles with wind shapes represent wind generation either connected directly to ultra-high voltage levels or connected through step-up transformers, while circles with dog bone shapes are conventional generators. The green area in this figure is Area2 and red area is a transmission system with 500kV. Also, Fig. 3.5 shows Area2 includes wind generation with three main transmission levels in this area, which are 345, 230, 138KV, and those levels represent a main path for transferring power to the rest of WTS456.

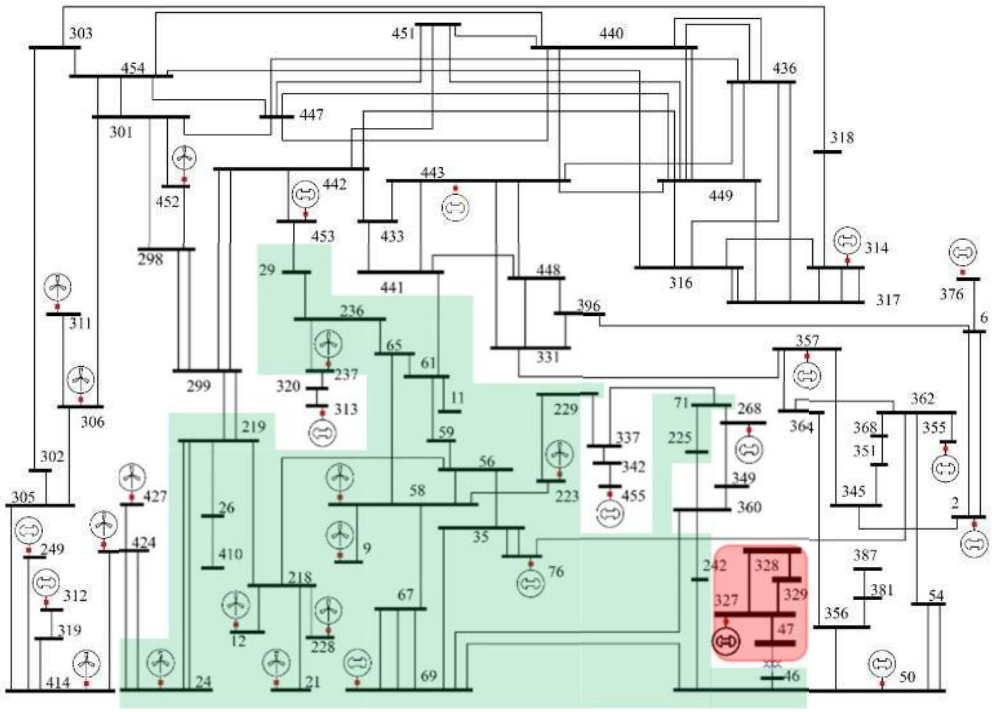

Fig. 3.4. One-line Diagram of 500kV and 345kV transmission system in WTS456 model.

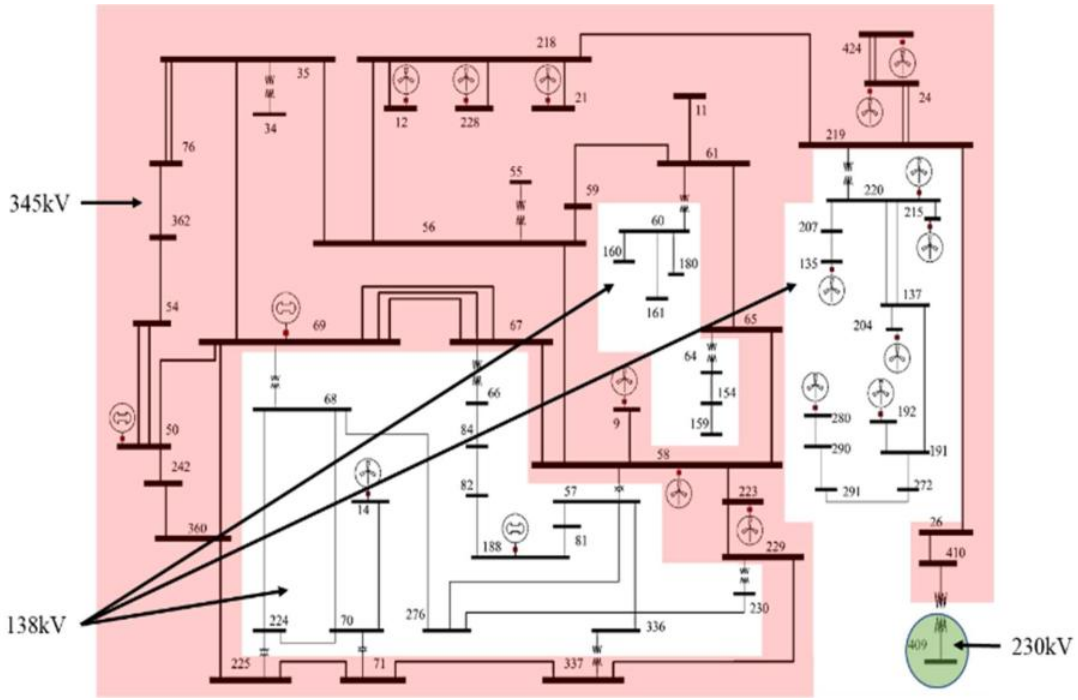

Fig. 3.5. One-line diagram of the wind farms area, Area2, in WTS456 model.

3.2.3 Validation Process

After building the new benchmark model, the validation process should take place. Power flow of WTS456 model must be examined to check its accuracy of its measurements compared with measurements of the initial system. WTS456 model is run in the PowerWorld simulator and an event is placed resulting in open a 345kV line similar to the real event in both the operational file and PMU data. The validation approach applied on the measurements of WTS456 model simulation consists of two main inspections; PMU measurements data comparison and Network6 operational files comparison.

3.2.3.1 Contingency Analysis

NERC advises utilities to validate small operational and planning systems using Synchrophasor data because the exact match for power flows between original and reduced models is not expected after reduction [71]. Therefore, different levels of errors are anticipated in producing reduction processes and it should be certain rules thay mention acceptable ranges of

errors. Model Validation Working Group (MVWG) of NERC recommends that power flow errors of new reduced systems should be within ±10% of measured values [72] and relying on this standard, validation part is necessary for obtaining the error rate.

The voltage angle error comparison is given in

$$\delta_{jk} = \delta_j - \delta_k, \tag{3.6}$$

$$\delta_{jk}{}^{error} = \delta_{jk}{}^{Model} - \delta_{jk}{}^{PMU} \tag{3.7}$$

where δ_j is voltage angle at bus *j,* δ_k is the voltage angle at bus *k,* δ_{jk} is the power angle between the buses *j* and *k*. $\delta_{jk}{}^{error}$ is the error between voltage phase angles of WTS456 and PMU measurements data, respectively. $\delta_{jk}{}^{Model}$ and $\delta_{jk}{}^{PMU}$ are the phase of the WTS456 and PMUs, respectively.

Other calculations are in this part to achieve the goal from PMU comparisons. Calculations such as, lower levels of error and those calculations that analyze error levels in measurements of both active power and reactive power. Obtained errors from the power comparison includes, the difference between WTS456 measurements and PMUs measurements, and the weight of line, w_i, which is a ratio of power passes through line *i* to the net of powers pass through the lines of WTS456. w_i is given in

$$w_i = \frac{P_i}{\sum_{i=1}^{n} P_i} \tag{3.8}$$

where w_i is the weight of line *i*, P_i is the power passes through line *i*, *n* is the number of lines in the new model, which is WTS456. The accuracy of comparisons is obtained like in [71] through calculating the relative error, ε

$$\varepsilon = \frac{\left[\frac{1}{n}\sum_{i=1}^{n}\left(X_{i\,pmu} - X_{i\,benchmak}\right)^2 w_h\right]^{\frac{1}{2}}}{\left[\frac{1}{n}\sum_{i=1}^{n} X_{i\,\mathrm{pmu}}{}^2\right]^{\frac{1}{2}}} \tag{3.9}$$

where $X_{i\,pmu}$ represents a power measured by PMUs for line i, $X_{i\,benchmak}$ is a power measured in the new model simulation for line i, ε is utilized to derive a measure of confidence "σ" as it is given in

$$\sigma = 100\%(1-\varepsilon) \tag{3.10}$$

This examination is deemed to be a quantitative exam because it focuses on the values of power flow variables and it is required to see different aspects of checks in next sections to give more credit to the proposed approach.

3.2.3.2 Direction Examination

The second inspection in the validation part is testing the direction of power flow in WTS456 compared with the initial operational files provided by Network6. The direction of power flow variables could be diagnosed form PMUs data. However, the novel method adopts this second path to check its new model (in addition to PMUs comparison) to reduce error percentage if there is shortage of information in PMUs measurement data. Different elements are selected in this comparison depending on the location of them from the studied area to emphasize accuracy of the reduced model. By this step, two main comparisons validate both quantitative and directional values of power flow to achieve error within ±10% of actual data in both PMUs and operational models. However, if all validation steps do not produce the targeted percentage error, all reduction steps in the first part of the novel method would be repeated.

3.2.4 Error Reduction Section

This section could be referred to an error reduction technique (ECT) and is the final part of the SVM. This section works on minimizing the percentage of error from ±10% to ±5% of measured values in the small models to avoid mismatching conditions if there is a disturbance or component placed. The ECT section functions through adjusting *PV* and *PQ* buses and this set

depends on PMUs measurements to simulate the same studied conditions. In *PV* buses, the magnitude of injection power by generators, left without any change in this method to make generators and its transformers experience the studied conditions. However, voltage magnitude in those buses is set with values extracted from PMUs data and this change helps increase accuracy of reactive power and variables related to dynamic stability. If error percentage ±5% is not gotten in this step, adjusting *PQ* buses is the next step.

This step stirs in four aspects, increasing *PQ* load, decreasing *PQ* load, increasing *P* load and decreasing *Q* load, and vice-versa. These variations are applied in areas where a high error of measurements is diagnosed. This step impacts the fourth reduction in the first section, Internal Reduction, through increasing elements inside substations, but this influence would reduce relative errors and make small models more realistic, especially in the main section of the system. In other words, the new model will have a main section that should have low errors due to it mimicking the original systems with low complexity and that can be explained as following

$$V_o \cong V_r, \tag{3.10}$$

And

$$P_o \cong P_r, \tag{3.11}$$

Then

$$V_o Y_o \cong V_r Y_r, \tag{3.12}$$

Where

$$Y_{red} = \begin{bmatrix} Y_{11} & . & Y_{1j} \\ . & Y_r & . \\ Y_{i1} & . & Y_{ij} \end{bmatrix}. \tag{3.13}$$

Y_{red} is admittance matrix of the reduced model, V_o, V_r are the voltage magnitude of original and studied part of reduced model, respectively, P_o, P_r are the active power of original and studied part

of reduced model, respectively, Y_o, Y_r are the admittance of original and studied part of reduced model, respectively. From (3.10) to (3.13), equality of values for powers and voltages of the targeted area could come from having same values of admittance for the original and the reduced model or

$$Y_o \cong Y_r, \tag{3.14}$$

If ECT does not produce the required relative error with completing all potential buses, the reduction method goes towards the first section, reduction part and all steps are shown in Fig. 3.6. In Fig. 3.6, *iE* is number of the event, *Pei* is the initial error percentage which is below ±10% , *Pe* is the final error percentage which is below ±5% , *iPV* is the number of *PV* bus, *iPQ* is the number of *PQ* bus, and ε is the relative error.

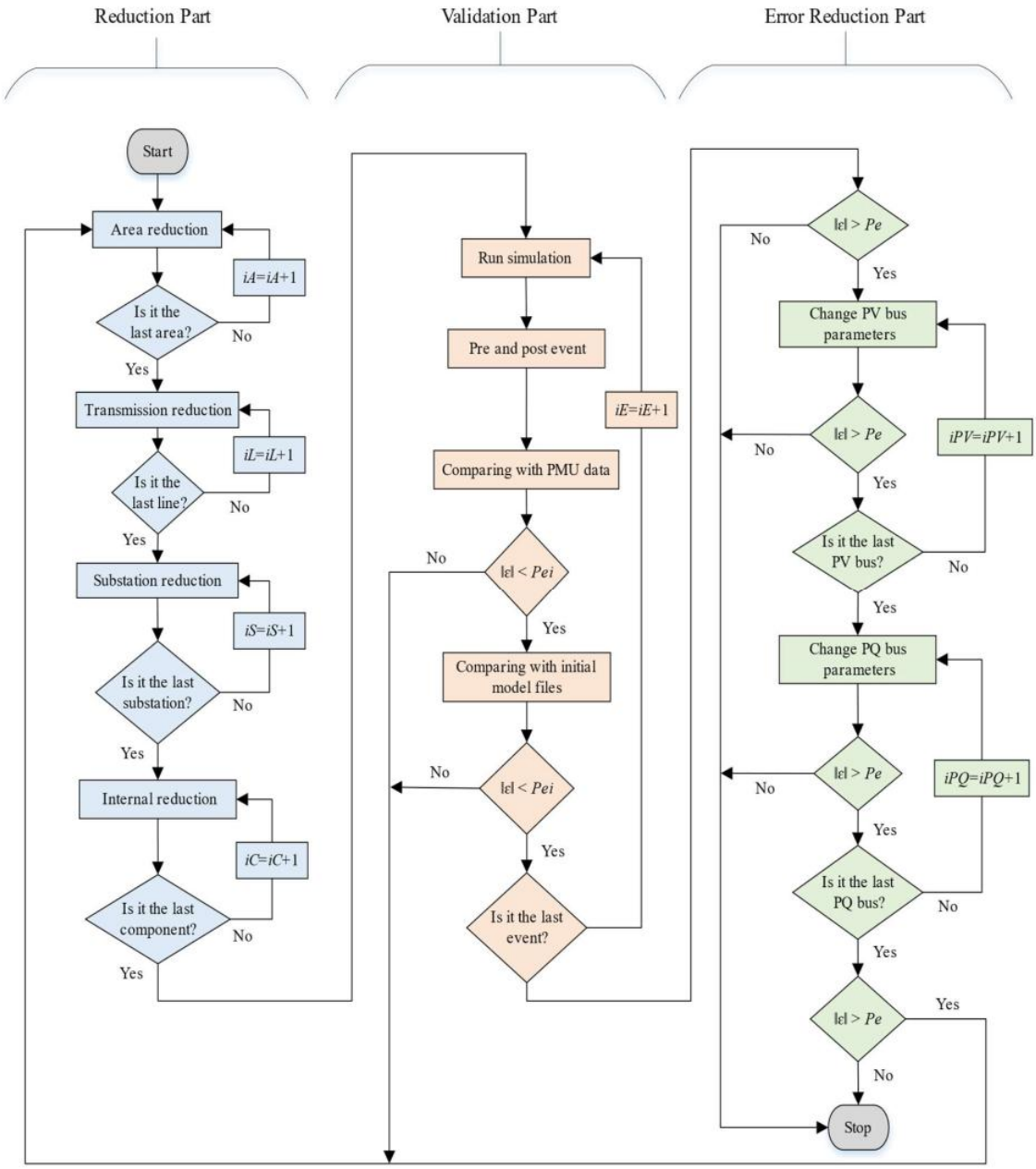

Fig. 3.6. Flow chart of the novel reduction method with its SVM steps.

3.2.5 WTS456 Model Results

For test purposes, a contingency event is applied on WTS456 to copy the actual event occurred in the Network6, Area2, and this event was recorded in PMUs data. This event is executed in the WTS456 model via outage line 58-67. This event is selected because the

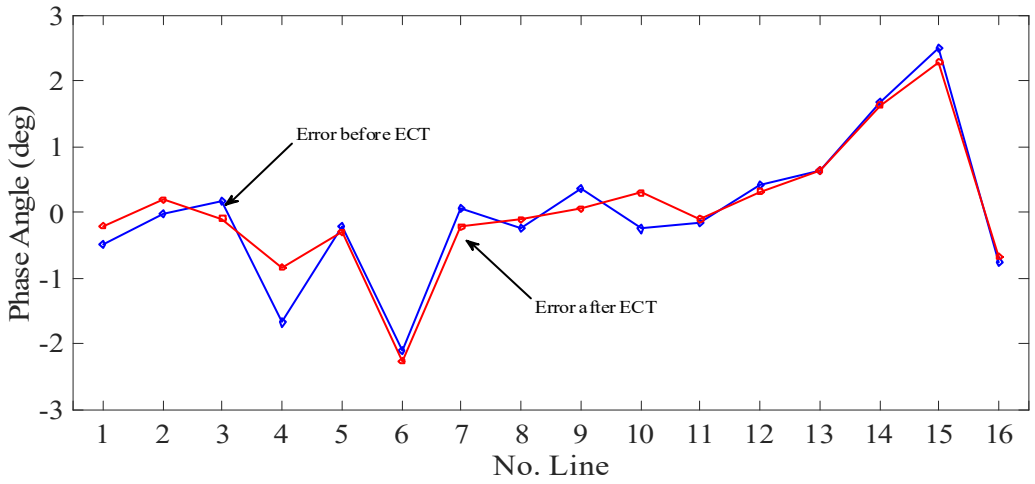

Fig. 3.7. Comparison of phase angle errors for pre-event condition.

disturbance occurred near several wind generation and its influences on them and transmission lines in the Area2. All comparisons in the second and third parts of the reduction method are accomplished through analyzing measurements of 16 lines of 345kV transmission level linked 16 buses of WTS456 and the comparisons analyze the model under pre and post-event conditions via three variables, phase angle, active power, and reactive power.

Investigation of the three variables, illustrated in Fig. 3.7 to Fig. 3.12, includes two results, the initial error percentage and the final error percentage, which are results of the validation part and the error reduction part, respectively. In Fig. 3.7, the initial error of phase angles, at line 4, is -1.68° and this error decreased to -0.8° after the reduction error part due to adjusting voltage magnitude and the *PQ* load amount near this line. Those differences between WTS456 system and PMUs measurements come from variations in the power flow amount after the SVM process that changes power production of some generators due to the change of demand in the model. However, other lines may not experience high differences between results after the reduction error part, some even have high error, because any change around those lines could impact power flow in the whole system and produce inaccurate measurements. In comparison with errors of line 4th in Fig. 3.8, errors have increased after having the disturbance because the load flow suffered big

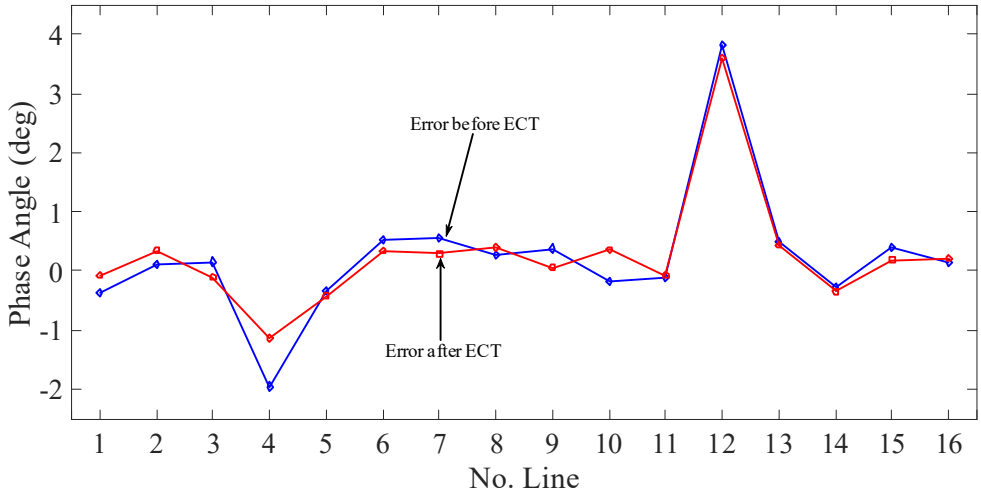

Fig. 3.8. Comparison of phase angle errors for post-event condition.

changes and is shown in line 12. Line 12 has big differences between Fig. 3.7 and Fig. 3.8 and those differences are because this line is the tripped line in this simulation and the load flow around it will make big differences impacting phase angle levels.

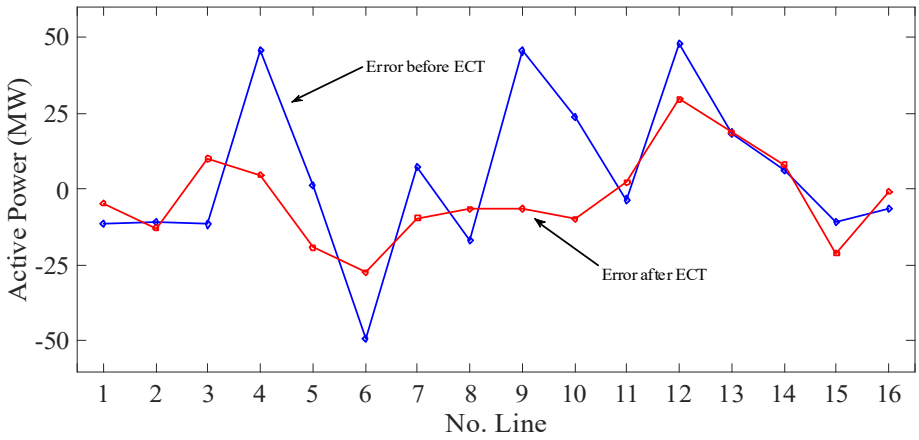

Fig. 3.9. Comparison of active power errors for pre-event condition.

From active power aspects, errors between WTS456 and PMUs measurements shown in Fig. 3.9 and Fig. 3.10 have different ranges that are from -50 to 50 MW and -40 to 65 MW, respectively. These errors come either from eliminating some generators, load nodes, and lines or adjusting the load values in WTS456 model and those acts influence values of active power in the

studied area significantly. However, the error levels are decreased to minimum values after the ECT part. For instance, line 4 in Fig. 3.9 has the error measurement equal to 45.71 MW and this value is decreased to 4.61 MW after setting *PV* load in the ECT part. Another explanation that cause could cause those errors is the change in production of the generating unit and this can be seen in line 6.

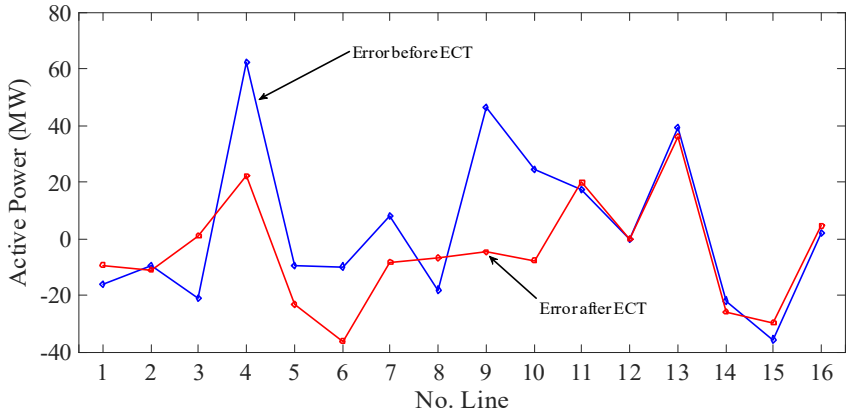

Fig. 3.10. Comparison of active power errors for post-event condition.

This line has a significant power error, which is -49.16 MW as the initial error. The cause of this error comes from the wind generation at Bus12, near 6th, and this wind generation increases its production from 152.02 MW in the operational files to 169.8 MW in WTS456 model to fulfill changes in power flow after SVM processes. Previous acts exhibit the same effects on other lines in both Fig. 3.9 and Fig. 3.10, which are for pre and post-event conditions, respectively.

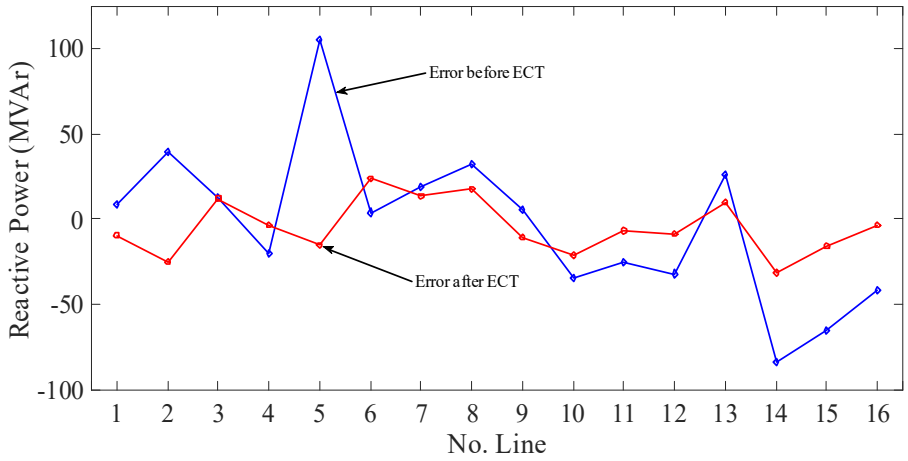

Fig. 3.11. Comparison of reactive power errors for pre-event condition.

The third variable is analyzed in this research is reactive power that is illustrated in Fig. 3.11 and Fig. 3.12. In these figures, both situations show noticeable errors of reactive power within ±100MVAr. Those large errors are results of changes in configuration of WTS456 system with the original model removing the external network and relinking the boundary buses together. This change is a result of inadequate reactive power produced by removed shunt capacitance of transmission lines [67, 70]. The high range of errors is minimized in ECT to values within ±25MVAr in pre-event and ±40MVAr in post-event conditions. After validation of ECT parts, measures of confidence for all pervious variables under pre and post event conditions can be seen in Table 2 and Table 3.

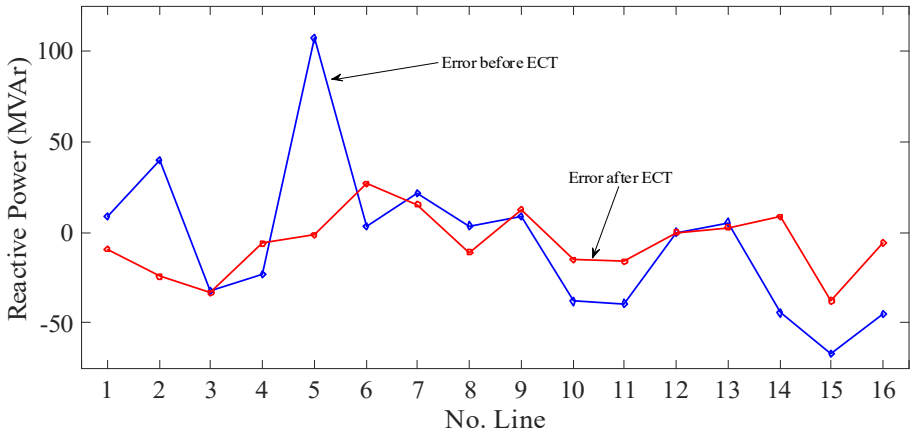

Fig. 3.12. Comparison of reactive power errors for post-event condition.

Table 2. Accuracy of WTS456 model for pre-event conditions

Variable	Before ECT (%)	After ECT (%)
Phase Angle (°)	99.80	99.74
Active Power (MW)	99.12	99.53
Reactive Power (MVAr)	92.50	97.70

Table 3. Accuracy of WTS456 model for post-event conditions

Variable	Before ECT (%)	After ECT (%)
Phase Angle (°)	97.78	99.37
Active Power (MW)	98.85	98.89
Reactive Power (MVAr)	92.72	97.55

The second inspection in this work is examining the power flow direction in WTS456 compared with the initial model files provided by Network6 corporation. This check is conducted through matching the direction of power flow in the initial operational file with direction of power flow in the WTS456 model. The test includes two buses and one of them is in the middle of targeted area, located near wind generation, and another one is far from the wind generation. The first bus is Bus58 located in the middle of the wind generation area and has some wind generation connected to it. The direction of active power flow for all lines and generators linked to this bus are the same for both the operational model and WTS456. Also, the comparison is applied on Bus361 and the power flow of active and reactive power for the initial files and WTS456 model have the same directions. For clarification, power flow in two lines connected to the mentioned buses are matched and tabulated in Table 4 with taking in account comparing with PMUs data. Both active and reactive power for both lines in WTS456 model have the same directions compared to files of the operational files and PMUs data.

Table 4. Comparison of power flow direction

Line	WTS456		Original Model		PMU	
	MW	MVAr	MW	MVAr	MW	MVAr
58 – 223	42.7	-48.9	46.8	-49.3	48.2	-75.83
69 – 361	37.5	-91.8	0.7	-85.7	3.0	-88.92

The previous comparisons are taken under steady state conditions. In other words, they show the performance of WTS456 before and after a fault condition in a certain time and they do not show response of the model under dynamic conditions. Therefore, an additional test is applied on WTS456 model to simulate dynamic performance during the fault occurrence. This final simulation is dependent on the PMUs measurements and compares them with the dynamic simulation of WTS456 in PowerWorld environment. Three lines in WTS456, which are 58-65, 219-218, and 58-56, are selected to analyze their phase angles and active power flow when the fault is applied and compares them with the same lines in PMUs data.

Selection of those lines is because their locations are near both wind generation and an open line. Performances of phase angles and active power calibrated with PMUs data are exhibited in Fig. 3.13 and Fig. 3.14. In those figures, WTS456 model conducts in similarly to the original system through mimicking the changes in load flow variables when the fault occurs at 0.5 seconds. In Fig. 3.14, phase angles of the three lines show the same actions with small errors for both measurements of WTS456 model and PMUs data. For Fig. 3.14, active power for three lines experience same changes after tripping line58-67 either for WTS456 model or for PMUs data.

From previous quantity and direction checks, the new benchmark model shows some common aspects with the initial system by either comparing with PMUs measurements data or comparing with Network6 files. The differences that appeared in the measurements of WTS456 model are related to changing size of the original system through eliminating undesired areas, buses, generators, and others. However, the accuracy of the WTS456 model is within NERC

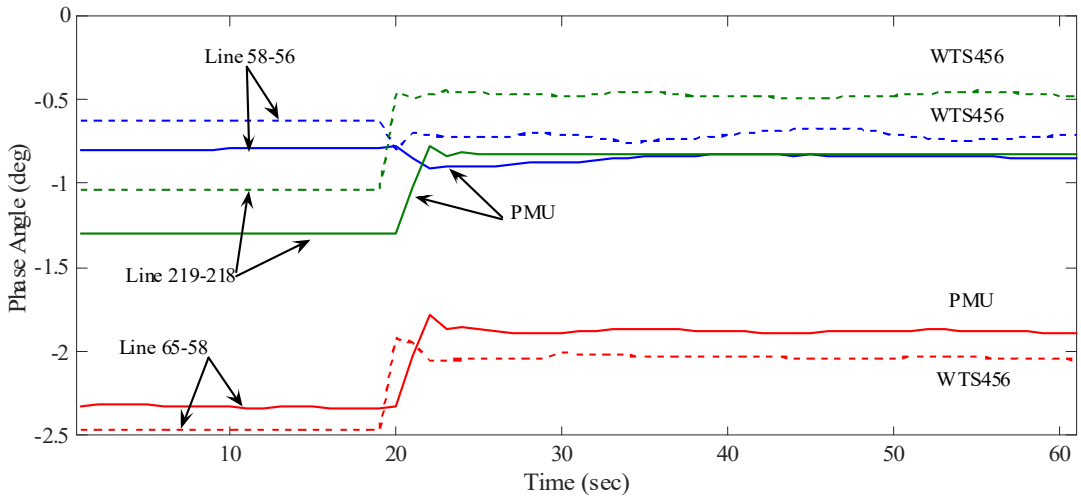

Fig. 3.13. Phase angle comparison of three lines after open line 58-67.

requirements for validation of new models. Therefore, the suggested SVM steps in this work provides a valid reduced system to analyze power systems for various conditions, and WTS456 could be used for planning purposes, especially with a high penetration of wind generation.

The proposed strategy in this research is to produce reduction models to help researchers and planners to use small power system imitating large networks with high accuracy, especially with wind generation. Reduction, validation, and reduction error parts of SVM are explained. PMUs measurements data is employed in both validation and reduction error parts. Those processes are

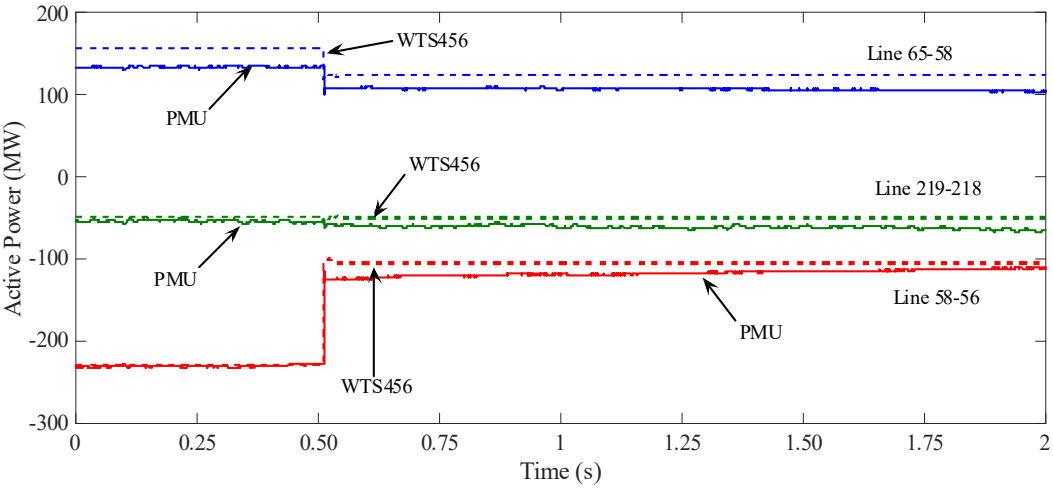

Fig. 3.14. Power comparison of three lines after open line 58-67.

applied on Newtork6 and resulted in producing WTS456 model. WTS456 model shows small errors that meets requirements of NERC standards for validations. WTS456 model with its extensive details like circuit breakers, could be used for analyzing aims under various operational circumstances, especially with wind power sent remotely to load areas.

4 Wide Area Control Method

4.1 Need for Control Approach in Power System

Modern power grids with large amount of wind turbine generators could produce complicated risks of inter-area oscillations relying on location and volume of wind generation. Wide-area control (WAC) designs, with participation of advanced WAM technologies like PMUs, can effectively diminish wide oscillations of power systems. Optimal modification of transient stability, using WAC and the incorporation of wind generation, can enhance capability of power transfer of transmission grids and block power systems from generators or load disconnection, or large failure following a sequence of disturbances [33]-[35]. This work offers a WAC approach based on a modified H_2 control method, one of robust control techniques, to dampen frequency oscillation and power swing through adjusting variables in both HVDC links and FACTS devices particularly static synchronous series compensators (SSSC).

One of the techniques employed in various systems as a robust control is the H_2 control method. [73] addresses using a composite of linear and nonlinear parts to produce a controller that is designed to meet the required H_2 performance and offset the quantization error. [74] presents a H_2 method to design a robust controller for optimizing the vertical ride quality of the wheel-rail forces and improving the ride comfort of the railway vehicle. The investigation in [75] deals with designing a H_2 controller for linear uncertain models with input quantization in the existence of common encoder/decoder mismatch. A H_2 controller optimal design is suggested in [76] which meets and satisfies requirements of a robust control benchmark model. The aim of H_2 control method in [77] is to develop a feedback controller for placing the desired eigenvalues in some desired stable regions and weaken the disturbance between the output vector and the

disturbance vector. Also, [78] offers a study on a robust H_2 LMI-based controller to treat damping issues and improve the inter-area mode oscillations of power systems. [79] develops continuous time H_2 and H_∞ controllers for FACTS devices through two types of vibration modes subjected to large load variations that makes the control of devices difficult. [80] states utilizing a LMI-based mixed H_2/H_∞ state-feedback control technique for controlling Distributed Generation (DG) units in an islanded operation of a microgrid system under load uncertainties. Mixed H_2/H_∞controllers in [81] prove to be functional in minimizing road disturbances and tackling different inputs. [82] explains designing of H_2 controller for robust stability of individual generators in multi-machine systems via feedback controlled static VAR compensators. From previous research, it is clear that H_2 control method can be used in various systems to attenuate disturbances and set poles or eigenvalues in stable regions.

4.2 The Modified H_2 Control Method

It is known that the transfer matrix in terms of state-space systems, for linear-time invariant systems (LTI), could be given in the following forms

$$\dot{x}(t) = Ax(t) + Bu(t), \tag{4.1}$$

$$y(t) = Cx(t) + Du(t), \tag{4.2}$$

Or in different form, which is

$$G(s) = \begin{bmatrix} A & B \\ C & D \end{bmatrix}. \tag{4.3}$$

With denoting $G(s) = D + C(sI - A)^{-1}B$.

These systems could be investigated to increase stability through designing controller. Several researches utilized the H_2 controller to get optimal LTI system feedback that functions

properly to reduce influences of disturbance and meet standard requirements [82]-[85]. This research considers the following LTI formula, shown in Fig. 4.1, as in

$$P = \begin{bmatrix} A & B_2 & B_1 \\ C_2 & D_{11} & D_{12} \\ C_1 & D_{21} & D_{22} \end{bmatrix} = \begin{bmatrix} P_{11} & P_{12} \\ P_{21} & P_{22} \end{bmatrix}, \tag{4.4}$$

Where $P_{ij}(s) = C_i(sI - A)^{-1}B_j + D_{ij}$, for $|I - P_{22}K| \neq 0$.

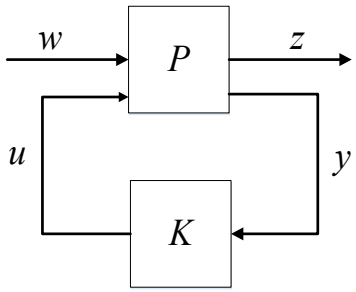

Fig. 4.1. Generalized block diagram of H_2 control method [86].

A generalized plant, *P*, that consists of the studied system with its controlled and variable inputs, is designated with a specific arrangement given in [86]-[87] and this formula could be given as

$$\dot{X}(t) = Ax(t) + B_2\, w(t) + B_1\, u(t), \tag{4.5}$$

$$z(t) = C_2x(t) + D_{11}\, w(t) + D_{12}\, u(t), \tag{4.6}$$

$$y(t) = C_1x(t) + D_{21}\, w(t) + D_{22}\, u(t). \tag{4.7}$$

where $x \in \mathbb{R}^n$ is the state, B_1 is controlled input, B_2 is disturbance input, $C_1$is sensor or measurement output, C_2 is the performance or cost output, and $D_{11}, D_{12}, D_{21}, D_{22}$ represent constant variables change with the system design. The H_2 control method has been chosen in this work because is a proper approach to find a real rational K that stabilizes *G*(*s*) internally and minimizes the H_2 norm of the *P* matrix from *w* to *z* and the action of H_2 control method would be

fast compared with the H_∞ controller. Also, the H_2 controller works on minimizing the maximum error while the H_∞ controller functions on reducing the function [86]-[87].

The inputs and outputs for the controller design are vector signals and the input generated by the feedback controller, *K*, is *u,* while the output or sensor measurement of *K* is y, *z* and *w* represent the desired variable to control and exogenous inputs to *P*, respectively. Therefore, this work takes benefits of the H_2 controller approach, dealing with exogenous inputs, to accomplish the goals of this research with reducing the impacts of disturbances that have sudden and unexpectable variations with time.

All equations (4.5)-(4.7) would be correct with assumptions that D_{11} is equal to 0, $[A \quad B_2]$ is stabilizable, $[A \quad C_2]$ is detectable, $V = \begin{bmatrix} B_1 \\ D_{21} \end{bmatrix} [B_1^T \quad D_{21}^T] \geq 0$, $R = \begin{bmatrix} C_1^T \\ D_{21}^T \end{bmatrix} [C_1 \quad D_{21}] \geq 0$ [23].

The proposed controller design method in this research, illustrated in Fig. 4.2, requires that variables of any test system with respect to equations (4.4) to (4.7) and that they should be defined with proper forms in order to achieve optimal results. Then the method takes in account changing values of K_x and T_x that represent the controller gain and time of enhancing devices would be connected to the system adjusted and set by H_2 controllers. Variation in values K_x and T_x will influence directly *A* matrix and lead to change in calculations of gain of H_2 controllers. For instance, let's assume there is a system with $A \in \mathbb{R}^2$ and K_x and T_x are elements in the *A* matrix and that impact gain of H_2 controllers, which is given in

$$K = \begin{bmatrix} \frac{A+B_2F_2+L_2C_2+L_2D_{22}F_2}{F_2} & -L_2 \\ F_2 & 0 \end{bmatrix}, \tag{4.8}$$

$$F_2 = -R_{uu}^{-1}(R_{xu}^T + B_2^T X_2), \tag{4.9}$$

$$L_2 = -(Y_2 C_2^T + V_{xy}) V_{yy}^{-1}, \tag{4.10}$$

Where

$$R = \begin{bmatrix} R_{xx} & R_{xu} \\ R_{ux} & R_{uu} \end{bmatrix} = \begin{bmatrix} C_{11}^2 & C_{11}D_{12} \\ D_{12}C_{11} & D_{12}^2 \end{bmatrix}, \tag{4.11}$$

And X_2 and Y_2 are the unique, positive semidefinite solutions to the following Riccati equations [84];

$$0 = X_2A_r + A_r^TX_2 + R_{xx} - R_{xu}R_{uu}^{-1}R_{xu}^T - X_2B_2R_{uu}^{-1}B_2^TY_2, \tag{4.12}$$

$$0 = A_eY_2 + Y_2A_e^T + V_{xx} - V_{xy}V_{yy}^{-1}V_{xy}^T - Y_2C_2^TV_{yy}^{-1}C_2Y_2, \tag{4.13}$$

Where

$$A_r = (A - B_2R_{uu}^{-1}R_{xu}^T), \tag{4.14}$$

and

$$A_e = \left(A - V_{xy}V_{yy}^{-1}C_2\right). \tag{4.15}$$

From all mentioned variables it is clear that A matrix would influence directly three of four elements in (4.8) and produce different weights. Therefore, generating different controller weight, will produce different performances of system due to adjustment of the controller weight with the difference value could result in having proper outcomes and the criteria for γ.

The values of K_x and T_x would be within a range to avoid divergence results. After having these variables, the P plant would be built and then the H_2 controller is calculated with forming inputs and outputs and a comparison between sensor outputs of systems with conventional controllers and sensor outputs of systems with H_2 controllers is made. After getting all results for all conditions, the two criteria are used to select the optimal K_x from lower cases have low

measurement output deviations of system. The first criterion is based on the H_2 optimal cost (γ), which is given in

$$\gamma = \|f(P,K)\|^2. \tag{4.16}$$

If differences between low optimal cost (γ) for three different cases are lower than 0.1, then chosen the minimum of maximum output deviation, min (max (*ST*)), would be the second criterion to select the optimal K_x.

In other words, the K_x value would have three different current or frequency deviations as examples and the maximum values of these deviations are used to make a comparison of the second criterion. The case has lower current or frequency deviation in any area can be selected to choose K_x. If differences between low optimal cost (γ) for three different cases are higher than 0.1, then selection of K_x is dependent on a case that has lower γ and all these steps are explained in Fig. 4.2.

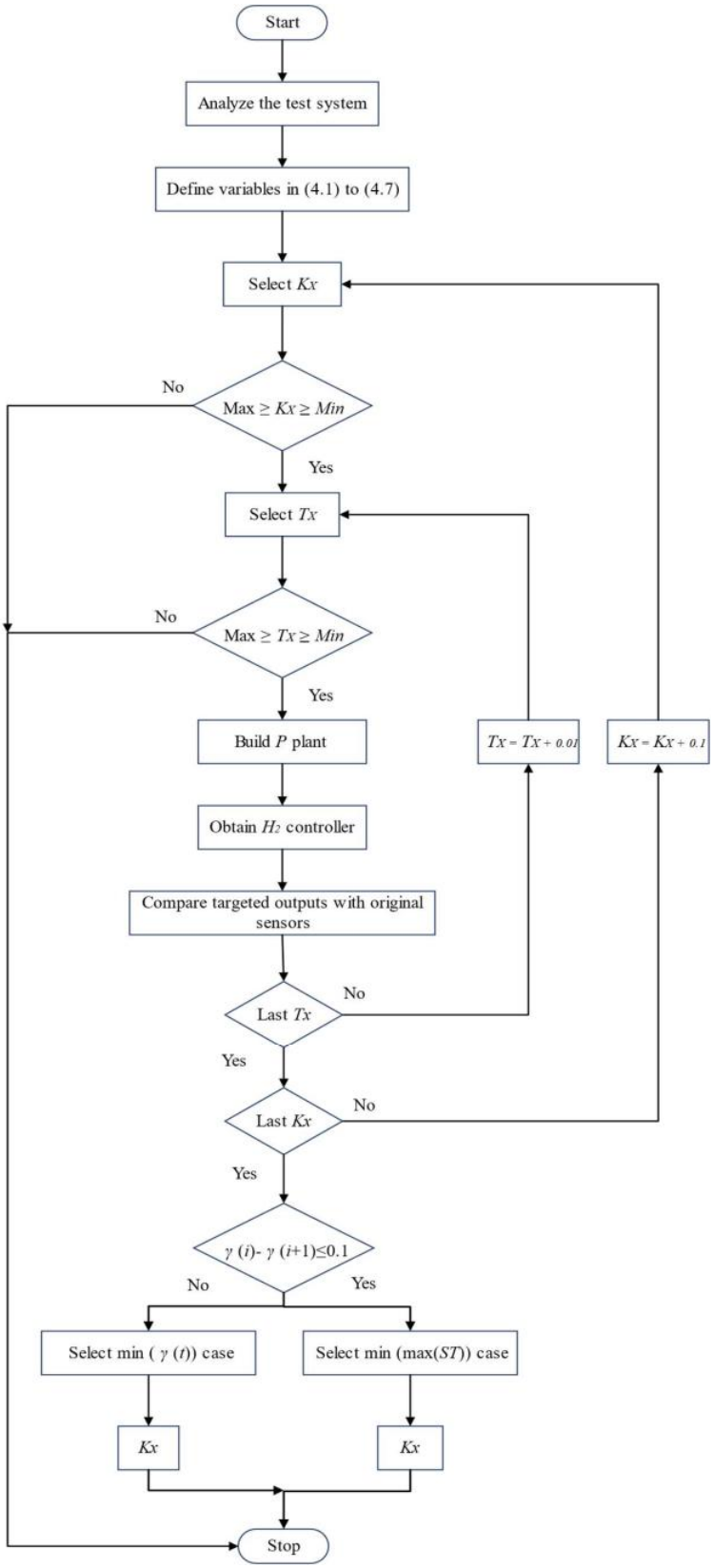

Fig. 4.2. Flow chart of the proposed control method.

Designing the system with an H_2 controller could be done in several configurations and that is dependent on the type of inputs and outputs [88, 89]. In this research, two types of disturbance inputs are suggested to be within the suggested configuration of H_2 control feedback design, shown in Fig. 4.3, while the error of sensor outputs would be as inputs of the controller.

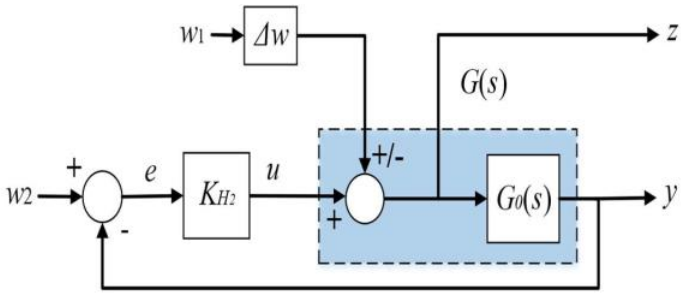

Fig. 4.3. The unstructured uncertainty model for the suggested control method.

In this figure, the unstructured uncertainty model for the H_2 controller is built on additive model of uncertainty [90] where the first disturbance input, w_1, is assumed to have variables with transfer functions to simulate complex components and this is added to the system plant producing a new plant as following

$$G(s) = G_0(s) + w_1\Delta w. \tag{4.17}$$

Where G_0 is the original system plant, G is the new system plant with the disturbance input, and Δw is the disturbance deviation and it is considered in this work as a band-limited white noise. The second disturbance input, w_2, is employed to be as a reference for the sensor outputs to reduce errors passes through the controller. The sign of w_1 could be positive or negative and that relies on the nature of the disturbance's influence on the whole test system. The input of the system, u, is the output of the H_2 controller in addition to w_1 and performance output, z, is taken from this part and the error in outputs, e, is selected to be the input of H_2, shown in Fig. 4.3.

4.3 The H_2 Controller in AGC Models

Various papers related to AGC models function with H_2 controller for predictive approaches, damping oscillations, and multi-area power flow through SSSC devices or HVDC links purposes [82],[88]-[97]. Defining variables, related to control and disturbance inputs and emphasizing performance and sensor outputs in power systems in LFC models, is an essential part in those researches to come up with optimal consequences that meet required standards.

SSSC devices or HVDC links are enhancing equipment that would be placed in the test system. The values of K_x and T_x, represent the controller gain and time of SSSC or HVDC connections, would be within a range to avoid divergence results. After having these variables, the P plant would be built and then the H_2 controller is calculated and a comparison between sensor outputs of systems with ACE controllers and sensor outputs of systems with H_2 controllers is made. After getting all results for all conditions, there are two criteria that are used to select the optimal K_x from lower cases that have low frequency deviations or power deviation of areas in a test system, which are the H_2 optimal cost (γ) or the minimum of maximum frequency deviation, min (max (ST)). The case that has lower frequency deviation in any area can be selected to choose K_x and this criterion is important for this work in order to check violating the NERC frequency standard, Bal-003-1.

The outputs of LFC models, $[\Delta f \ \ \Delta P_{tie-line}]$, are selected in all works to display successes of control methods and this research is considered sensor outputs to make the controller develop its weight in order to reduce errors. Also, disturbance inputs in LFC models could be either renewable generation, wind or solar generation, or load variation or faults and these inputs may be simulated through transfer functions to demonstrate more realistic performance.

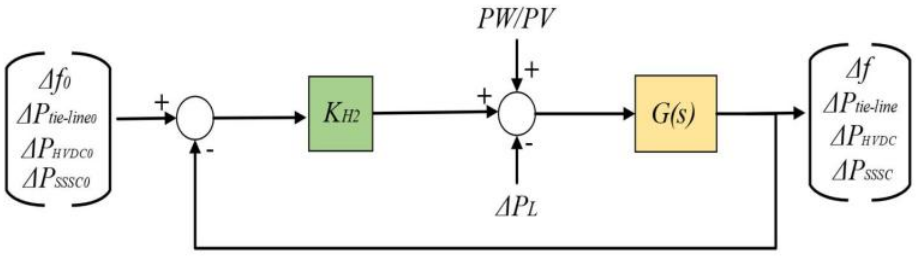

Fig. 4.4. The proposed approach to implement the H_2 controller in the LFC test system.

4.4 The H_2 Controller with Inverter-based Devices

This work employs these components of LFC models, as state-space variables, after adding the SSSC device or HVDC link, as the other output, and replacing the ACE controller with the H_2 controller [96] for multiple area systems. The proposed approach, shown in Fig. 4.4, deals with several areas and each area has its own outputs, which are $[\Delta f \;\; \Delta P_{tie-line}]$, in addition to power deviation via either the SSSC device, ΔP_{SSSC}, or HVDC links, ΔP_{HVDC}. In addition to the outputs, disturbances inputs, which are *PW* is wind power, *PV* is solar power, and ΔP_L is the load variation, influence frequency response and power swing in the model widely and this increase the complexity of power systems. As part of the suggested methods in Fig. 4.3, the sensor outputs, $\Delta f, \Delta P_{tie-line}$, ΔP_{SSSC} and ΔP_{HVDC} are normalized with reference values, $\Delta f_0, \Delta P_{tie-line0}$, ΔP_{SSSC} and ΔP_{HVDC} (set to be zero) in order to reduce errors, shown in Fig. 4.4. These reference values are also considered disturbance inputs to the test system for processing in the system and getting low errors as inputs for the suggested controller. The normalized outputs are turned back to the model, with various disturbances, through the H_2 controller with an integrator and these steps should be counted in equations (4.1) to (4.4). After arrangement in (4.5) to (4.7), the control law for the suggested approach can be written with the configuration in Fig. 4.4 as

$$\begin{bmatrix} y_1(t) \\ y_3(t) \\ y_2(t) \\ y_4(t) \\ y_5(t) \\ y_6(t) \end{bmatrix} = \begin{bmatrix} -\Delta f \\ -\Delta P_{tie-line1} \\ -\Delta f_2 \\ -\Delta P_{tie-line2} \\ -\Delta P_{SSSC} \\ -\Delta P_{HVDC} \end{bmatrix}^T x(t) + \begin{bmatrix} \Delta f_0 \\ \Delta P_{tie-line0} \\ \Delta f_0 \\ \Delta P_{tie-line0} \\ \Delta P_{SSSC} \\ \Delta P_{HVDC} \end{bmatrix} w(t) + \begin{bmatrix} 0 \\ 0 \\ 0 \\ 0 \\ 0 \\ 0 \end{bmatrix} u(t). \quad (4.18)$$

This approach makes the controller deal with its input variables, displayed in (4.18), which is dealing with each area, and outputs of the area, and this assists the controller to set the weight of areas. This will help in having results with low error and cost and meeting requirements of agencies standards.

4.4.1 Static Synchronous Series Compensator (SSSC)

One of the substantial members in flexible ac transmission system devices is SSSC that would be installed in series with lines of transmission systems connecting two areas, as shown in Fig. 4.5, to control the real power flow, voltage profile, and frequency damping in acceptable ranges [95]-[97]. One of the SSSC characteristics is the ability of absorbing active power from one area and injecting it to another area under change load in the power system [96], [98, 99]. The dynamic model of SSSC used in AGC system requires knowing the way to calculate its variables to represent them properly in LFC models. In the existence of SSSC between areas *i* and *j*, deviation of active power flow between the two areas can be given as follow

$$\Delta P_{i-j} = \Delta P_{tie\ i-j} + \Delta P_{SSSC} \quad (4.19)$$

Where ΔP_{i-j} is the deviation of power flow in tie-line *i-j* with SSSC, $\Delta P_{tie\ i-j}$ is deviation of power flow in tie-line *i-j* without SSSC, ΔP_{SSSC} is power flow between areas *i* and *j* due to SSSC and this power flow will have different signs (+/-) due to its performance dynamically [96],[98, 99].

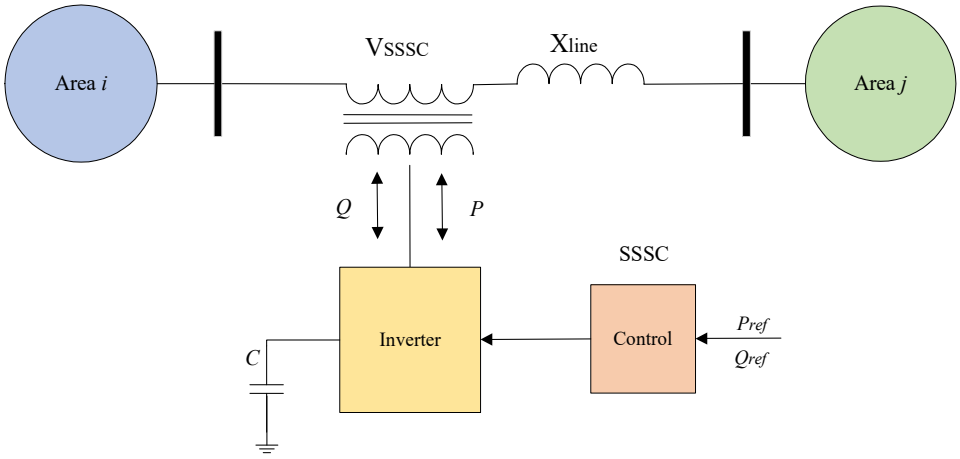

Fig. 4.5. Configuration of a two-area power system equipped with a SSSC device [96].

To represent the SSSC device in LFC models with taking in account with respecting to state-space formulas, linearized model of SSSC device with its power flow control consists of four blocks, as shown in Fig. 4.6, that represent a lead/lag compensator, a High Pass Filter (HPF) and a controller gain [96]. Where, K_{SSSC} is a controller gain, T_W is a washout time constant, T_1, T_2, T_3 and T_4 are time constants of lead/lag controller. Time constant of HPF, i.e. T_W is between 0.5 and 20 s. In this study, it is fixed to 10 seconds while T_2 and T_4 are set to be 0.01 seconds [96, 100].

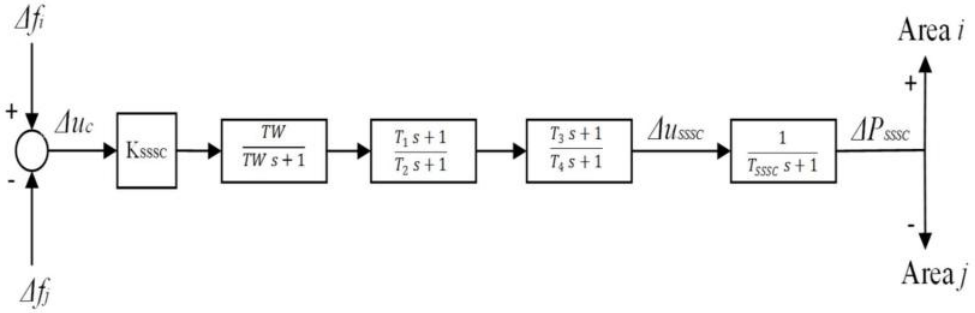

Fig. 4.6. Linearized model of the SSSC device [100].

Dynamic characteristic of SSSC is modeled by first order transfer function or first order differential equation as [96]:

$$\Delta u_{SSSC} + T_{SSSC}\Delta\dot{u}_{SSSC} = \Delta P_{SSSC} \tag{4.20}$$

where u_{SSSC} is control signal of SSSC, and T_{SSSC} is time constant of SSSC. The input signal of the compensator for the SSSC is defined as:

$$U_C = \Delta f_i - \Delta f_j \tag{4.21}$$

where, Δf_i and Δf_j are frequency deviations of areas *i* and *j*, respectively. From Fig. 4.6, the SSSC controller uses frequency deviation of Area *i* and *j* and frequency deviation of Area *i* is a local signal while the frequency deviation of Area *j* would be transmitted via communication channels to the controller. The SSSC control unit will vary power flow in the tie-lie between two areas and assist in stabilizing the frequency oscillations. For the proposed H_2 control method, four variables, which are K_{SSSC}, T_{SSSC}, T_1 and T_3, would be examined to find optimal values of K_X and T_X.

4.4.2 High Voltage Direct Current (HVDC) Link

Development of the HVDC transmission system, due to economy, environment and performance's advantages over the other alternative techniques, improves dynamic performance

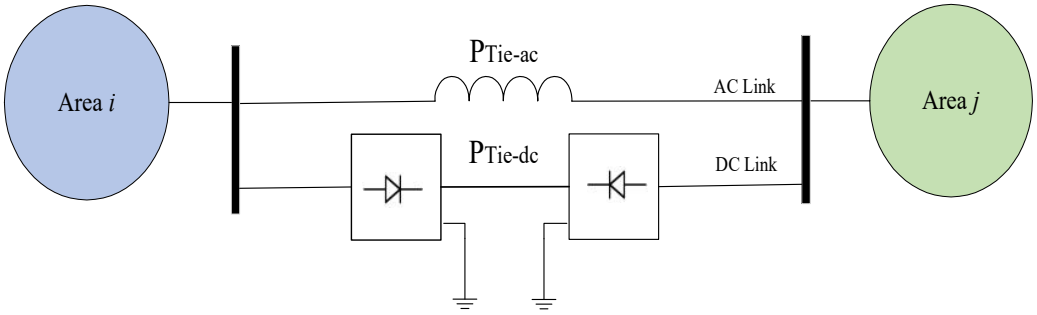

Fig. 4.7. Configuration of a two-area power system equipped with a HVDC link [99].

of power systems, especially with greater stabilization margins or edges under small changes in power systems. Therefore, this work considers LFC models of interconnected power systems with a dc tie-line in parallel with an ac tie-line, shown in Fig. 4.7 [99, 101]. The HVDC system provides better flexibility in the power system operation and control by utilizing the power electronics

equipment. In each HVDC link, the sending end converter acts as a rectifier and the receiving end converter functions as an inverter, as shown in Fig. 4.7. With fast control action of the converters, the parallel combination of AC tie-line and HVDC link (AC/DC link) improves in reducing power oscillation and frequency deviation in systems have variable generation and disturbances is a main purpose in this research in addition to enhanced power flow in tie-lines for international connections [102].

Tie-lines in interconnected areas are utilized for increasing a power exchange between the control areas while providing inter area support during abnormal conditions[103]. However, due to issues in ac transmission systems such as power flow oscillations, increasing fault current level, frequency droop, and disturbance effects of transmission faults from one area to other could result in deterioration of overall system performance. These issues are solved by adoption of HVDC links that participate in reducing power instability associated with ac lines of the interconnected power systems, especially with renewable generation [99],[104]-[106]. The fast act of power electronics within HVDC converter stations could vary power flow rapidly through the HVDC line and help in power oscillation damping (POD). The potential for power injection control at non-generator buses (where HVDC systems are typically installed) has been shown that HVDC systems can be used to damp inter-area electromechanical oscillations produced by abnormal events or renewable generation [107].

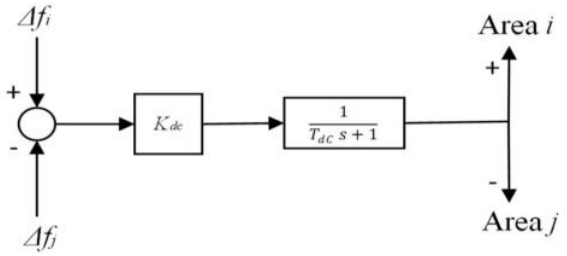

Fig. 4.8. Linearized model of the HVDC link [99].

In this work, a simple block diagram of AC/DC transmission system is used in LFC models to simulate HVDC tie-lines. An equivalent first order transfer function with appropriate AC/DC gain constant, K_{dc}, and time constant, T_{dc} are shown in Fig. 4.8. Similar to the SSSC device, the difference between Δf_i and Δf_j is used as input to the HVDC controller i and j, respectively. For the proposed H_2 control method, four variables, which are K_{dc}, and T_{dc}, would be examined to find optimal values of K_X and T_X.

The suggested control method and calculating optimal values of inverter-based equipment's parameters are applied in two real test systems in the following chapters. One of these systems is an electrical network with high penetration of wind generation built relying on SVM. While the other system is an electrical network planned to have solar generation and be a hub for connecting different countries through ac tie-lines and HVDC links.

5 The Modified H_2 Control Method with Three Area System

5.1 Three Area Test System

The main aim of this dissertation is applying the suggested control method on real power systems to achieve two goals; offering new models created and validated via the proposed reduction technique, SVM, and presenting more realistic results that could help in determining proper actions for potential events. Also, it is preferred to have simple reduced systems of large ones to run LFC models to avoid complexity during the calculations and the outcome model from SVM in chapter 3 is employed to be the test system required to be a simple LFC model.

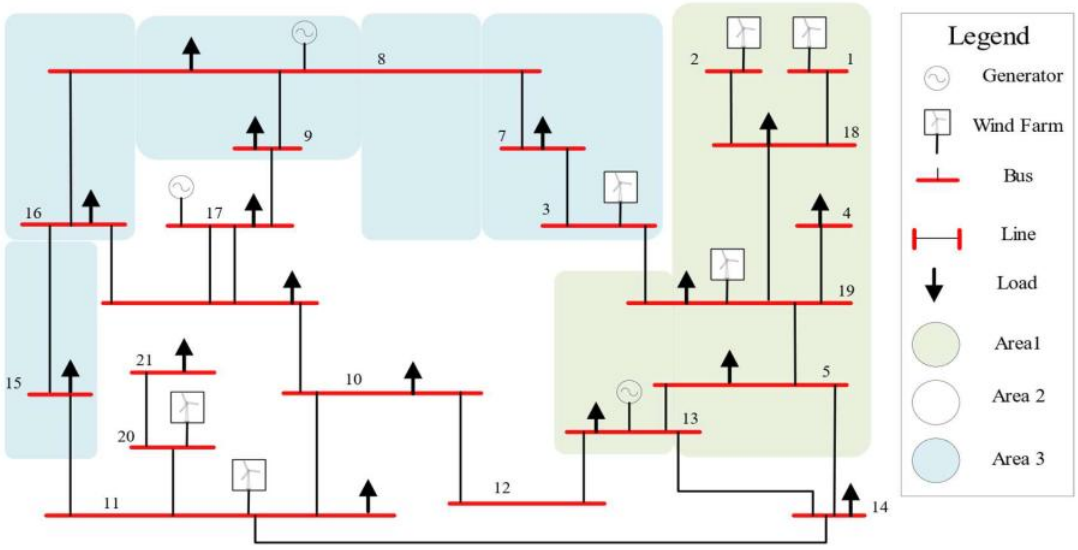

Fig. 5.1. The 21 buses three-area system.

Area 2, in Fig. 3.5, in the WTS456 model includes 237 buses, 414 lines, and 35 generators with total generation 4300 MW, and 40% of the installed generation is from wind generation, whose percentage would be increased or reduced with time compared with the conventional generators. This model is reduced by the novel reduction method to 21 bus system. The reduced system consists of nine generators, six of them are wind generation, and 27 lines, shown in Fig.

5.1. This area is built in this work as a LFC model in order to simulate power systems with wind generation under H_2 control method with both SSSC device and HVDC link.

The new model, shown in Fig. 5.2, is divided into three areas and each area has a conventional generator and different numbers of wind generation and these areas are connected together through three tie-lines. Both SSSC device and HVDC link is placed or connected second and third areas. Also, there is a disturbance with 0.05pu as a magnitude is set at 30 seconds in the first area and it is cleared after 0.5 seconds and frequency deviation and power change in tie-lines are outputs used to be inputs for the H_2 controller.

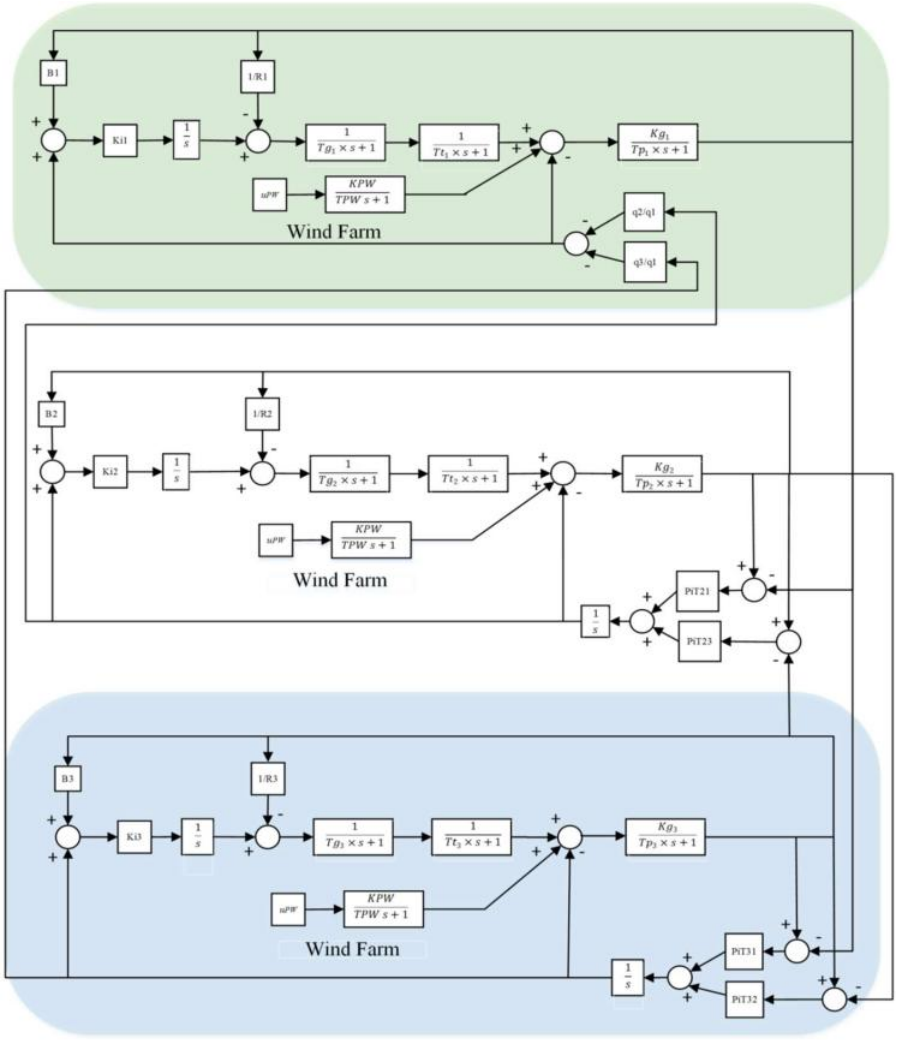

Fig. 5.2. Block diagram of three area system with wind farms.

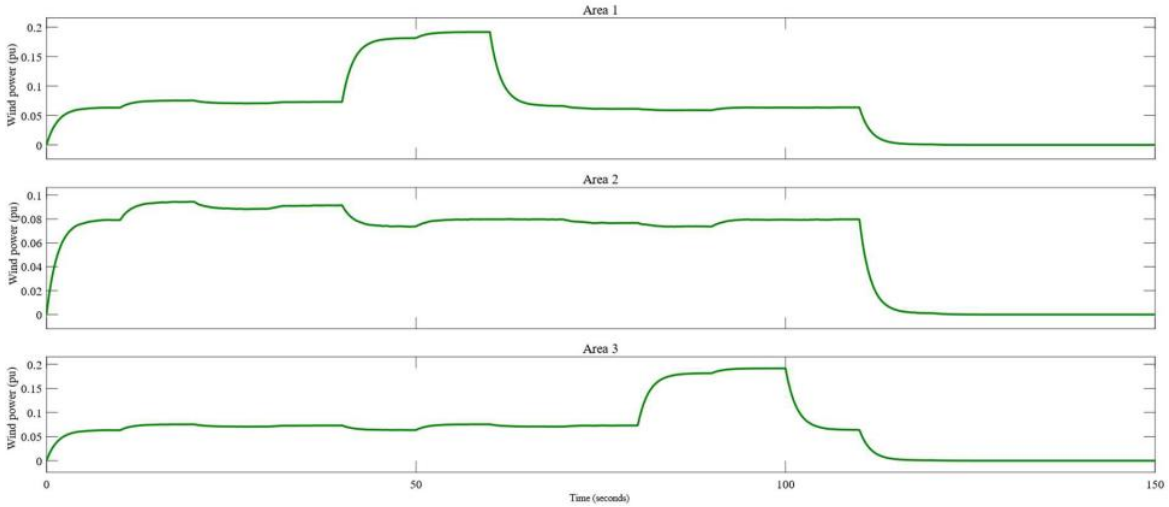

Fig. 5.3. Generation of wind farms in the three-area system.

The wind generation in each area has a different generation that is varied with time and that is shown in Fig. 5.3 and this impacts directly the frequency and power in tie-lines. The frequency for the three-area system, shown in Fig. 5.4, has a range which is between 60.2 and 59.6Hz and this violates frequency standard within 0.06Hz. Several dips and peaks display in each frequency recovery due to varying generation of the wind generation. Also, the frequency shows a significant dip at the time when the disturbance is placed in the first area while it does not

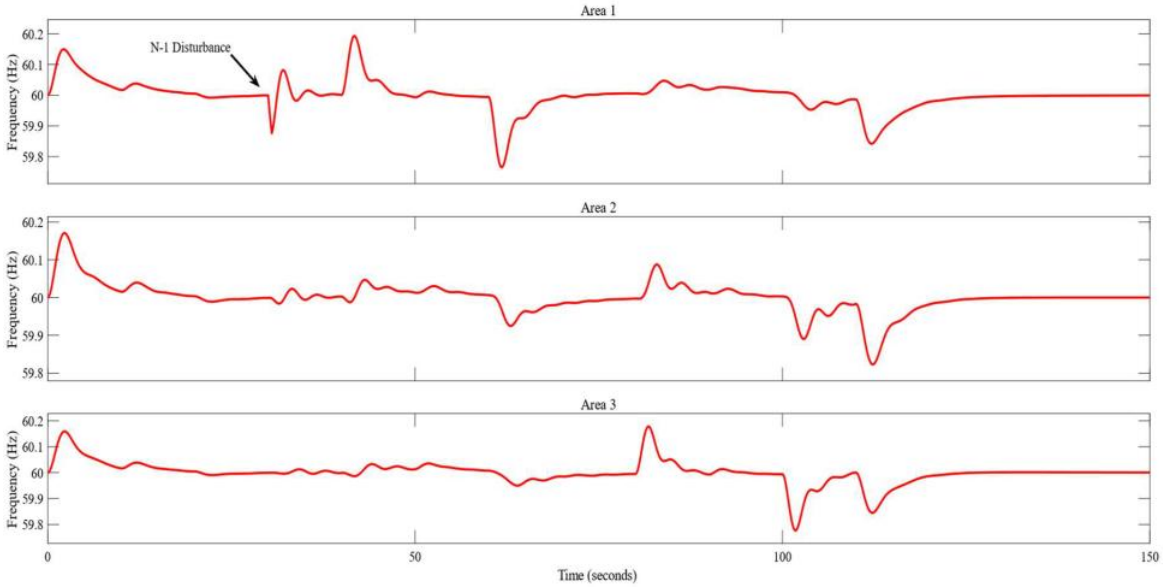

Fig. 5.4. Frequency response of the three-area test system with wind farms and a disturbance.

have high influences on other areas. Generators in this system are considered as thermal units and transfer functions of those units are given in Generator:

$$\frac{Kg_i}{Tp_i s+1}, \tag{5.1}$$

Governor transfer function:

$$\frac{1}{Tg_i s+1}, \tag{5.2}$$

Steam turbine:

$$\frac{1}{Tt_i s+1}, \tag{5.3}$$

while the ACE in all the three areas are given as in

$$ACE_i = \Delta Ptie_i + B_i \Delta f_i, \tag{5.4}$$

where, s: Laplace operator, i: the number of areas, Kg: gain constant, Tp: time constant, Tg: governor time constant, Tt: turbine time constant, $\Delta Ptie$: tie-line power changes among different areas, B: biasing constant, Δf: the incremental frequency deviation [108].

The system calculations are built on state-space variables equations in order to check stability and design the H_2 controller. The check shows that the system, which has 15 state variables, before having time delay, and wind generation is unstable and the reason for this condition is the existence of a zero eigenvalue. The zero eigenvalue is brought to this system because of integrators in the $\Delta Ptie$ transfer function, given by

$$\frac{2\pi T_{ij}}{s}, \tag{5.5}$$

where, T_{ij}: power synchronizing coefficient between area i and j. Therefore, a reduced row echelon form is utilized to reduce number of tie-line power changes in the three- area system. After several calculations, $\Delta Ptie_i$ is replaced with both $\Delta Ptie_2$ and $\Delta Ptie_3$ after multiplication with constants and that is given in

$$x_4^{old} = -\frac{q_2}{q_1}x_8 - \frac{q_3}{q_1}x_{13}, \tag{5.6}$$

Where, X_4^{old}: state-space variable of $\Delta Ptie_1$pre-replacement, X_8: state-space variable of $\Delta Ptie_2$, X_{13}: state-space variable of $\Delta Ptie_3$, q_1, q_2, q_3: reduction constants. The state-space equations after this reduction are given in

$$\dot{x_1} = \frac{-1}{Tp_1}x_1 + \frac{Kg_1}{Tp_1}x_2 + \frac{Kg_1q_2}{Tp_1q_1}x_8 + \frac{Kg_1q_3}{Tp_1q_1}x_{13} + \frac{Kg_2}{Tp_2}x_{15} + \frac{Kg_1}{Tp_1}u, \tag{5.7}$$

$$\dot{x_2} = \frac{-1}{Tt_1}x_2 + \frac{1}{Tt_1}x_3, \tag{5.8}$$

$$\dot{x_3} = \frac{-1}{R_1Tg_1}x_1 - \frac{1}{Tg_1}x_3 + \frac{1}{Tg_1}x_4, \tag{5.9}$$

$$\dot{x_4} = -Ki_1B_1x_1 + \frac{Ki_1q_2}{q_1}x_8 + \frac{Ki_1q_3}{q_1}x_{13}, \tag{5.10}$$

$$\dot{x_5} = \frac{-1}{Tp_2}x_5 + \frac{Kg_2}{Tp_2}x_6 + \frac{Kg_2}{Tp_2}x_8 + \frac{Kg_2}{Tp_2}x_{16} + \frac{Kg_2}{Tp_2}u, \tag{5.11}$$

$$\dot{x_6} = \frac{-1}{Tt_2}x_6 + \frac{1}{Tt_2}x_7, \tag{5.12}$$

$$\dot{x_7} = \frac{-1}{R_2Tg_2}x_5 - \frac{1}{Tg_2}x_7 + \frac{1}{Tg_2}x_9, \tag{5.13}$$

$$\dot{x_8} = -2\pi T_{21}x_1 + 2\pi(T_{21} + T_{23})x_5 - 2\pi T_{23}x_{10}, \tag{5.14}$$

$$\dot{x_9} = -Ki_2B_2x_5 - Ki_2x_8, \tag{5.15}$$

$$\dot{x_{10}} = \frac{-1}{Tp_3} x_{10} + \frac{Kg_3}{Tp_3} x_{11} - \frac{Kg_3}{Tp_3} x_{13} + \frac{Kg_3}{Tp_3} x_{17} + \frac{Kg_3}{Tp_3} u, \tag{5.16}$$

$$\dot{x_{11}} = \frac{-1}{Tt_3} x_{11} + \frac{1}{Tt_3} x_{12}, \tag{5.17}$$

$$\dot{x_{12}} = \frac{-1}{R_3 Tg_3} x_{10} - \frac{1}{Tg_3} x_{12} + \frac{1}{Tg_3} x_{14}, \tag{5.18}$$

$$\dot{x_{13}} = -2\pi T_{31} x_1 - 2\pi T_{32} x_5 + 2\pi (T_{31} + T_{32}) x_{10}, \tag{5.19}$$

$$\dot{x_{14}} = -Ki_3 B_3 x_{10} - Ki_3 x_{13}, \tag{5.20}$$

$$\dot{x_{15}} = \frac{-1}{TW} x_{15} + \frac{K_t}{TW}\ KWT \tag{5.21}$$

$$\dot{x_{16}} = \frac{-1}{TW} x_{16} + \frac{K_t}{TW}\ KWT \tag{5.22}$$

$$\dot{x_{17}} = \frac{-1}{TW} x_{17} + \frac{K_t}{TW}\ KWT \tag{5.23}$$

where, Ki_1, Ki_2, Ki_3: three area controllers, R_1,R_2, R_3: speed regulation parameter, *U*: state-space input, *TW*: Wind turbine time constant, which is 1.5 seconds in this work, K_t: Wind power percentage of total generation, KWT: Wind variable input.

The state space equations for (5.7)-(5.23) are written as:

$$\dot{x} = Ax(t) + Bu(t), \tag{5.24}$$

$$y(t) = Cx(t) + Du(t). \tag{5.25}$$

Six of the test system's variables, $x_1, x_5, x_{10}, (-\frac{q_2}{q_1} x_8 - \frac{q_3}{q_1} x_{13}), x_8, x_{13}$, are connected to the H_2 controller through a time delay function, which is $\frac{1}{\frac{1}{2} T_d\, s+1}$. All these variables are added to the system resulting in a test system with 23 state-space variables. The modified, highlighted by *, and new state-space variables can be given as

$$\dot{x_1} = \frac{-1}{Tp_1}x_1 + \frac{Kg_1}{Tp_1}x_2 + \frac{Kg_1q_2}{Tp_1q_1}x_8 + \frac{Kg_1q_3}{Tp_1q_1}x_{13} + \frac{Kg_1}{Tp_1}x_{15} + \frac{Kg_1}{Tp_1}u_2, \quad (5.7^*)$$

$$\dot{x_4} = x_{18} + x_{19} + u_1, \quad (5.10^*)$$

$$\dot{x_5} = \frac{-1}{Tp_2}x_5 + \frac{Kg_2}{Tp_2}x_6 + \frac{Kg_2}{Tp_2}x_8 + \frac{Kg_2}{Tp_2}x_{16} + \frac{Kg_2}{Tp_2}u_2, \quad (5.11^*)$$

$$\dot{x_9} = x_{20} + x_{21} + u_1, \quad (5.15^*)$$

$$\dot{x_{10}} = \frac{-1}{Tp_3}x_{10} + \frac{Kg_3}{Tp_3}x_{11} - \frac{Kg_3}{Tp_3}x_{13} + \frac{Kg_3}{Tp_3}x_{17} + \frac{Kg_3}{Tp_3}u_2, \quad (5.16^*)$$

$$\dot{x_{14}} = x_{22} + x_{23} + u_1, \quad (5.20^*)$$

$$\dot{x_{18}} = \frac{B_1}{T_d}x_1 - \frac{1}{T_d}x_{18}, \quad (5.26)$$

$$\dot{x_{19}} = \left(\frac{-1}{T_d}\frac{q_2}{q_1}\right)x_8 - \left(\frac{1}{T_d}\frac{q_3}{q_1}\right)x_{13} - \frac{1}{T_d}x_{19}, \quad (5.27)$$

$$\dot{x_{20}} = \frac{B_2}{T_d}x_5 - \frac{1}{T_d}x_{20}, \quad (5.28)$$

$$\dot{x_{21}} = \frac{1}{T_d}x_8 - \frac{1}{T_d}x_{21}, \quad (5.29)$$

$$\dot{x_{22}} = \frac{B_3}{T_d}x_{10} - \frac{1}{T_d}x_{22}, \quad (5.30)$$

$$\dot{x_{23}} = \frac{1}{T_d}x_{13} - \frac{1}{T_d}x_{23}, \quad (5.31)$$

where U_1, U_2: controlled input and variable input, such as renewable power or random load. After running these state-space equations in the MATLAB environment, the results of the system pre and post having the H_2 controller are obtained.

The power flow deviation shown in Fig. 5.5 has obvious changes with time due to impacts of wind generation and these changes vary from -0.02 to 0.04pu. However, the power in tie-lines

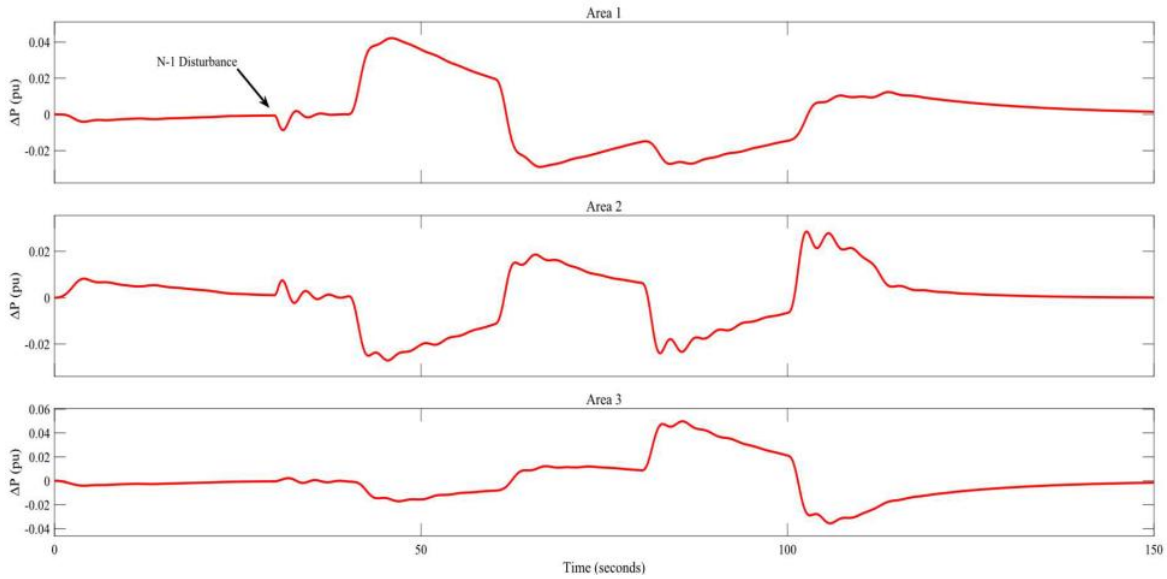

Fig. 5.5. Power deviation of tie-lines in the three-area test system.

does not display large dips or peaks at the time of disturbance and this may come from influences of renewable generation.

The performance of the system illustrated in previous figures is an outcome of a conventional controller, which is ACE, and this controller does not give a proper act to reduce large variations and fluctuations. The proposed control method is applied on this system to show the required response and similar to the approach in Fig. 4.2. From Fig. 5.6 and Fig. 5.7, the improvement of system's response for both frequency and power deviation of tie-lines exists and this enhancement is a result of an adoption of the H_2 control method. The frequency recovery shown in Fig. 5.6 is reduced from the range 60.14-59.74Hz to the range 60.08-59.92Hz and this outcome is because of the considering disturbances or varying inputs by the H_2 controller and its function to keep the frequency and power deviation near the reference values. Also, frequency has a high swing when the disturbance is placed evenly. The H_2 controller tries to reduce it and keep it within the range between 60.06 and 59.94Hz and that is required to avoid violating the frequency standards. However, the H_2 controller act causes some oscillations in frequency that are present

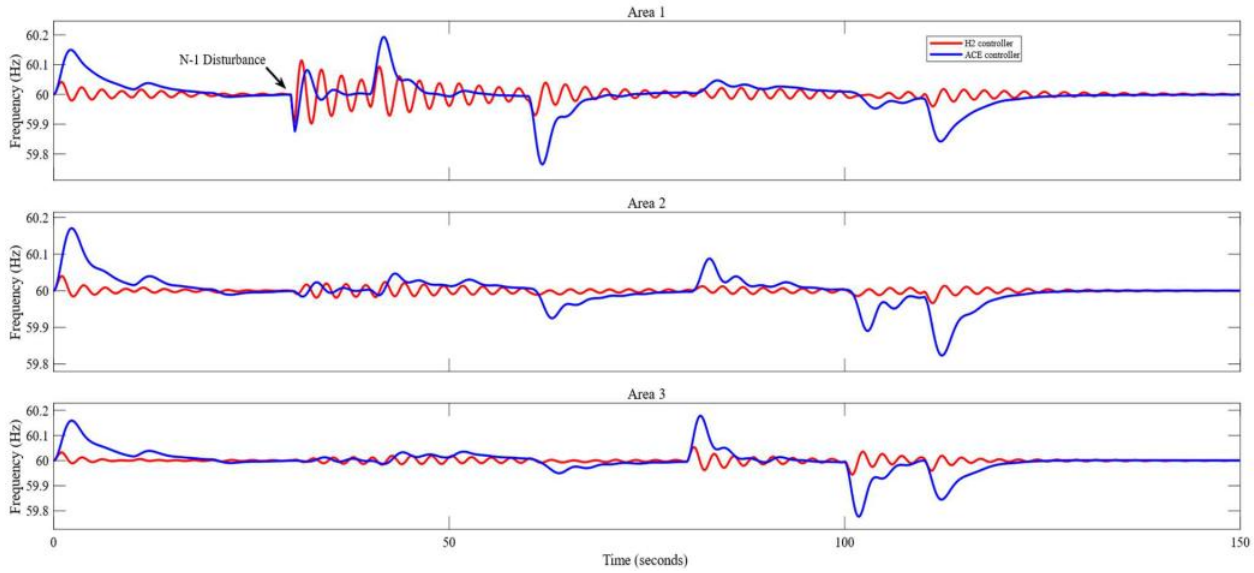

Fig. 5.6. Frequency response of the test system with both ACE and H_2 controllers.

in the original system with the conventional controller even these oscillations do not have high values compared with original system.

From the power flow in tie-lines aspect, the system with the H_2 controller shows low power deviation for all three areas compared with the original system where the range of deviation has been reduced from 0.09 to 0.03pu, Fig. 5.7, and that is optimal in load flow, especially if the system

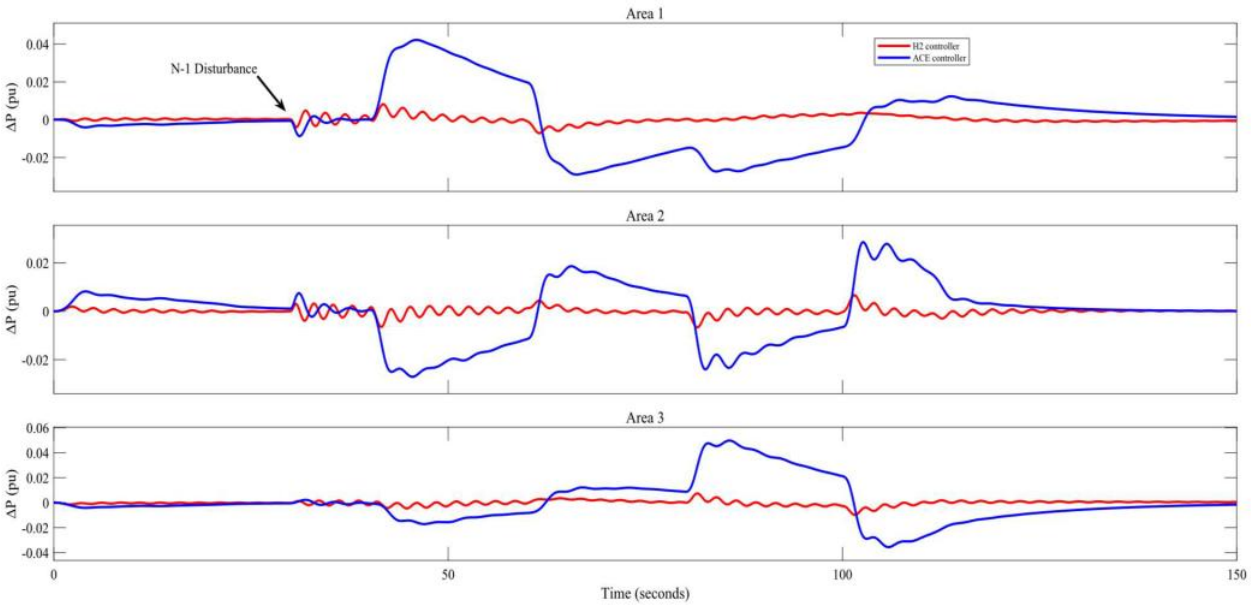

Fig. 5.7. Power deviation response of the test system with both ACE and H_2 controllers.

experiences abnormal conditions. Similar to frequency recovery, the power deviation has little oscillations with the H_2 controller. This phenomenon could be an effect of power generation by wind generation and this could be seen when wind generation have high amount of production injected into the system. Some techniques are going to be adopted in this work to reduce those oscillations and others and these techniques consist of inserting a SSSC device and HVDC link in the test system in addition to placing N-1 and N-1-1 contingency events.

5.2 HVDC Link Installation

One of methods used to improve and enhance power flow and reduce frequency deviation is installing HVDC links in transmission systems. The HVDC link is placed between two areas, Area 2 and Area 3, to reduce impacts of disturbances, Fig. 5.8. The modified method is applied to obtain the optimal values of T_{dc} and K_{dc} with considering the time communication delay is 200ms. After running the proposed method in Fig. 4.2 in MATLAB environment for 1900 cases in 4.45 hours, the optimal values for T_{dc} and K_{dc} that achieve optimal cost γ for three areas, depending on criterion min(max(*ST*)) , are 3.15, 3.11, and 3.12, respectively, and minimum frequency deviations for the areas are 60.0651, 60.0312, and 60.0330Hz, respectively, shown in Table. 5.

Table 5. Minimum frequency (Hz) and optimal cost values for the HVDC case

Case No.	f_1	f_2	f_3	γ
1	60.0651	60.0321	60.0444	3.1510
2	60.0654	60.0312	60.0336	3.1094
3	60.0654	60.0318	60.0330	3.1241

The first case is chosen to be optimal values for T_{dc} and K_{dc} with and their values are 0.5 second and 0. 2pu, respectively. Selection of these values from others is because all mentioned cases achieve the condition ($\gamma(i+1)$-$\gamma(i)$ = 0.1) and then the optimal values selection would depend

on the lowest value of frequency deviation, which can be seen in the first area. Also, other conditions will be ignored even they have lowest frequency deviation or optimal cost because they have a HVDC link connected them together in addition their ac tie-line. This connection would help in reducing frequency deviations and power swings and that would be seen in next part.

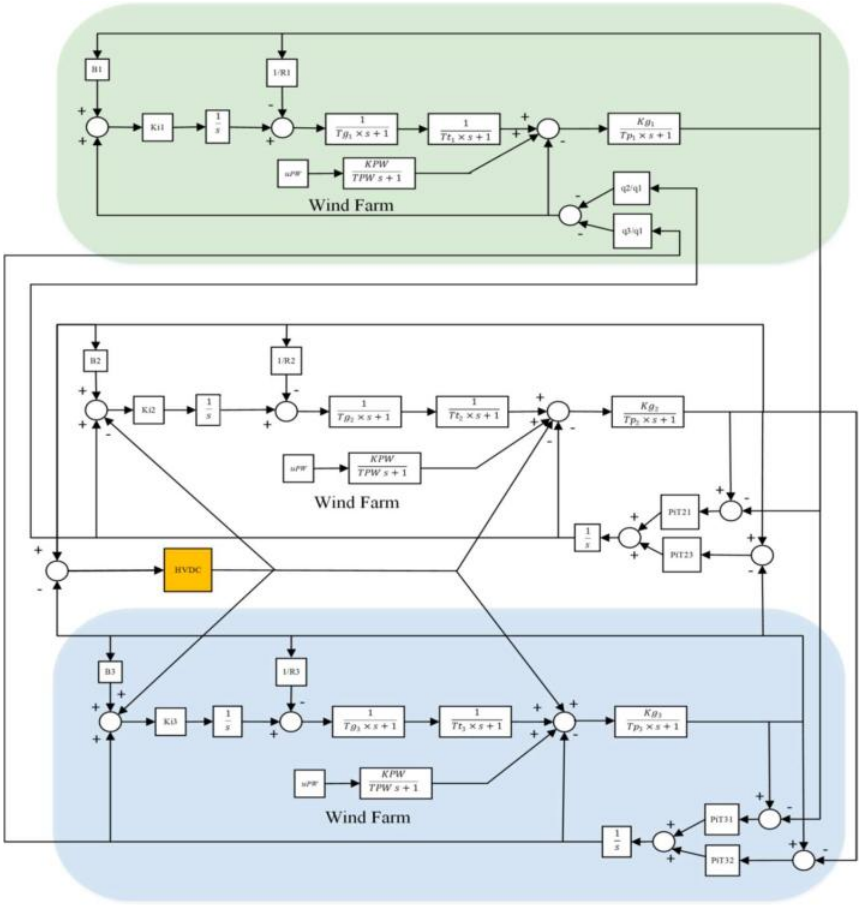

Fig. 5.8. Block diagram of three area system with wind farms with HVDC link.

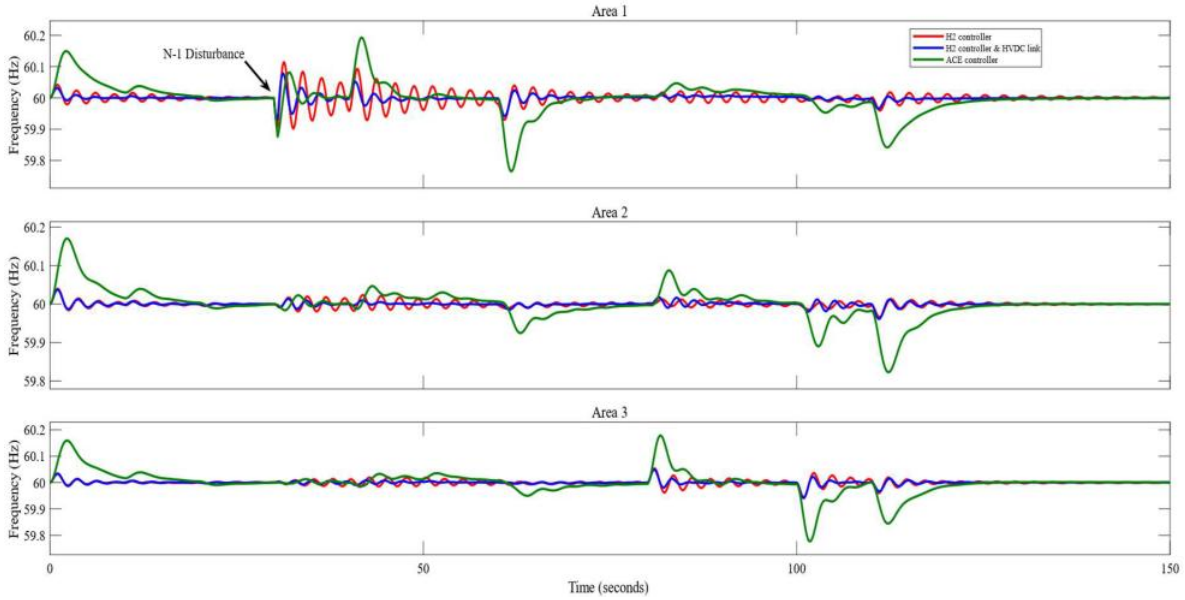

Fig. 5.9. Frequency response of three areas in three cases; ACE controller, H_2 controller, and H_2 controller + HVDC link.

The optimal values are placed in the transfer function of HVDC link and a comparison between three different cases, ACE controller, H_2 controller, and H_2 controller with HVDC link, respectively, under two scenarios will be done. The first scenario consists of the three-area system with wind generation and a disturbance in the first area. The system is run in MATLAB environment for 150 seconds and the comparison will be between the three cases as shown in Fig. 5.9. In this figure, frequency deviation has been reduced to lower values in H_2 controller, and H_2 controller with HVDC link compared with ACE controller case. However, the H_2 controller case shows high frequency oscillations during the simulation time and that could exhaust generators and their controllers and may lead to overloading conditions in lines with high power flow. This case would be a result of H_2 controller's dealing with wind generation or disturbances because these oscillations begin with increasing of wind volume or disturbance occurrence, shown in Fig. 5.3. Therefore, adoption of HVDC link technique helps in mitigating this issue along with reducing frequency oscillations.

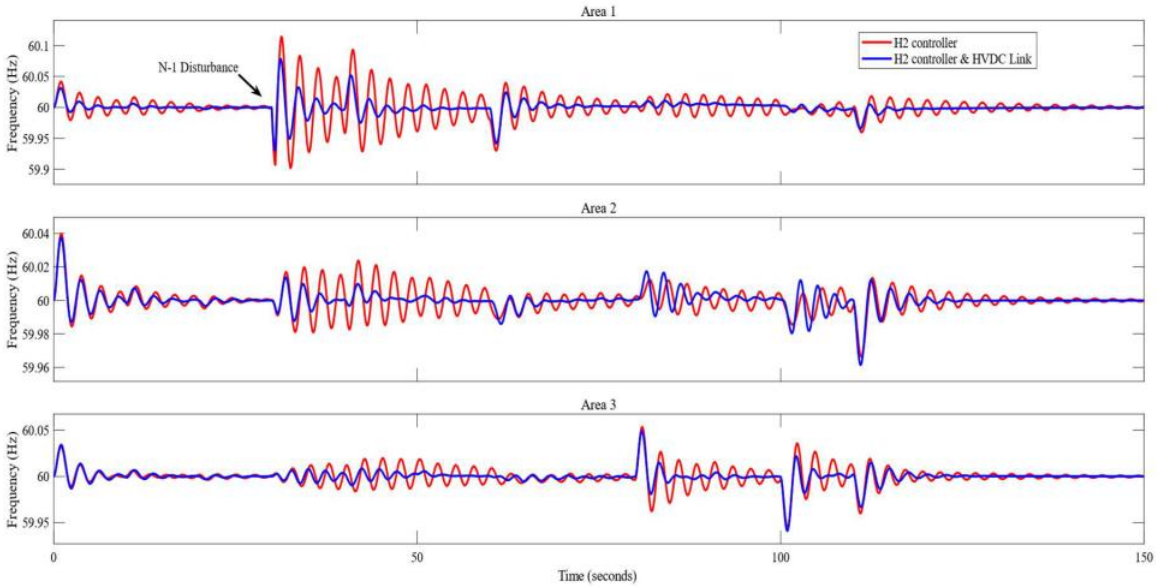

Fig. 5.10. Frequency response of three areas in two cases; H_2 controller, and H_2 controller + HVDC link.

In Fig. 5.10, the system with HVDC links shows a smoother response compared with the condition without an HVDC link and it maintains the frequency deviation with ±0.06Hz to meet the regulatory requirements. However, the first area has a frequency deviation over 0.06 Hz and this issue is due to influence of the disturbance at 30. Also, frequency deviations of the third case has the same value of frequency deviation of the second condition and this phenomenon is due to injection of wind generation or placement of disturbances. Therefore, the HVDC link functions to reduce this issue gradually with time after the moment of the event.

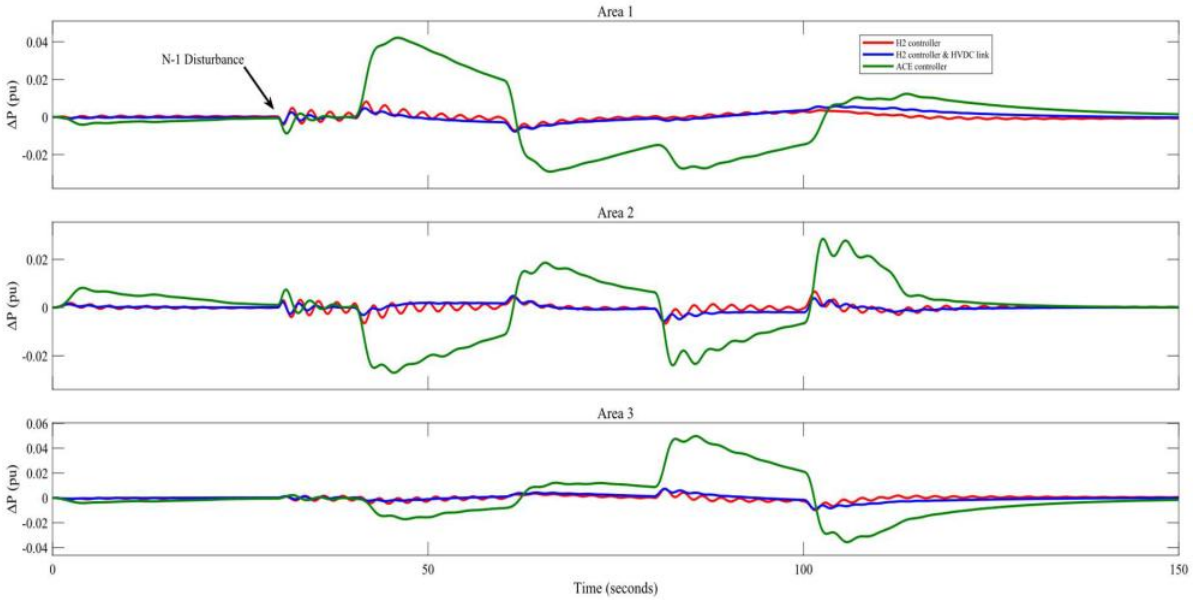

Fig. 5.11. Power deviation of tie-lines of three areas in three cases; ACE controller, H_2 controller, and H_2 controller + HVDC link.

From the power flow in tie-line aspect, the comparisons are repeated for power deviation in tie-lines and the deviation has been reduced largely, as shown in Fig. 5.11. In this figure, power deviation for the second and third cases are within ±0.02pu due to the impact of the H_2 controller while the system with ACE controller has conditions with power deviation reaches 0.1pu as in the third area.

5.3 N-1-1 Contingency Event with HVDC Link

The three-area system experiences N-1-1 contingency events through setting a disturbance with 0.05pu as magnitude after 2 seconds from clearing the first fault, cleared at 30.5 seconds, and the second fault would be clear by 33 seconds. In this simulation, selection of T_{dc} and K_{dc} is left relying on the previous values to analyze response of the system under unpredictable conditions or without pre-preparations. After placing the disturbances, the comparisons are applied again on the three cases, ACE controller, H_2 controller, and H_2 controller with HVDC link, respectively.

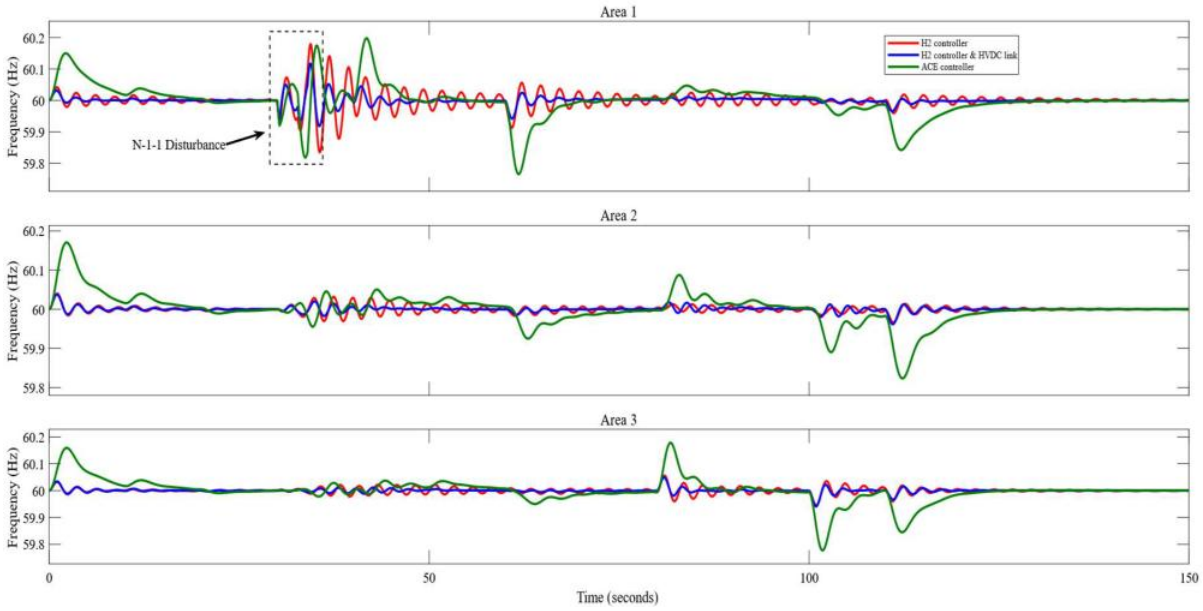

Fig. 5.12. Frequency response of three areas in three cases; ACE controller, H_2 controller, and H_2 controller + HVDC link under N-1-1 contingency events.

The first comparison is related to frequency deviation that is displayed in Fig. 5.12 and this figure shows the system has high frequency deviation during the disturbance period for all cases, especially in the first area that reached 60.1 Hz. This issue comes from the influence of faults that occur in a sequence where the impacts of first the fault are increased by the second fault instead of damping. However, the system responds to this type of events in a proper way through reducing frequency deviation in all areas and these changes have been enhanced from a response with high oscillations to smooth variations that are illustrated in Fig. 5.13. For the issue in the first area, the frequency deviation during the N-1-1 condition that reaches over 60.1 Hz and this is related to the impact of disturbances of 5% of the system load.

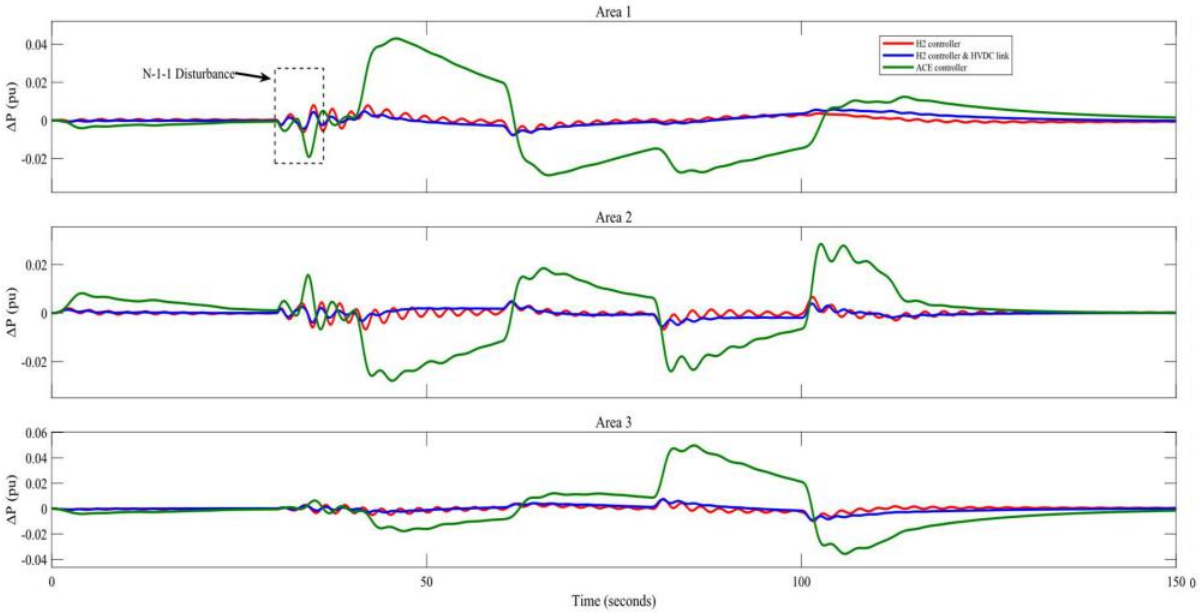

Fig. 5.14. Power deviation of tie-lines of three areas in three cases; ACE controller, H_2 controller, and H_2 controller + HVDC link under N-1-1 contingency events.

This disturbance could be considered a large change in power system conditions and that is used in this work to show a worst-case situation. Moreover, another comparison is made for the power deviation in tie-lines and is similar to a previous scenario. The power deviation for the system under N-1-1 contingency event does not show high changes in the second and third cases in contrast with the first case that have large variations, shown in Fig. 5.14.

Another type of event is applied on the test system with the HVDC link and this event is an outage of two lines sequentially. These lines area selected to be in tie-lines 1-2 and 1-3 and these trips occur at 30 and 32 seconds, respectively, and these lead to increased values of power synchronizing coefficients ten times, to emphasize outage of lines as shown in Fig. 5.15. In this figure, it is obvious that the N-1-1 event impacts power flow in the system largely and that can be seen during wind generation periods where there are big differences in values of power deviation between pre and post-event condition.

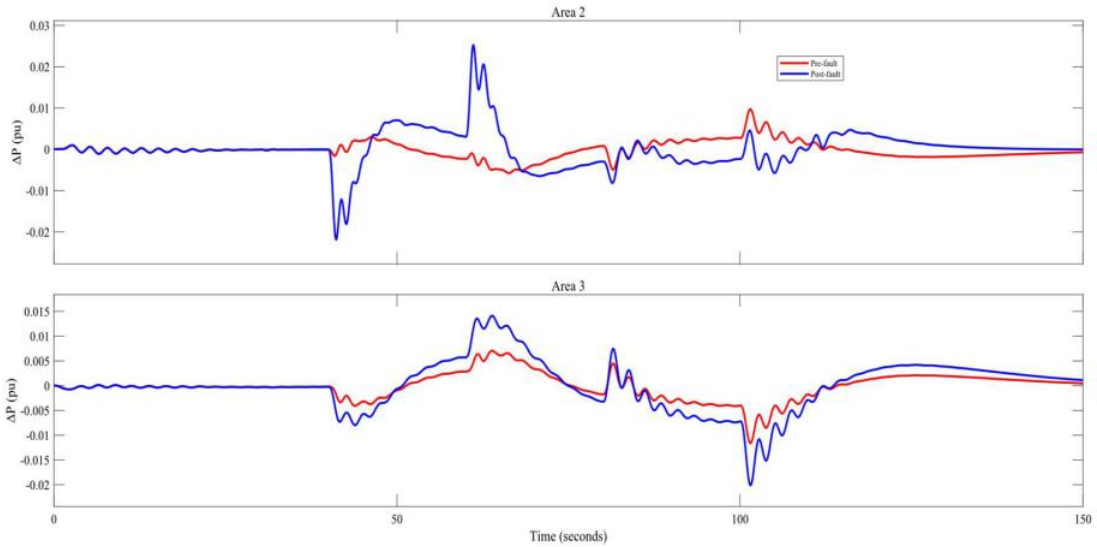

Fig. 5.15. Power deviation of tie-lines of two areas under N-1-1 contingency events.

This event is simulated for the system in three cases and the results are shown in Fig. 5.16 and Fig. 5.17. In Fig. 5.16, the system with only the H_2 controller or with the H_2 controller and HVDC link have better frequency recovery compared with ACE controller. The HVDC link simulation shows smooth response keeping within the NERC frequency requirements. Also, Fig. 5.17 displays that power deviation with the H_2 controller have reduced values and maintain with

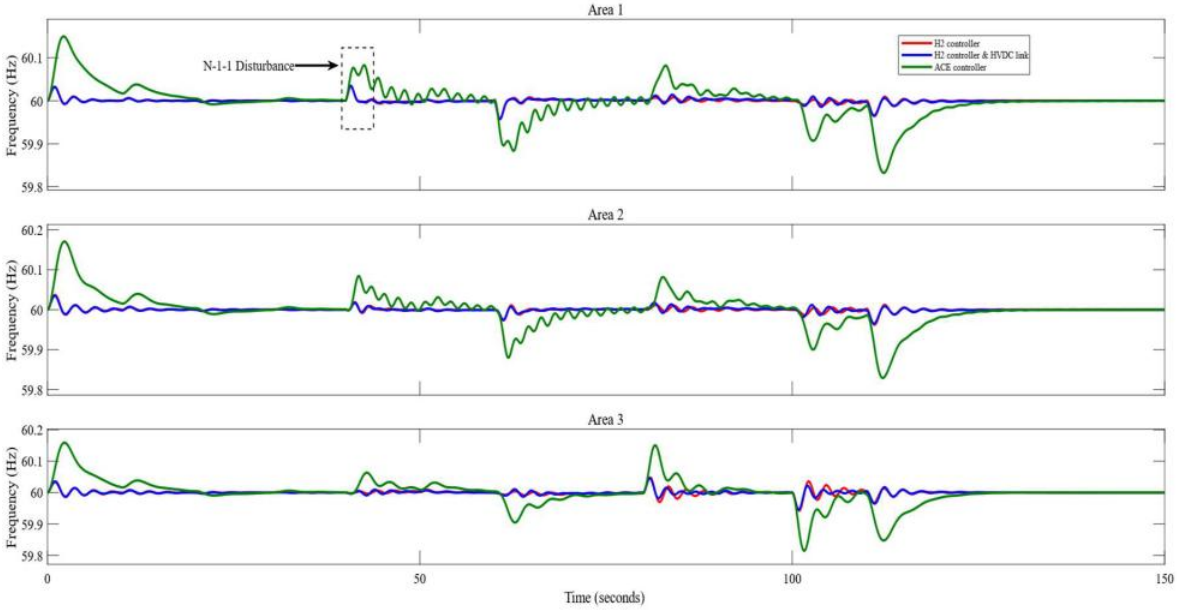

Fig. 5.16. Frequency response of three areas in three cases; ACE controller, H_2 controller, and H_2 controller + HVDC link under N-1-1 contingency events in lines.

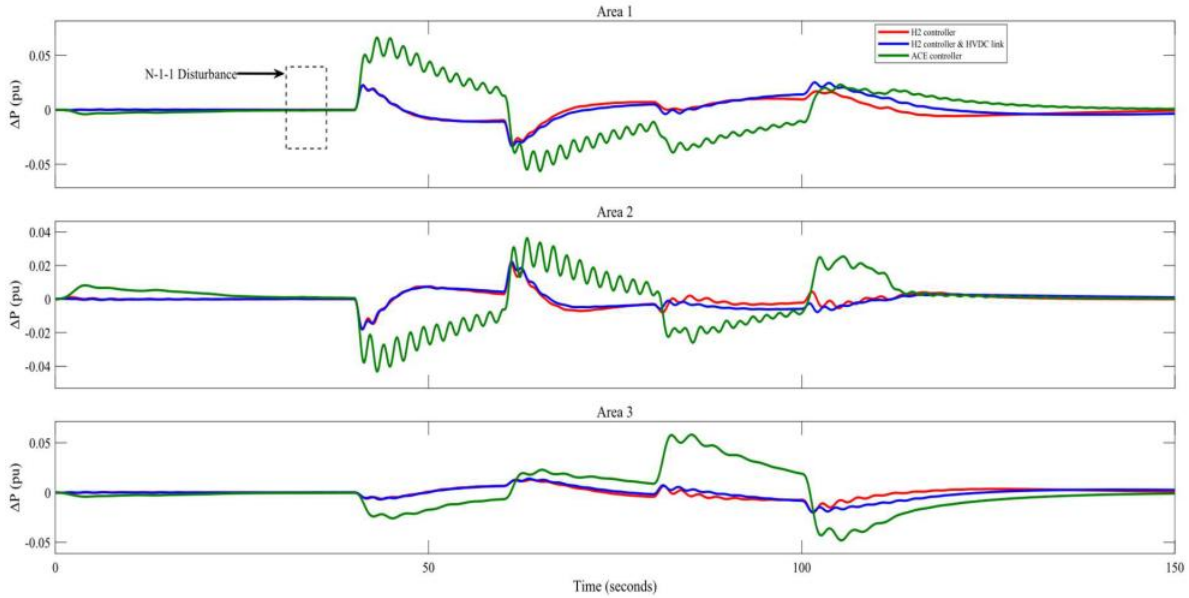

Fig. 5.17. Power deviation of tie-lines of three areas in three cases; ACE controller, H_2 controller, and H_2 controller + HVDC link under N-1-1 contingency events in lines.

the range of 0.05pu while the system with a conventional controller has larger power deviations. The H_2 controller with HVDC link produces lower power deviation even when there are several disturbances and variable resources influence the power system.

5.4 SSSC Device Installation

The modified approach for use of FACTS devices is applied on the three-area system through setting a SSSC device between the second and third area, Fig. 5.18. This step is to test the response of the system for dynamic circumstances and the influence of the SSSC device to reduce power oscillation and frequency swings. The modified method calculates the optimal values of K_{SSSC} and T_{SSSC}, T_1, and T_3 with considering the time communication delay is 200ms and fixing T_W, T_2, and T_4 to be 10, 0.01, 0.01.

The suggested approach is simulated in MATLAB environment for 2.2 hours, the optimal values for K_{SSSC} and T_{SSSC}, T_1, and T_3 that achieve optimal cost γ for three areas, depending on criterion min(max(ST)) , are 3.30, 3.24, and 3.27, respectively, and minimum frequency deviations

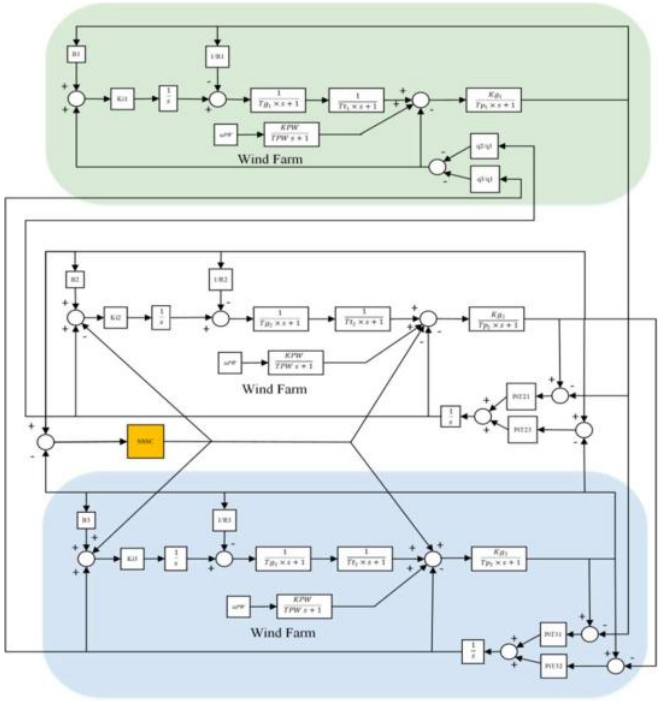

Fig. 5.18. Block diagram of three area system with wind farms with SSSC.

for the areas are 60.0360, 60.0370, and 60.0352Hz, respectively, illustrated in Table 6. Similar to the HVDC link conditions, the first case is chosen to be optimal values for K_{SSSC} and T_{SSSC}, T_1, and T_3 with and their values are 0.2pu and 0.1, 0.1, and 0.1 seconds, respectively.

Table 6. Minimum frequency (Hz) and optimal cost values for SSSC case

Case No.	f_1	f_2	f_3	γ
1	60.0360	60.0374	60.0467	3.2959
2	60.0372	60.0370	60.0355	3.2363
3	60.0370	60.0374	60.0352	3.2660

Like the analysis with an HVDC installment, three cases are studied to make a comparison to evaluate the system response with having the SSSC device. The first comparison is for the frequency recovery that is shown in Fig. 5.19.

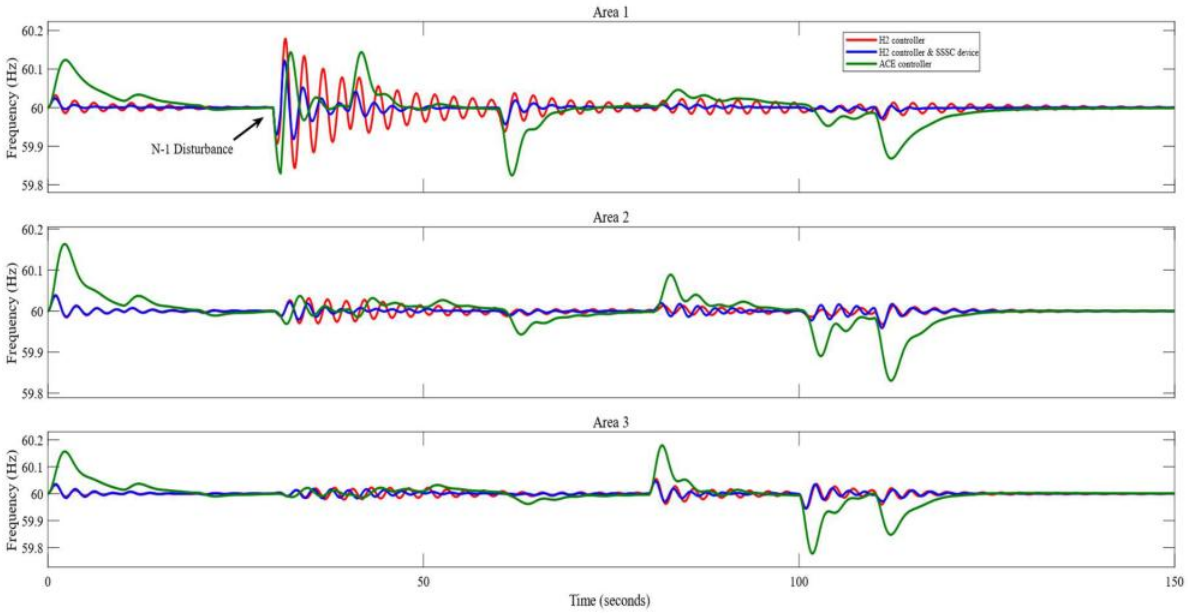

Fig. 5.19. Frequency response of three areas in three cases; ACE controller, H_2 controller, and H_2 controller + SSSC device.

In this figure, frequency recovery of the system either with only H_2 controller or with H_2 controller and SSSC device functions better that frequency recovery of the system with an ACE controller. The H_2 controller helps the power system to reduce its frequency deviation created either by wind generation or by disturbances. The controller decreases frequency variations range from over 0.4 to 0.2Hz but it has a frequency deviation due to the disturbance around 60.17Hz while the system has a frequency deviation in the conventional condition that reaches 59.8Hz. However, the H_2 controller participates in producing some frequency oscillation around the nominal value of frequency, 60Hz, and that is increased by wind generation and faults.

Performance of the three-area system with the SSSC device does show significant differences in contrast with the system without the FACTS equipment and these cases are with the H_2 controller and are shown in Fig. 5.20. The system with the SSSC connection has stable behavior and the deviations are reduced from 0.2 to 0.1 Hz. However, the system for both the second and third cases have almost the same recovery time although reaching over 60.1Hz at the

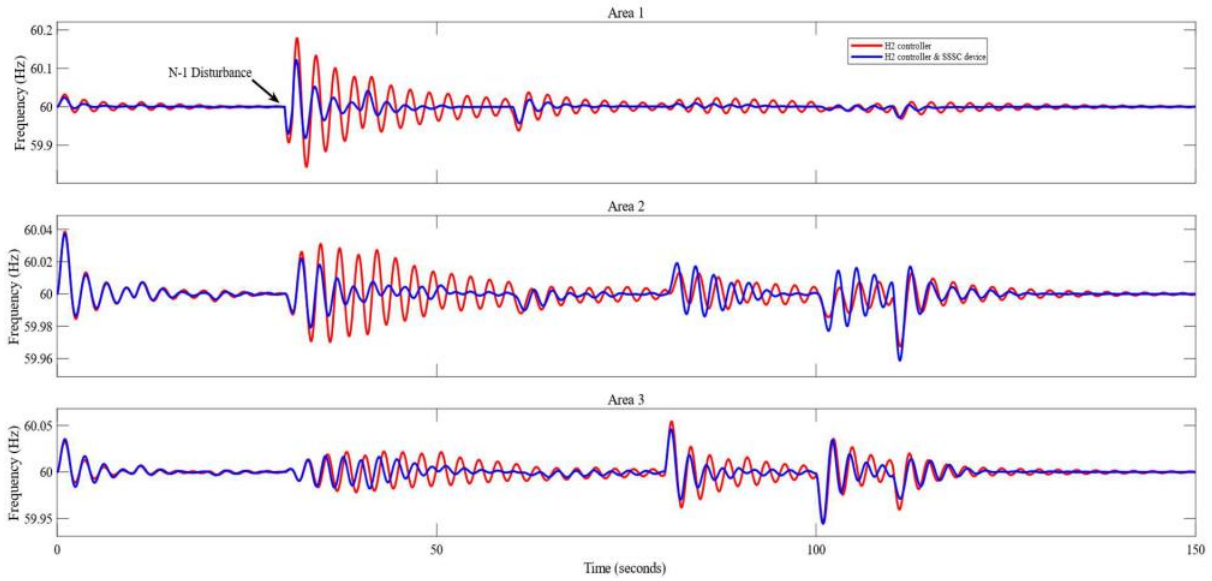

Fig. 5.20. Frequency response of three areas in two cases; H_2 controller, and H_2 controller + SSSC device.

disturbance moment, for the first area, and the system starts having lower values in time after that. In the other areas, the system with SSSC has a smooth recovery and maintains the range of frequency deviation within ±0.05Hz and that is illustrated in Fig. 5.21.

In power flow aspect, power variation range has been mitigated from 0.12pu in ACE controller case to 0.01pu in the H_2 controller cases, without and with SSSC device, and that is

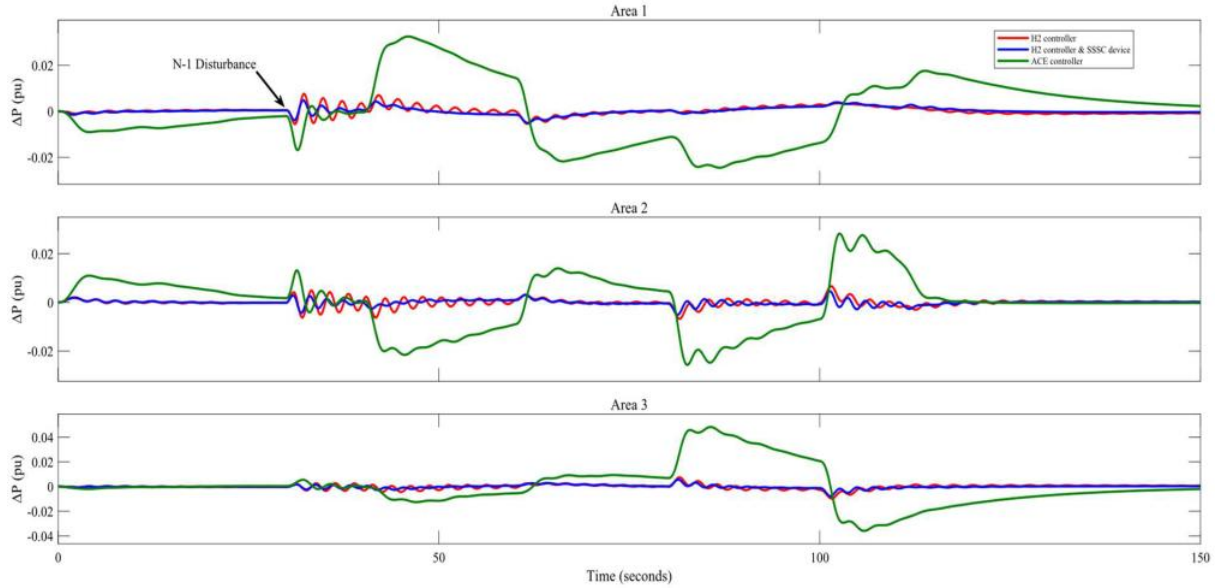

Fig. 5.21. Power deviation of tie-lines of three areas in three cases; ACE controller, H_2 controller, and H_2 controller + SSSC device.

illustrated clearly in Fig. 5.19. The difference between H_2 controller cases is lower than 0.003pu and the system performs smoothly with SSSC compared with only H_2 controller case the during the simulation. The second and third areas present small variations with time compared with the first area due to the impact of the SSSC device. These variations between the two cases would be the same at the beginning of the disturbances produced by wind generation or by faults and that could be seen in Fig. 5.21 at 25, 75, 120 seconds and then the SSSC would help the system to have damped power oscillations. This concludes that the SSSC device would have a significant influence in the power system with an H_2 controller and would assist in reducing frequency and power deviations and keep them within acceptable ranges of NERC power system requirements.

5.5 N-1-1 Contingency Event with SSSC Device

A sequence of two events also are evaluated in the system with SSSC device in order to investigate the dynamic response. The first event is applying the same disturbances as in the HVDC link example, with 0.05pu magnitude and at 30 and 32 seconds, respectively, and these events are placed in the first area. From Fig. 5.22, the system has a different response for the three-area depending on the fault and SSSC locations. The first area experiences high effects of the disturbances and the frequency reaches range between 60.16 and 59.8Hz in the conventional controller condition. Both the H_2 controller cases witness a high frequency swing at the disturbance moment due to the N-1-1 consequences and the only H_2 controller case has over 60.1 Hz and under 59.9 Hz which violates the NERC frequency standard. However, the H_2 controller functions within limits 60.12 to 59.97Hz and then this is reduced to be under 0.06Hz. In other areas, the last two cases do not exceed the NERC frequency standard.

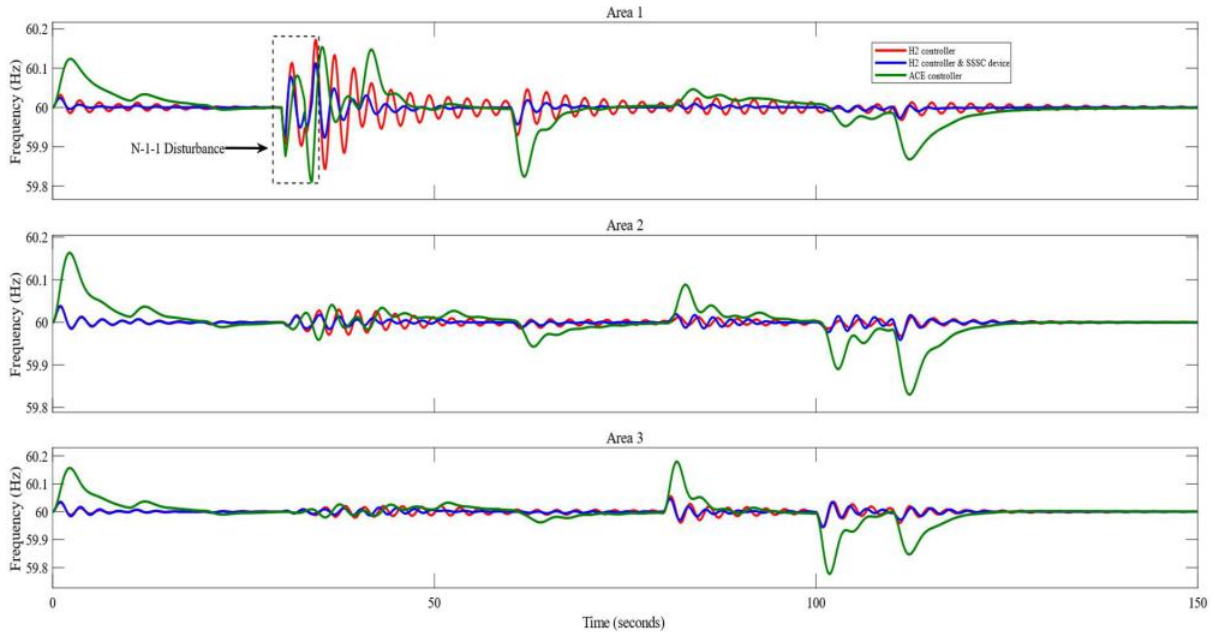

Fig. 5.22. Frequency response of three areas in three cases; ACE controller, H_2 controller, and H_2 controller + SSSC device under N-1-1 contingency events.

From a power deviation aspect, the range of power swing under the H_2 controller cases is within 0.02pu as shown in Fig. 5.23, and this is an improvement compared to a range of 0.04pu in ACE controller method. In the other scenario of an N-1-1 disturbance, there is no violation in frequency standards for all cases as shown in Fig. 5.24 where the frequency recovery has been

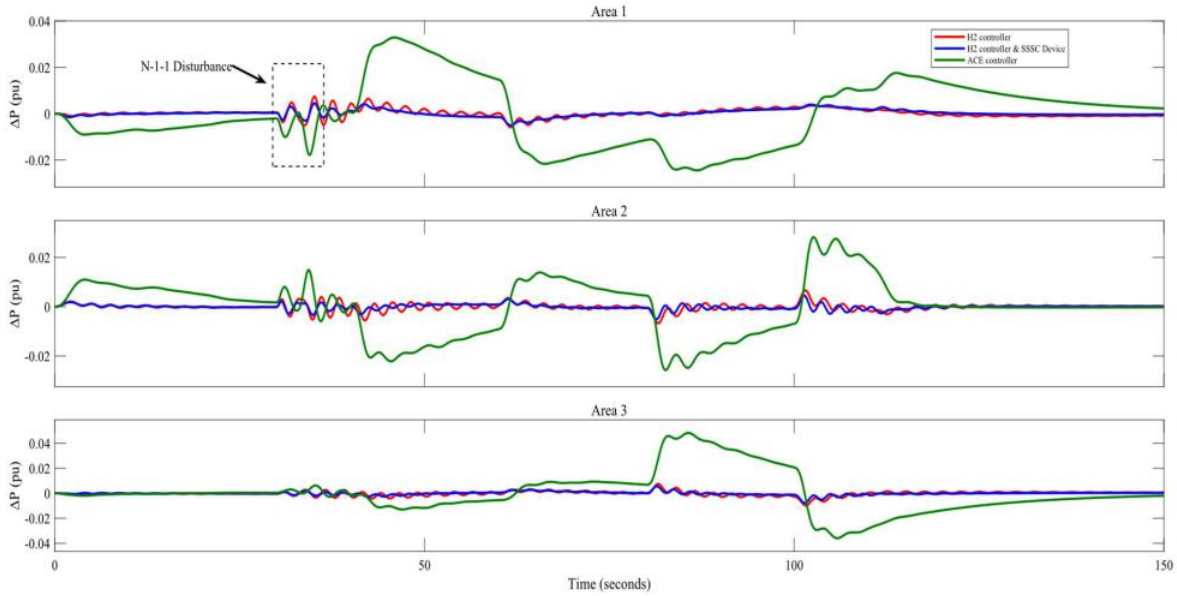

Fig. 5.23. Power deviation of tie-lines of three areas in three cases; ACE controller, H_2 controller, and H_2 controller + SSSC device under N-1-1 contingency events.

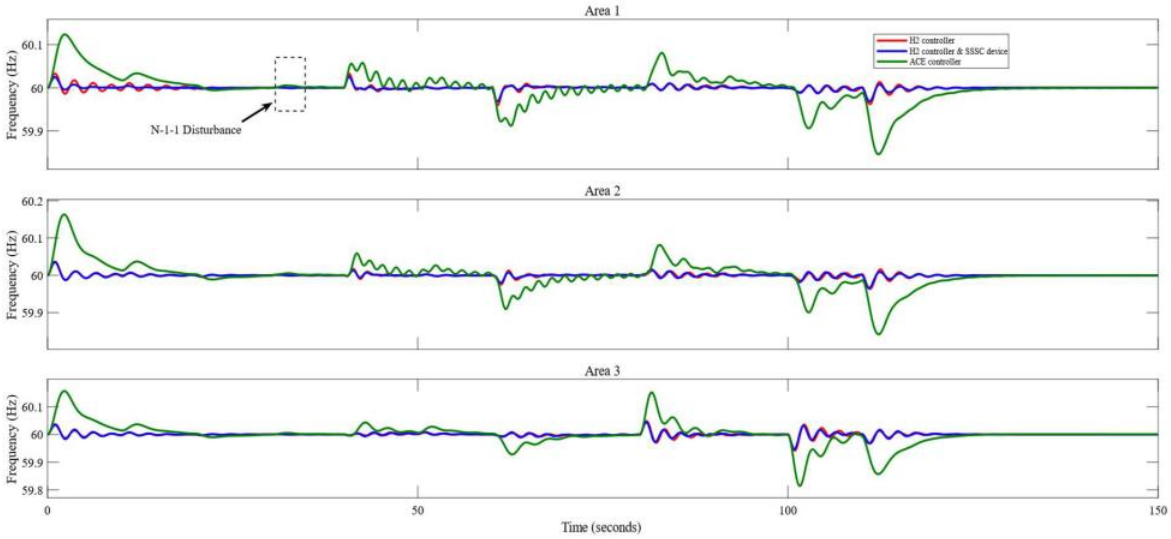

Fig. 5.24. Frequency response of three areas in three cases; ACE controller, H_2 controller, and H_2 controller + SSSC device under N-1-1 contingency events in lines.

enhanced under the H_2 control method. Installing an SSSC in the three-area system improves frequency recovery with time and that is displayed in Fig. 5.25, particularly with increasing wind penetration. From a power flow aspect, the range of power deviation has been decreased from 0.11pu in the ACE controller case to 0.04pu in the H_2 controller case. The H_2 controller with an SSSC device shows a smooth response as illustrated in Fig. 5.26.

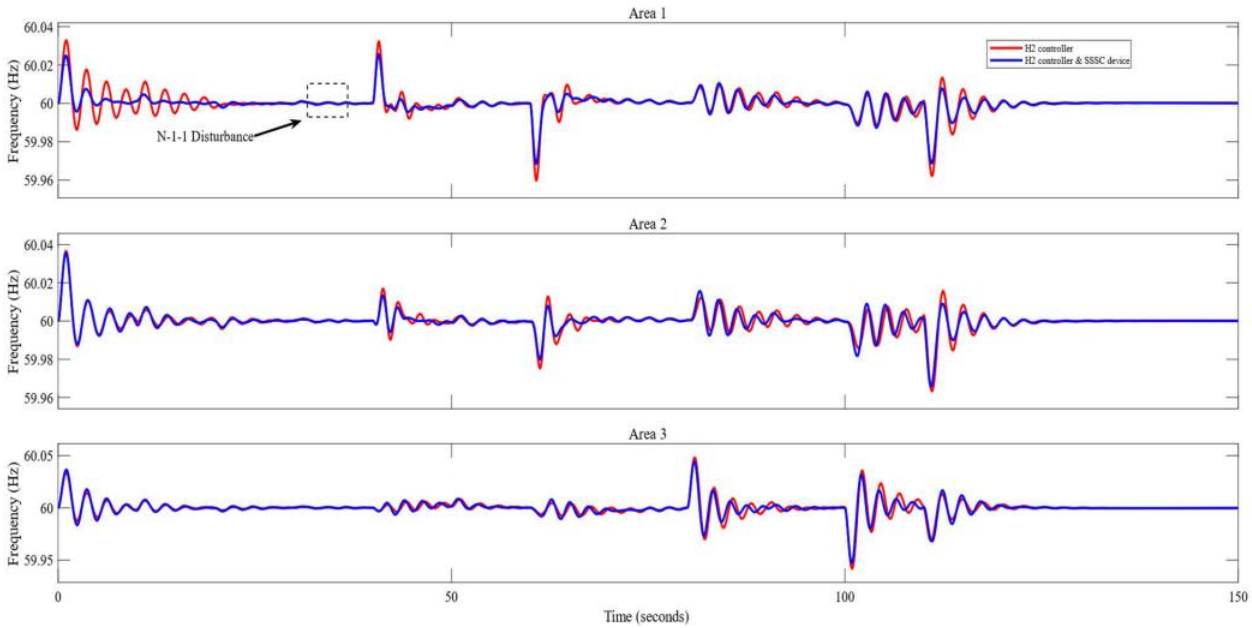

Fig. 5.25. Frequency response of three areas in two cases; H_2 controller, and H_2 controller + SSSC device under N-1-1 contingency events in lines.

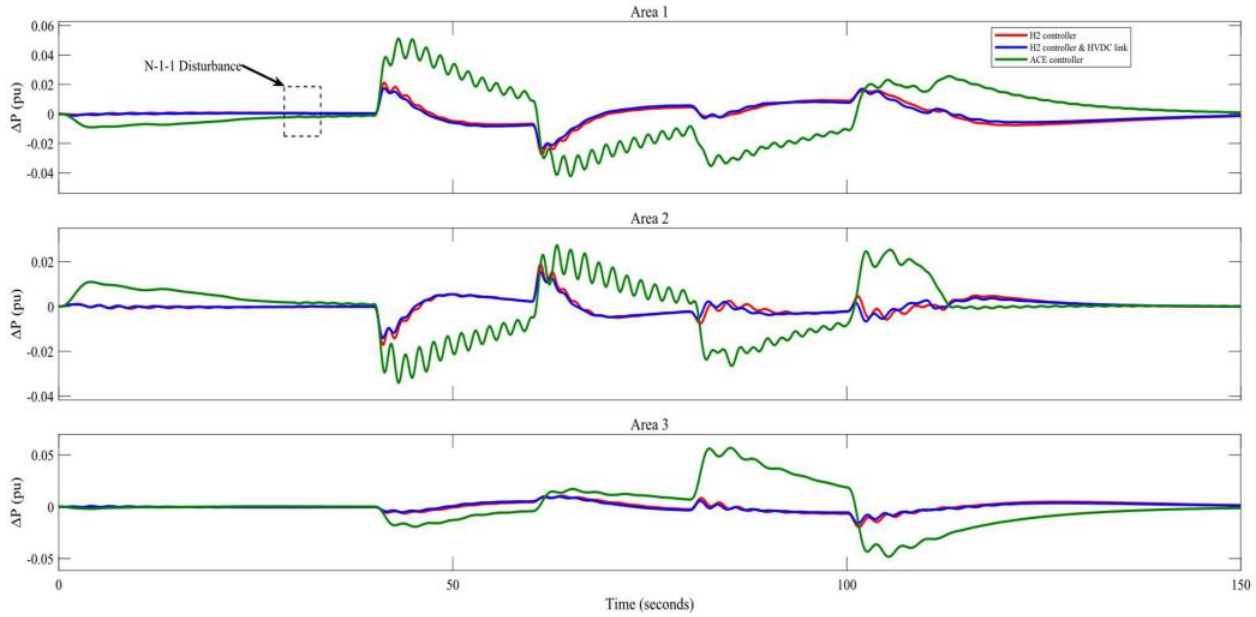

Fig. 5.26. Power deviation of tie-lines of three areas in three cases; ACE controller, H_2 controller, and H_2 controller + SSSC device under N-1-1 contingency events in lines.

5.6 HVDC Link and SSSC Device Comparison

Two different techniques are added to the three-area system with high penetration of wind turbines. An HVDC link and an SSSC device are considered to emphasize their roles in reducing frequency deviations and improved power damping. There is a comparison between the two cases for the three-area system under N-1 condition with the HVDC link and SSSC device. The first comparison is for frequency deviation, shown in Fig. 5.27, where both techniques produce almost the same response. However, the HVDC presents almost the same response during pre- and post-disturbances compared with the SSSC device and has a low frequency deviation. It ranges from 59.95 to 60.05Hz, in contrast with the SSSC device which has a frequency deviation range from 59.93 to 60.12Hz during the disturbance. This change also can be seen in other periods of the simulation when there is high penetration of wind generation.

Power flow in tie-lines for the three-area system has its own comparison between the HVDC and SSSC techniques. In Fig. 5.28, the HVDC case has a fast and smooth response with

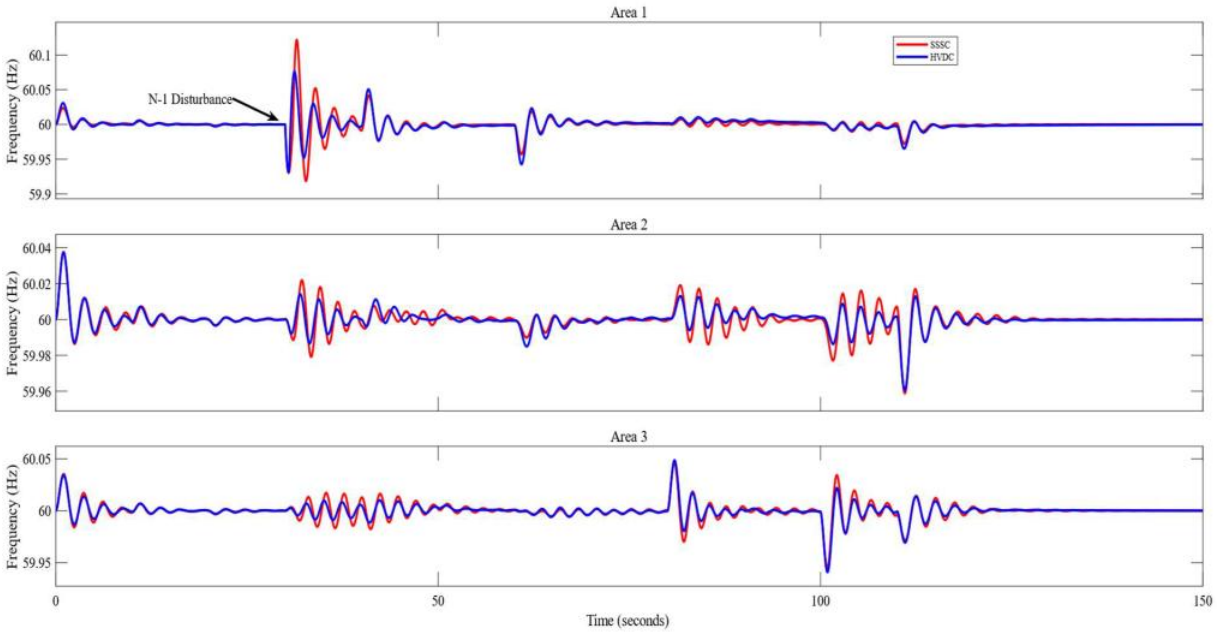

Fig. 5.27. Frequency deviation of three areas with H_2 controller in two cases; HVDC link and SSSC.

obvious differences in contrast to the SSSC case and that is shown in the second and third area. These areas display that the HVDC case has power deviation with large range if this range is checked with the SSSC case, shown between 80 to 120 seconds, and this comes from the order of the transfer functions that represent both techniques used in this work in addition to design of the

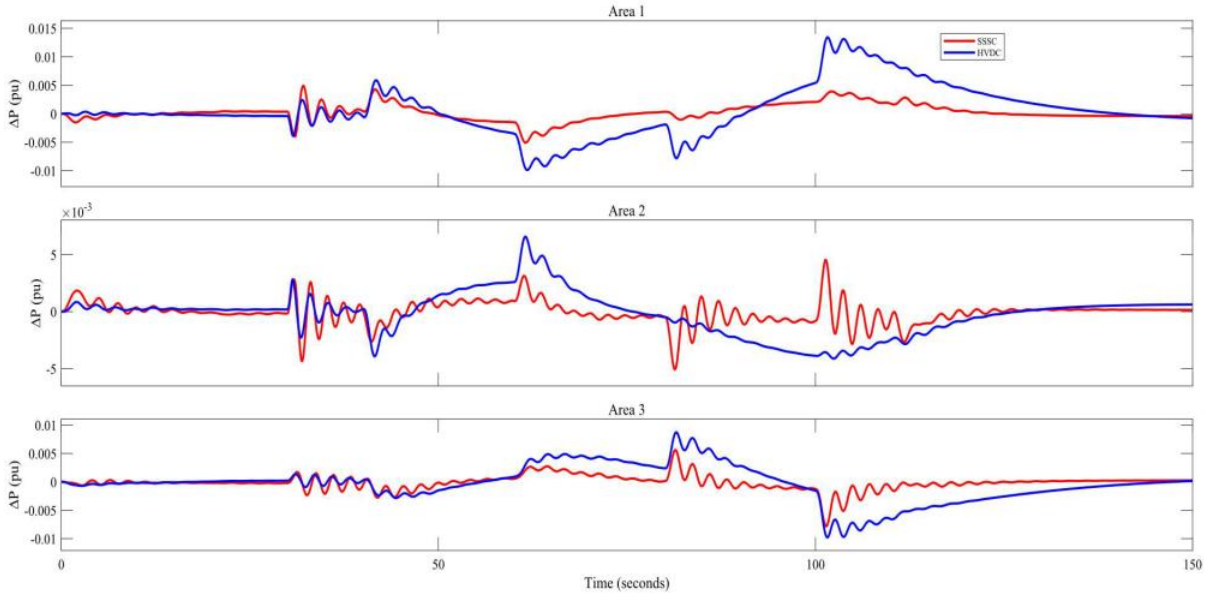

Fig. 5.28. Power deviation of three areas with H_2 controller in two cases; HVDC link and SSSC.

H_2 controller. The first-order transfer function of HVDC link assists in having fast and large deviations in power flow for tie-lines while the third-order transfer function of SSSC device offers low response with time. These differences and others would give the priority to adopt HVDC links in power systems rather than SSSC devices to increase the time response and reduce frequency oscillations and power damping, especially with systems suffering a large volume of wind generation and dynamic events.

5.7 Eigenvalues Examination

One of the ways to show stability optimization of the system with the H_2 controller and HVDC link or SSSC device is examination of eigenvalues through comparison the original eigenvalues. The eigenvalues of the total system can be evaluated from (4.1) and (4.2) via $\lambda_i = \sigma_i \mp j\omega_i$, and $\sigma_i = \zeta\omega_n$ and $\omega_n\sqrt{\zeta^2 - 1}$ where ζ is the damping ratio and ω_n is the natural frequency. This work will focus on eigenvalues near the imaginary axis because they are least damped and correspond to reduced stability margins. For the three-area system, it looks from Fig. 5.29 that performance of the original system with black + has been improved through shifting of eigenvalues away from the imaginary axis. The performance is enhanced through increasing ζ

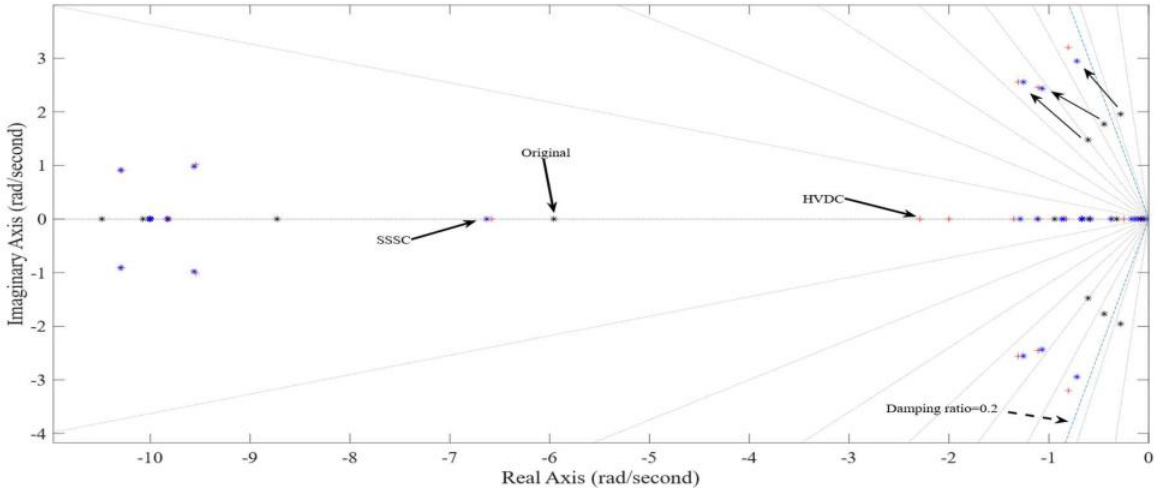

Fig. 5.29. Results of comparison between original system with ACE controller and system with H_2 controller and HVDC link and SSSC device.

from 0.142, the lowest eigenvalue in the system with conventional controller, to 0.244 in the system with HVDC link, with red *, and 0.237 in the system with SSSC device, with blue +. These eigenvalues are improved after considering a damping ratio limit ζ equal to 0.2. From the figure, it shows that eigenvalues of HVDC and SSSC move toward left *s*-plane and that helps in increasing the stability of the system. All changes in the eigenvalues of the system under different conditions, illustrated in Table 7 through Table 9.

Table 7. Mode Characteristics of the Original Study System

Eigenvalue	Damping	Freq. (rad/s)
-0.281+1.96i	0.142	1.98
-0.281-1.96i	0.142	1.98
-0.446+1.77i	0.244	1.83
-0.446-1.77i	0.244	1.83
-0.606+1.48i	0.380	1.60
-0.606-1.48i	0.380	1.60

Table 8. Mode characteristics of the study system with H_2 controller and HVDC link

Eigenvalue	Damping	Freq. (rad/s)
-1.110+2.46i	0.411	2.69
-1.110-2.46i	0.411	2.69
-1.310+2.56i	0.455	2.87
-1.310-2.56i	0.455	2.87
-0.804+3.20i	0.244	3.30
-0.804-3.20i	0.244	3.30
-9.540+1.01i	0.994	9.60
-9.540-1.01i	0.994	9.60

Table 9. Mode characteristics of the study system with H_2 controller and SSSC device

Eigenvalue	Damping	Freq.(rad/s)
-1.07+2.44i	0.401	2.66
-1.07-2.44i	0.401	2.66
-1.25+2.55i	0.441	2.85
-1.25-2.55i	0.441	2.85
-0.719+2.95i	0.237	3.03
-0.719-2.95i	0.237	3.03
-9.56+0.979i	0.995	9.61
-9.56-0. 979i	0.995	9.61

6 The H_2 Control Method for the Iraqi National Super Grid System

6.1 Iraqi National Super Grid System (INSGS)

The Iraqi national electrical system includes hundreds of lines and buses, 400kV and 132kV, and this network experienced several circumstances resulting in a lack of generation and an imbalance between electricity production and demand, especially during between 1991 and 2014. This causes unstable condition in the Iraqi electrical system network in addition to the delay of replacement or maintenance of power components. Various works dealt with Iraqi national super grid system (INSGS) to show the optimal control methods to increase the stability and reliability [109]-[112]. This work will apply the proposed H_2 control method on INSGS model in [110, 112] that consists of 19 buses and 29 transmission lines for 400KV transmission level, INSGS is the backbone of Iraqi electrical network shown in Fig. 6.1. This system is divided into six areas, two hydro turbines, three steam non-reheat turbines, and one steam reheat turbine area and loads are represented by static admittance while lines are expressed by equivalent π representation model, Fig. 6.2a. All network data are in per-unit to refer a common base power of 100MVA for 400kV as base voltage and all this data is tabulated in the appendix [110, 112].

This system is evaluated to receive various modifications in the future to reduce unstable conditions and increase reliability and stability. The modifications include installing PV generation in the third area and HVDC link between the first and sixth area to reduce short circuit levels and transfer power through peak load times seasonally. Moreover, there is a plan, adopted by the Ministry of Electricity in Baghdad to start power marketing with synchronizing ac tie-lines between Iraq and Turkey and Iran. There are isolated areas in the eastern part of Iraq that are fed

by Iran ac tie-lines presently, and a HVDC link with Kuwait to transfer power to Turkey and then to Europe [113]. The studied case and future case of INSGS are demonstrated in Fig. 6.2b.

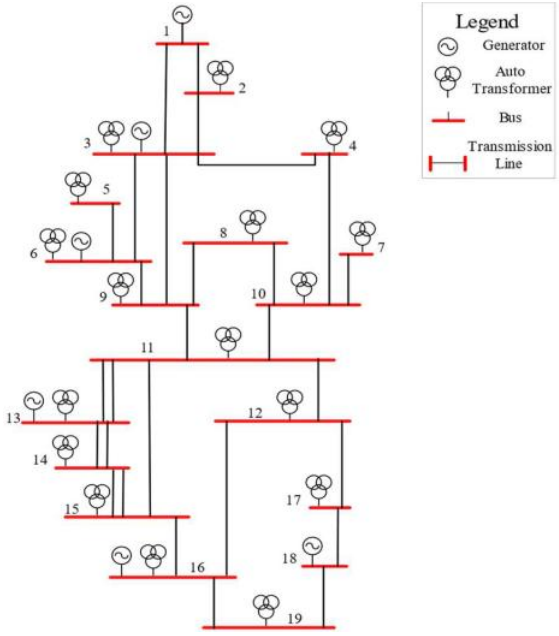

Fig. 6.1. One-line diagram for Iraqi National Super Grid System (INSGS) [109, 111].

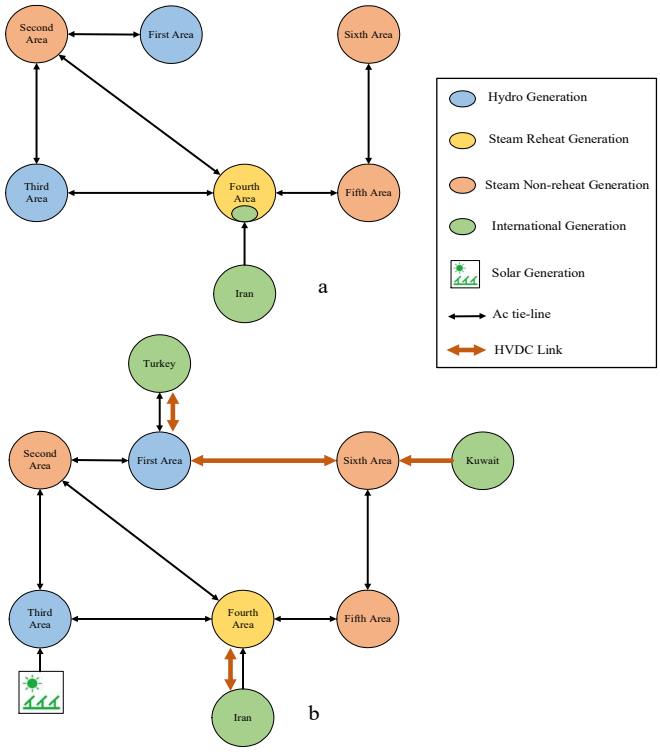

Fig 6.2. INSGS areas; a) recent system, b) future plan.

6.2 Load Frequency Control Model of INSGS

The studied LFC model of INSGS, before the modifications, is linearized and represented in the state-space like in (4.1) and (4.2), shown in Fig. 6.3.

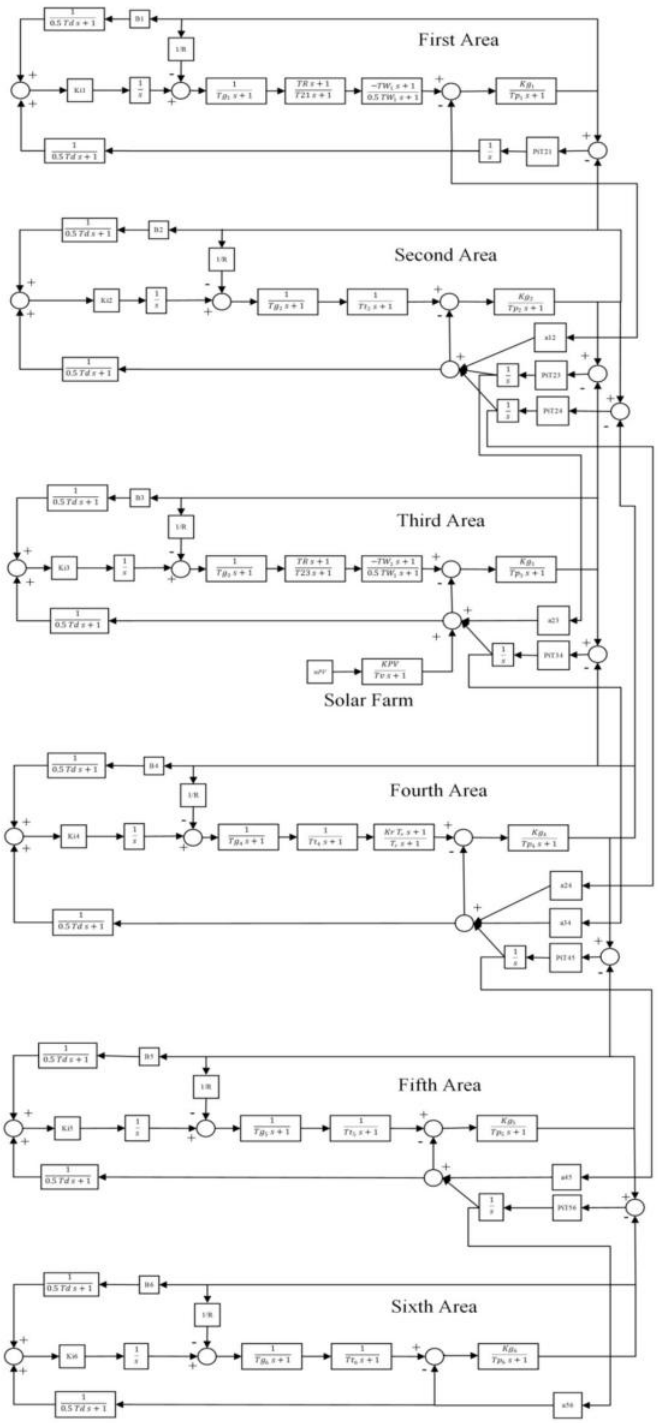

Fig. 6.3. Block diagram of INSGS for LFC model.

The power system investigated in this work is given in [110] and this system is modified with time delay transfer function and common ACE control approach. The state-space variables controlled through the ACE approach are shown in Fig. 6.3. Generators in this system are considered as thermal units and transfer functions of those units are given in

Reheat turbine:

$$\frac{Kr_i Tr_i s+1}{Tr_i s+1}, \tag{6.1}$$

Hydro turbine:

$$\frac{-TW_i s+1}{0.5TW_i s+1}, \tag{6.2}$$

Hydro governor:

$$\frac{TR\ s+1}{T2_i s+1}, \tag{6.3}$$

Time delay:

$$\frac{1}{0.5\ Td\ s+1}, \tag{6.4}$$

while the ACE in all six areas are given as in

$$ACE_i = \Delta Ptie_i + B_i \Delta f_i\ , \tag{6.5}$$

where, Kr is a reheat constant, and T_r reheat time constant, T_W: water starting time, T_R: dashpot time constant of hydro-governor, T_2: hydro-governor time constant, Δf: the incremental frequency deviation [108]. The state-space equations for this system, for each area before placing the time delay and the solar generation, are given in

Area One:

$$\dot{x_1} = \frac{-1}{Tp_1} x_1 + \frac{Kg_1}{Tp_1} x_2 - \frac{Kg_1}{Tp_1} x_5, \tag{6.6}$$

$$\dot{x_2} = -\frac{2}{TW_1} x_2 - 2\dot{x}_3 + \frac{2}{TW_1} x_3, \tag{6.7}$$

$$\dot{x_3} = -\frac{1}{T2_1} x_3 + \frac{TR}{T2_1} \dot{x}_4 + \frac{1}{T2_1} x_4, \tag{6.8}$$

$$\dot{x_4} = \frac{-1}{R_1 Tg_1} x_1 - \frac{1}{Tg_1} x_4 + \frac{1}{Tg_1} x_6, \tag{6.9}$$

$$\dot{x_5} = 2\pi T_{12} x_1 - 2\pi T_{12} x_7, \tag{6.10}$$

$$\dot{x_6} = -Ki_1 B_1 x_1 - Ki_1 x_5. \tag{6.11}$$

Area Two:

$$\dot{x_7} = \frac{-1}{Tp_2} x_7 + \frac{Kg_2}{Tp_2} x_8 + a_{12} \frac{Kg_2}{Tp_2} x_5 - \frac{Kg_2}{Tp_2} x_{10} - \frac{Kg_2}{Tp_2} x_{11}, \tag{6.12}$$

$$\dot{x_8} = \frac{-1}{Tt_2} x_8 + \frac{1}{Tt_2} x_9, \tag{6.13}$$

$$\dot{x_9} = \frac{-1}{R_2 Tg_2} x_7 - \frac{1}{Tg_2} x_9 + \frac{1}{Tg_2} x_{12}, \tag{6.14}$$

$$\dot{x_{10}} = 2\pi T_{23} x_7 - 2\pi T_{23} x_{13}, \tag{6.15}$$

$$\dot{x_{11}} = 2\pi T_{24} x_7 - 2\pi T_{24} x_{19}, \tag{6.16}$$

$$\dot{x_{12}} = -Ki_2 B_2 x_7 - Ki_2 x_{10} - Ki_2 x_{11} + a_{12} Ki_2 x_5. \tag{6.17}$$

Area Three:

$$\dot{x_{13}} = \frac{-1}{Tp_3} x_{13} + \frac{Kg_3}{Tp_3} x_{14} + a_{23} \frac{Kg_3}{Tp_3} x_5 - \frac{Kg_3}{Tp_3} x_{17}, \tag{6.18}$$

$$\dot{x_{14}} = -\frac{2}{TW_3} x_{14} - 2\dot{x}_{15} + \frac{2}{TW_3} x_{15}, \tag{6.19}$$

$$\dot{x_{15}} = -\frac{1}{T2_3}x_{15} + \frac{TR}{T2_3}\dot{x}_{16} + \frac{1}{T2_3}x_{16}, \tag{6.20}$$

$$\dot{x_{16}} = \frac{-1}{R_3 Tg_3}x_{13} - \frac{1}{Tg_3}x_{16} + \frac{1}{Tg_3}x_{18}, \tag{6.21}$$

$$\dot{x_{17}} = 2\pi T_{34}x_{13} - 2\pi T_{34}x_{19}, \tag{6.22}$$

$$\dot{x_{18}} = -Ki_3 B_3 x_{13} - Ki_3 x_{17} + a_{23}Ki_3 x_{10}. \tag{6.23}$$

Area Four:

$$\dot{x_{19}} = \frac{-1}{Tp_4}x_{19} + \frac{Kg_4}{Tp_4}x_{20} + a_{24}\frac{Kg_4}{Tp_4}x_{11} + a_{34}\frac{Kg_4}{Tp_4}x_{17} - \frac{Kg_4}{Tp_4}x_{23}, \tag{6.24}$$

$$\dot{x_{20}} = -\frac{1}{Tr}x_{20} + Kr\,\dot{x}_{21} + \frac{1}{Tr}x_{21}, \tag{6.25}$$

$$\dot{x_{21}} = \frac{-1}{Tt_4}x_{21} + \frac{1}{Tt_4}x_{22}, \tag{6.26}$$

$$\dot{x_{22}} = \frac{-1}{R_4 Tg_4}x_{19} - \frac{1}{Tg_4}x_{22} + \frac{1}{Tg_4}x_{24}, \tag{6.27}$$

$$\dot{x_{23}} = 2\pi T_{45}x_{19} - 2\pi T_{45}x_{25}, \tag{6.28}$$

$$\dot{x_{24}} = -Ki_4 B_4 x_{19} - Ki_4 x_{23} + a_{24}Ki_4 x_{11} + a_{34}Ki_4 x_{17}. \tag{6.29}$$

Area Five:

$$\dot{x_{25}} = \frac{-1}{Tp_5}x_{25} + \frac{Kg_5}{Tp_5}x_{26} + a_{45}\frac{Kg_5}{Tp_5}x_{23} - \frac{Kg_5}{Tp_5}x_{28}, \tag{6.30}$$

$$\dot{x_{26}} = \frac{-1}{Tt_5}x_{26} + \frac{1}{Tt_5}x_{27}, \tag{6.31}$$

$$\dot{x_{27}} = \frac{-1}{R_5 Tg_5}x_{25} - \frac{1}{Tg_5}x_{27} + \frac{1}{Tg_5}x_{29}, \tag{6.32}$$

$$\dot{x_{28}} = 2\pi T_{56}x_{25} - 2\pi T_{56}x_{30}, \tag{6.33}$$

$$\dot{x_{29}} = -Ki_5 B_5 x_{25} - Ki_5 x_{28} + a_{45} Ki_5 x_{23}. \tag{6.34}$$

Area Six:

$$\dot{x_{30}} = \frac{-1}{Tp_6} x_{30} + \frac{Kg_6}{Tp_6} x_{31} + a_{56} \frac{Kg_6}{Tp_6} x_{28}, \tag{6.35}$$

$$\dot{x_{31}} = \frac{-1}{Tt_6} x_{31} + \frac{1}{Tt_6} x_{32}, \tag{6.36}$$

$$\dot{x_{32}} = \frac{-1}{R_6 Tg_6} x_{30} - \frac{1}{Tg_6} x_{32} + \frac{1}{Tg_6} x_{33}, \tag{6.37}$$

$$\dot{x_{33}} = -Ki_6 B_6 x_{30} + a_{56} Ki_6 x_{28}. \tag{6.38}$$

where, $Ki_1, Ki_2, Ki_3, Ki_4, Ki_5, Ki_6$: six ACE area controllers, $R_1, R_2, R_3, R_4, R_5, R_6$: speed regulation parameters. After simulating the original system in [110, 112] without time delay or the solar generation, it shows during the analysis that there is a critical condition because of the one eigenvalue, which is almost equal to zero, causes this issue and this eigenvalue, which is λ_{33}, comes from one of the six tie-lines of the INSGS. Therefore, a reduced row echelon form technique is utilized to reduce number of tie-line power changes in the six-area system.

To reduce the size of the A-matrix due to having the critical eigenvalue, the reduced row echelon form or Gauss-Jordan elimination method is used and applied on synchronizing power coefficients, as given in

$$\begin{bmatrix} \dot{x_5} \\ \dot{x_{10}} \\ \dot{x_{11}} \\ \dot{x_{17}} \\ \dot{x_{23}} \\ \dot{x_{28}} \end{bmatrix} = \begin{bmatrix} 2\pi T_{12} & -2\pi T_{12} & 0 & 0 & 0 & 0 \\ 0 & 2\pi T_{23} & -2\pi T_{23} & 0 & 0 & 0 \\ 0 & 2\pi T_{24} & 0 & -2\pi T_{23} & 0 & 0 \\ 0 & 0 & 2\pi T_{34} & -2\pi T_{34} & 0 & 0 \\ 0 & 0 & 0 & 2\pi T_{45} & -2\pi T_{45} & 0 \\ 0 & 0 & 0 & 0 & 2\pi T_{56} & -2\pi T_{56} \end{bmatrix} \begin{bmatrix} x_1 \\ x_7 \\ x_{13} \\ x_{19} \\ x_{25} \\ x_{30} \end{bmatrix} \tag{6.39}$$

After using the rref MATLAB command, the result of the reduced row echelon is written as

$$\begin{bmatrix} q_{11} & q_{12} & q_{13} & q_{14} & q_{15} & q_{16} \\ q_{21} & q_{22} & q_{23} & q_{24} & q_{25} & q_{26} \\ q_{31} & q_{32} & q_{33} & q_{34} & q_{35} & q_{36} \\ q_{41} & q_{42} & q_{43} & q_{44} & q_{45} & q_{46} \\ q_{51} & q_{52} & q_{53} & q_{54} & q_{55} & q_{56} \\ q_{61} & q_{62} & q_{63} & q_{64} & q_{65} & q_{66} \end{bmatrix} \begin{bmatrix} \dot{x_5} \\ \dot{x_{10}} \\ \dot{x_{11}} \\ \dot{x_{17}} \\ \dot{x_{23}} \\ \dot{x_{28}} \end{bmatrix} = \begin{bmatrix} 1 & 0 & 0 & 0 & 0 & -1 \\ 0 & 1 & 0 & 0 & 0 & -1 \\ 0 & 0 & 1 & 0 & 0 & -1 \\ 0 & 0 & 0 & 1 & 0 & -1 \\ 0 & 0 & 0 & 0 & 1 & -1 \\ 0 & 0 & 0 & 0 & 0 & 0 \end{bmatrix} \begin{bmatrix} x_1 \\ x_7 \\ x_{13} \\ x_{19} \\ x_{25} \\ x_{30} \end{bmatrix} \tag{6.40}$$

From the equation above, the last row could be used to coordinate which element would be reduced of the *A*-matrix.

$$[q_{61} \quad q_{62} \quad q_{63} \quad q_{64} \quad q_{65} \quad q_{66}] \begin{bmatrix} \dot{x_5} \\ \dot{x_{10}} \\ \dot{x_{11}} \\ \dot{x_{17}} \\ \dot{x_{23}} \\ \dot{x_{28}} \end{bmatrix} = [0 \quad 1 \quad -1.4 \quad 1.06 \quad 0 \quad 0] \begin{bmatrix} \dot{x_5} \\ \dot{x_{10}} \\ \dot{x_{11}} \\ \dot{x_{17}} \\ \dot{x_{23}} \\ \dot{x_{28}} \end{bmatrix} \tag{6.41}$$

In other words, q_{61}, q_{65}, and q_{66} are equal to zeros. Then

$$q_{62}x_{10} + q_{63}x_{11} + q_{64}x_{17} = 0, \tag{6.42}$$

$x_{17} = \frac{-q_{62}}{q_{64}} x_{10} - \frac{q_{63}}{q_{64}} x_{11}$ or

$$x_{17} = -0.94\, x_{10} + 1.32\, x_{11}. \tag{6.43}$$

Four equations from (6.21) to (6.41) would be modified with this equation and renumbered in a new sequence. Modified equations are given in

$$\dot{x_{13}} = \frac{-1}{Tp_3} x_{13} + \frac{Kg_3}{Tp_3} x_{14} - \frac{Kg_3}{Tp_3}(a_{23} - \frac{q_{62}}{q_{64}})x_{10} + (\frac{Kg_3}{Tp_3}\frac{q_{63}}{q_{64}})x_{11}, \tag{6.18*}$$

$$\dot{x_{14}} = \frac{-2}{TW_1} x_{14} - 2\dot{x_{15}} + \frac{2}{TW_1} x_{15}, \tag{6.19*}$$

$$\dot{x_{15}} = \frac{-1}{T_{23}} x_{15} - \frac{TR}{T_{23}} \dot{x_{16}} + \frac{1}{T_{23}} x_{16}, \tag{6.20*}$$

$$\dot{x_{16}} = \frac{-1}{R_3 Tg_3} x_{13} - \frac{1}{Tg_3} x_{16} + \frac{1}{Tg_{13}} x_{17}, \tag{6.21*}$$

$$\dot{x_{17}} = -Ki_3 B_3 x_{13} - Ki_3(a_{23} - \frac{q_{62}}{q_{64}})x_{10} + (Ki_3 \frac{q_{63}}{q_{64}})x_{11}, \quad (6.23^*)$$

$$\dot{x_{18}} = \frac{-1}{Tp_4} x_{18} + \frac{Kg_4}{Tp_4} x_{19} - \frac{Kg_4}{Tp_4} x_{22} - \frac{Kg_4}{Tp_4}(a_{24} - a_{34}\frac{q_{63}}{q_{64}})x_{11} + (a_{34}\frac{Kg_4}{Tp_4}\frac{q_{62}}{q_{64}})x_{10}, \quad (6.24^*)$$

$$\dot{x_{19}} = \frac{-1}{T_r} x_{19} - Kr\dot{x_{20}} + \frac{1}{T_r} x_{20}, \quad (6.25^*)$$

$$\dot{x_{20}} = \frac{-1}{Tt_4} x_{20} + \frac{1}{Tt_4} x_{21}, \quad (6.26^*)$$

$$\dot{x_{21}} = \frac{-1}{R_4 Tg_4} x_{18} - \frac{1}{Tg_4} x_{21} + \frac{1}{Tg_4} x_{23}, \quad (6.27^*)$$

$$\dot{x_{22}} = 2\pi T_{45} x_{18} - 2\pi T_{45} x_{24}, \quad (6.28^*)$$

$$\dot{x_{23}} = -Ki_4 B_4 x_{18} - Ki_4(a_{24} - a_{34}\frac{q_{63}}{q_{64}})x_{11} + (Ki_4 a_{34}\frac{q_{62}}{q_{64}})x_{10} - Ki_4 x_{22}, \quad (6.29^*)$$

$$\dot{x_{24}} = \frac{-1}{Tp_5} x_{24} + \frac{Kg_5}{Tp_5} x_{25} - \frac{Kg_5}{Tp_5} a_{45} x_{22} - \frac{Kg_5}{Tp_5} x_{27}, \quad (6.30^*)$$

$$\dot{x_{25}} = \frac{-1}{Tt_5} x_{25} + \frac{1}{Tt_5} x_{26}, \quad (6.31^*)$$

$$\dot{x_{26}} = \frac{-1}{R_5 Tg_5} x_{24} - \frac{1}{Tg_5} x_{26} + \frac{1}{Tg_5} x_{28}, \quad (6.32^*)$$

$$\dot{x_{27}} = 2\pi T_{56} x_{24} - 2\pi T_{56} x_{29}, \quad (6.33^*)$$

$$\dot{x_{28}} = -Ki_5 B_5 x_{24} - Ki_5 a_{45} x_{22} - Ki_5 x_{27}, \quad (6.34^*)$$

$$\dot{x_{29}} = \frac{-1}{Tp_6} x_{29} + \frac{Kg_6}{Tp_6} x_{30} - \frac{Kg_6}{Tp_6} a_{56} x_{27}, \quad (6.35^*)$$

$$\dot{x_{30}} = \frac{-1}{Tt_6} x_{30} + \frac{1}{Tt_6} x_{31}, \quad (6.36^*)$$

$$\dot{x_{31}} = \frac{-1}{R_6 Tg_6} x_{29} - \frac{1}{Tg_6} x_{31} + \frac{1}{Tg_6} x_{32}, \quad (6.37^*)$$

$$\dot{x_{32}} = -Ki_6 B_6 x_{29} - Ki_6 a_{56} x_{27}. \qquad (6.38^*)$$

The results of this modification could be shown in Table 10 that displays the difference between the eigenvalues of INSGS before and after removing the critical eigenvalue.

Table 10. Eigenvalue comparison for INSGS

Pre-Reduction	Post-Reduction
-0.064+14.24i	-0.064+14.24i
-0.064-14.24i	-0.064-14.24i
-0.078+12.58i	-0.078+12.58i
-0.078-12.58i	-0.078-12.58i
-0.042+9.1i	-0.042+9.1i
-0.042-9.1i	-0.042-9.1i
-0.066+7.16i	-0.066+7.16i
-0.066-7.16i	-0.066-7.16i
-10.47+0i	-10.47+0i
-10.18+0i	-10.18+0i
-8.344+0i	-8.35+0i
-8.35+0i	-8.34+0i
-0.054+3.62i	-0.041+3.61i
-0.054-3.62i	-0.041-3.61i
-3.826+0i	-3.826+0i
-3.164+0i	-3.087+0i
-2.71+0i	-2.634+0i
-2.04+0i	-2.014+0i
-1.19+0i	-1.43+0i
-0.432+0i	-0.414+0i
-0.21+0.27i	-0.16+0.24i
-0.21-0.27i	-0.16-0.24i
-0.083+0.18i	-0.14+0.19i
-0.083-0.18i	-0.14-0.19i
-0.051+0.15i	-0.19+0i
-0.051-0.15i	-0.08+0.09i
-0.09+0.1i	-0.08-0.09i
-0.09-0.1i	-0.112-0i
-0.14+0i	-0.018+0.052i
-0.12+0i	-0.018-0.052i
-0.014+0.05i	-0.011+0.01i
-0.014-0.05i	-0.011-0.01i
-2.36e-16	----------

After this reduction, a time delay and renewable resource are added to the INSGS in order to prepare it as a reference power model with the conventional ACE control method. A time delay transfer function is placed on each input entered to the ACE controller and by this step the system size increased from 32 state-space variable to 44 and those new variables are given as

$$\dot{x_{33}} = \frac{-1}{Td}x_{33} + \frac{B_1}{Td}x_1, \tag{6.44}$$

$$\dot{x_{34}} = \frac{-1}{Td}x_{34} + \frac{1}{Td}x_5, \tag{6.45}$$

$$\dot{x_{35}} = \frac{-1}{Td}x_{35} + \frac{B_2}{Td}x_1, \tag{6.46}$$

$$\dot{x_{36}} = \frac{-1}{Td}x_{36} + \frac{1}{Td}x_{10} + \frac{1}{Td}x_{11} + a_{12}\frac{1}{Td}x_5, \tag{6.47}$$

$$\dot{x_{37}} = \frac{-1}{Td}x_{37} + \frac{B_3}{Td}x_{13}, \tag{6.48}$$

$$\dot{x_{38}} = \frac{-1}{Td}x_{38} + (a_{23} - \frac{q_{62}}{q_{64}})\frac{1}{Td}x_{10} - \frac{q_{63}}{q_{64}}\frac{1}{Td}x_{11}, \tag{6.49}$$

$$\dot{x_{39}} = \frac{-1}{Td}x_{39} + \frac{B_4}{Td}x_{18}, \tag{6.50}$$

$$\dot{x_{40}} = \frac{-1}{Td}x_{40} + (a_{24} - a_{34}\frac{q_{63}}{q_{64}})\frac{1}{Td}x_{11} - a_{34}\frac{q_{62}}{q_{64}}\frac{1}{Td}x_{10} + \frac{1}{Td}x_{22}, \tag{6.51}$$

$$\dot{x_{41}} = \frac{-1}{Td}x_{41} + \frac{B_5}{Td}x_{24}, \tag{6.52}$$

$$\dot{x_{42}} = \frac{-1}{Td}x_{42} + \frac{1}{Td}x_{27} + \frac{a_{45}}{Td}x_{22}, \tag{6.53}$$

$$\dot{x_{43}} = \frac{-1}{Td}x_{43} + \frac{B_6}{Td}x_{29}, \tag{6.54}$$

$$\dot{x_{44}} = \frac{-1}{Td}x_{44} + \frac{a_{56}}{Td}x_{27}, \tag{6.55}$$

This placement of 12 variables in the system would change the configuration of the system and impacts the following state-space variables

$$\dot{x_6} = -Ki_1x_{33} - Ki_1x_{34}, \tag{6.11*}$$

$$\dot{x_{12}} = -Ki_2x_{35} - Ki_2x_{36}, \tag{6.17*}$$

$$\dot{x_{17}} = -Ki_3x_{37} - Ki_3x_{38}, \tag{6.22*}$$

$$\dot{x_{23}} = -Ki_4 x_{39} - Ki_4 x_{40}, \tag{6.28*}$$

$$\dot{x_{28}} = -Ki_5 x_{41} - Ki_5 x_{42}, \tag{6.34*}$$

$$\dot{x_{32}} = -Ki_6 x_{43} - Ki_6 x_{44}. \tag{6.38*}$$

Then a solar generation is added to the third area where is expected to place due to the high sunlight intensity in the western part of Iraq. This renewable generation would be connected to the third area through a transfer function $\frac{KPV}{Tv\,s+1}$ where the *KPV* is the gain of solar generation in per unit, represents 20% of solar generation to the total generation in INSGS, and *Tv* is the solar time constant. The new state-space variable can be given as

$$\dot{x_{45}} = \frac{-1}{Tv} x_{45} + \frac{KPV}{Tv} u_2, \tag{6.56}$$

Where u_2 is the disturbance input while (6.47) is modified with this add and given as

$$\dot{x_{13}} = \frac{-1}{Tp_3} x_{13} + \frac{Kg_3}{Tp_3} x_{14} - \frac{Kg_3}{Tp_3}(a_{23} - \frac{q_{62}}{q_{64}}) x_{10} + (\frac{Kg_3}{Tp_3}\frac{q_{63}}{q_{64}}) x_{11} + \frac{Kg_3}{Tp_3} x_{45}. \tag{6.18**}$$

The output of the solar generation is illustrated in Fig. 6.4 where the generation was 0.2pu of the generation of the system and goes down after 40 second to display low generation with high demand phenomenon.

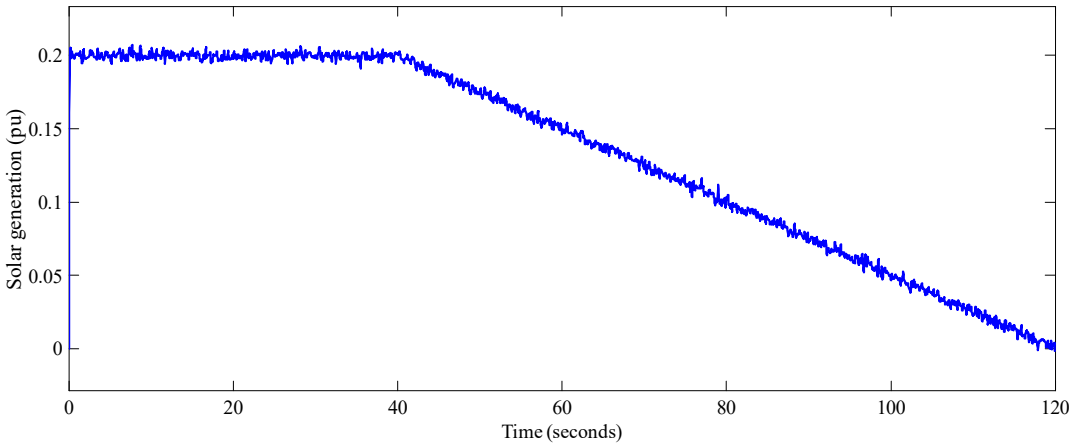

Fig. 6.4. Solar farm generation in the third area of INSGS.

Also, the load change (ΔP_L) in the system, shown in Fig. 6.5, is assumed to be in the second area and that impact the equation (6.12) and make it as written

$$\dot{x_7} = \frac{-1}{Tp_2}x_7 + \frac{Kg_2}{Tp_2}x_8 + a_{12}\frac{Kg_2}{Tp_2}x_5 - \frac{Kg_2}{Tp_2}x_{10} - \frac{Kg_2}{Tp_2}x_{11} - \frac{Kg_2}{Tp_2}\Delta P_L, \qquad (6.12^*)$$

In Fig. 6.5, the demand load is decreased from 0.018pu. to zero load at 80 seconds and then it starts increasing its value with time due to peak period at sunset as an example. This case tries to mimic real conditions when demand load begins to have high amount while the solar generation is in low level.

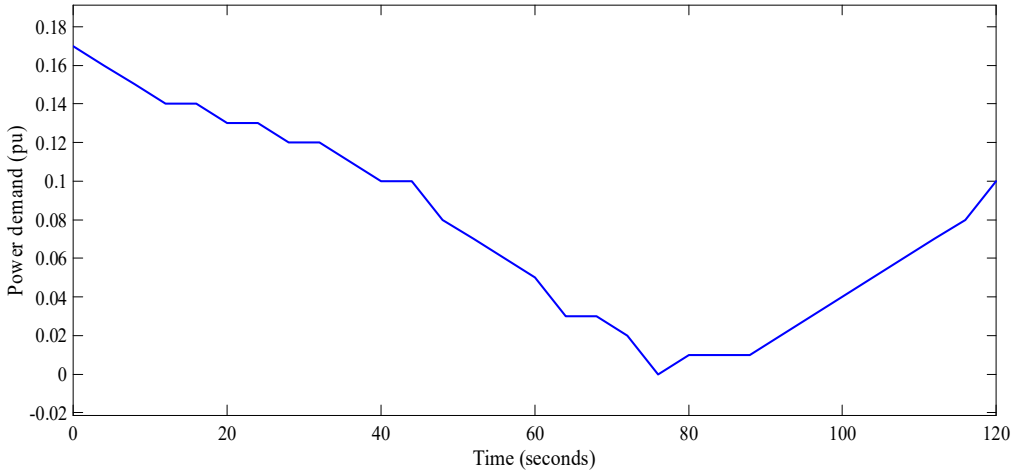

Fig. 6.5. Load change in INSGS added to the second area.

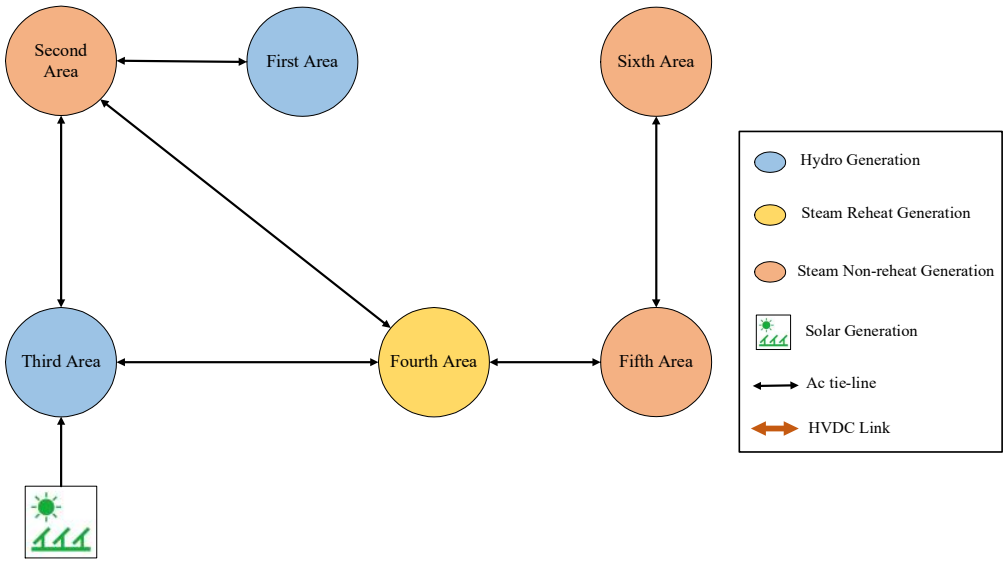

Fig. 6.6. INSGS model under the studied condition.

The Iraqi model, under the condition in Fig. 6.6, is simulated in MATLAB Simulink™ environment with all previous modifications in order to make the original model and compare it with the proposed control method. The frequency deviation output of each area is presented in Fig. 6.7 where influences of solar generation and load variation are in existence obviously. Moreover, power deviation for all areas are illustrated in Fig. 6.8. These figures explain the fluctuations of frequency and power flow in each area during normal case with changeable load and power generation.

6.3 The H_2 Controller in INSGS Model

The Iraqi system (INSGS) under a normal condition is analyzed with the proposed H_2 control approach. This study determines the design needed to operate this controller type. The number of variables in state-space form of INSGS is 45 variables. The arrangements of these variables with respect to the inputs and outputs is essential to produce a proper action of the controller. The controlled inputs matrix, B_1, of the system are six inputs and they are assumed to

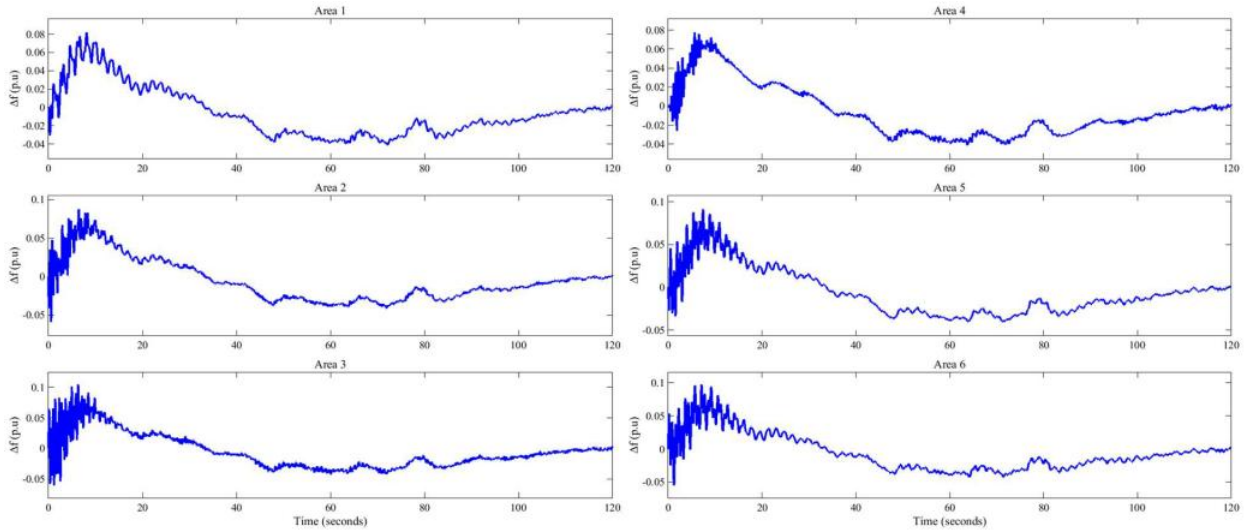

Fig 6.7. Frequency deviation of INSGS under studied case.

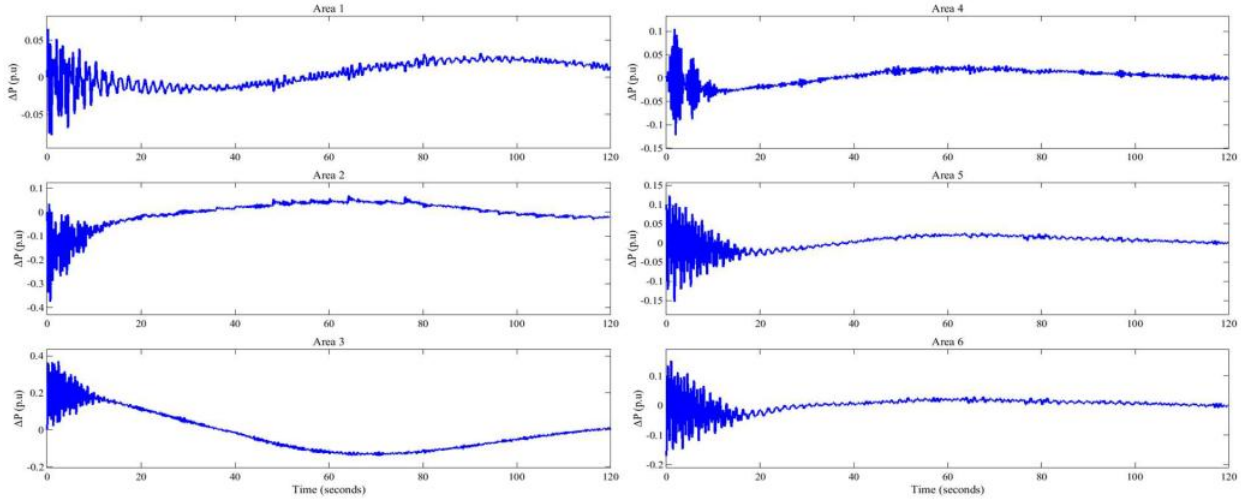

Fig. 6.8. Power deviation of INSGS under studied case.

be connected to six variables, which are x_6, x_{12}, x_{17}, x_{23}, x_{28}, and x_{32}. The sensor or measurement outputs matrix C_1, x_{33}, x_{34}, x_{35}, x_{36}, x_{37}, x_{38}, x_{39}, x_{40}, x_{41}, x_{42}, x_{43}, and x_{44}, are considered also as inputs of the controller after normalizing them with reference values depending on the modified H_2 control mothed. The disturbance inputs, B_2, in this system are 12 inputs; six of them are placed at x_1, x_7, x_{13}, x_{18}, x_{24}, and x_{29} and others represent disturbances inputs at each tie-line and these inputs are assumed to be load change, solar generation, or any disturbance impacts either generation or power flow in tie-lines.

The size of the A-matrix of INSGS is 45 rows by 45 columns, $B_1$is 45 rows by 6 columns, B_2 is 45 rows by 12 columns, C_1 is 12 rows by 45 columns, C_2 is 12 rows by 45 columns, D_{11} is 12 rows by 12 columns, D_{12} is 12 rows by 6 columns, D_{21} is 12 row by 12 columns, and D_{22} is 12 rows by 6 columns. D_{11}, D_{12}, and D_{22} are arranged to be zero matrices while D_{21} is assumed to be an identity matrix to simulate the reference values of sensor outputs. In other words, equation (4.18) could be written for INSGS model through following equation

$$\begin{bmatrix} y_1(t) \\ y_7(t) \\ y_2(t) \\ y_8(t) \\ y_3(t) \\ y_9(t) \\ y_4(t) \\ y_{10}(t) \\ y_5(t) \\ y_{11}(t) \\ y_6(t) \\ y_{12}(t) \end{bmatrix} = \begin{bmatrix} -\Delta f_1 \\ -\Delta f_2 \\ -\Delta f_3 \\ -\Delta f_4 \\ -\Delta f_5 \\ -\Delta f_6 \\ -\Delta P_{tie-line1} \\ -\Delta P_{tie-line2} \\ -\Delta P_{tie-line3} \\ -\Delta P_{tie-line4} \\ -\Delta P_{tie-line5} \\ -\Delta P_{tie-line6} \end{bmatrix}^T \begin{bmatrix} x_1(t) \\ x_7(t) \\ x_2(t) \\ x_8(t) \\ x_3(t) \\ x_9(t) \\ x_4(t) \\ x_{10}(t) \\ x_5(t) \\ x_{11}(t) \\ x_6(t) \\ x_{12}(t) \end{bmatrix} + \begin{bmatrix} -\Delta f_{10} \\ -\Delta f_{20} \\ -\Delta f_{30} \\ -\Delta f_{40} \\ -\Delta f_{50} \\ -\Delta f_{60} \\ -\Delta P_{tie-line10} \\ -\Delta P_{tie-line20} \\ -\Delta P_{tie-line3} \\ -\Delta P_{tie-line40} \\ -\Delta P_{tie-line5} \\ -\Delta P_{tie-line60} \end{bmatrix} w(t) + \begin{bmatrix} 0 \\ 0 \\ 0 \\ 0 \\ 0 \\ 0 \\ 0 \\ 0 \\ 0 \\ 0 \\ 0 \\ 0 \end{bmatrix} u(t). \quad (6.57)$$

The H_2 controller with this arrangement with P plant matrix of INSGS model is 69 rows by 63 columns. This system is simulated in MATLAB environment after building the LFC model and there is a comparison between frequency deviation of Area 1 and Area 2 and power deviation of tie-line 1-2 under the conventional control, ACE, and H_2 control methods.

In Fig. 6.9, INSGS has different responses of frequency deviation building on the type of controller. Under the ACE controller condition in red line, INSGS shows large frequency deviation far away from the nominal frequency of the Iraqi system, 50Hz. In other words, the frequency deviation varies between 50.082 to 49.959Hz for more than 80 seconds, which is too long a period, and this could cause violating frequency standards if the Ministry of Electricity in Iraq adopts standards similar to NERC frequency standard, BAL-003-1, requiring the frequency

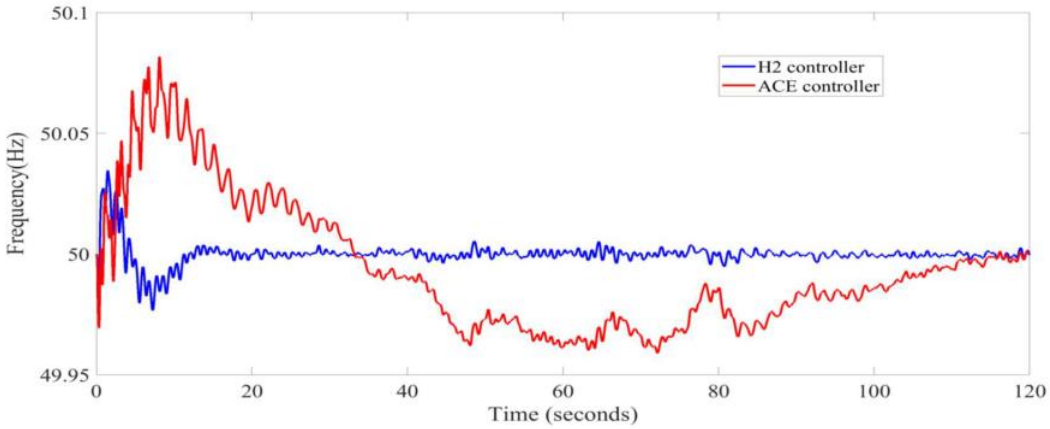

Fig. 6.9. Frequency deviation of the first area.

deviation within 0.06Hz of the nominal value. This high deviation from 50Hz could result in large disturbances, especially in transmission lines, if there is any sudden change in demand values or generation amounts of INSGS and can lead to cascade failures then total blackout.

However, the Iraqi system with an H_2 controller, blue line, shows more stable performance and low frequency deviation around 50Hz compared with the conventional method. The frequency begins with high fluctuation and moves from 50.04 to 49.98 Hz in 10 seconds, approximately, and this would be higher changes compared with the ACE control method, but after this time, the frequency gets low frequency deviation and this range is mitigated with time through having range between 50.005 and 49.995Hz after 40 seconds.

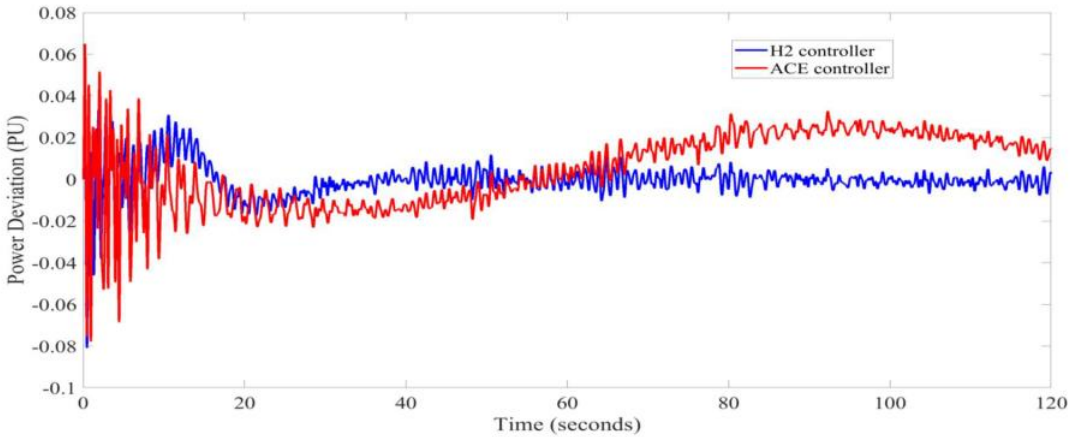

Fig. 6.10. Power deviation of tie-line 1-2.

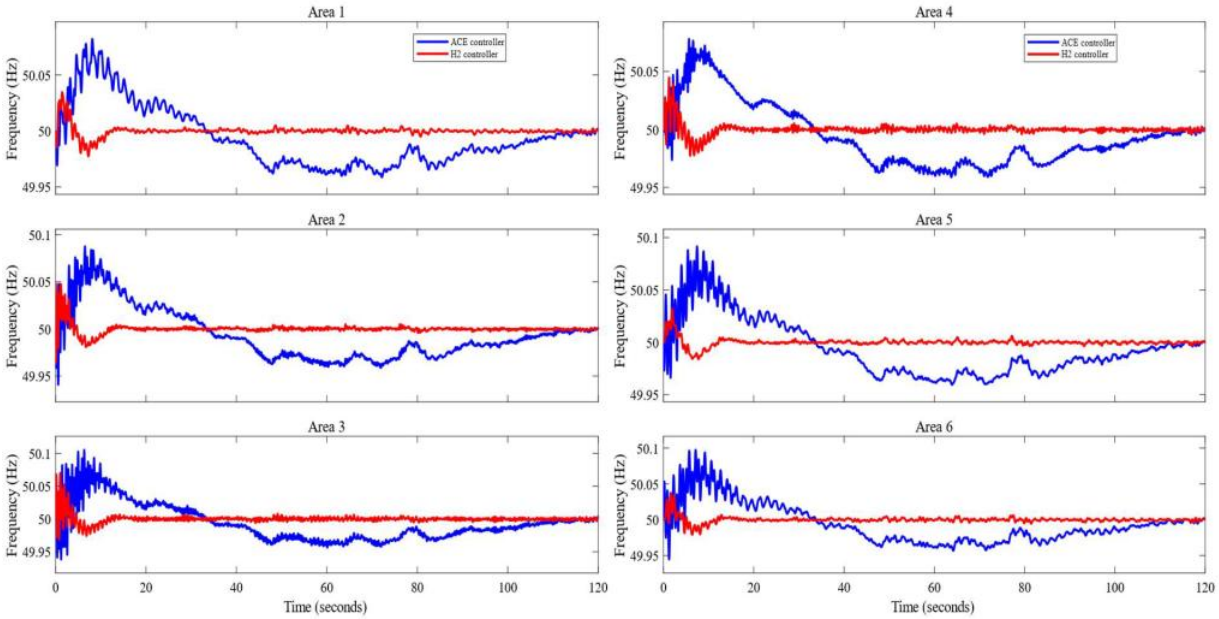

Fig. 6.11. Frequency deviation of INSGS with both ACE and H_2 controller.

From the power flow aspect, power deviation in tie-line 1-2 is investigated in Fig. 6.10 in order to compare changes with both the ACE controller and H_2 controller. The system with ACE control method shows high power deviation unlike the system with the proposed control method that has low range of deviation between 0.04 and -0.08pu this range goes in low range between 0.025 and -0.025pu. Also, the H_2 controller keeps the power deviation around 50Hz after 40 seconds while the other controller continues with frequency swings far away from zero pu as nominal value of power flow in the tie-line until finishing the simulation time.

In Fig. 6.11, results of frequency deviation are shown for all areas in terms of ACE and H_2 controller conditions. Frequency deviations for all areas have a faster response with the H_2 controller. Deviation values in all areas have been reduced to within 0.07pu ranges for 12 seconds and be within 0.02 range for the rest of the simulation time. In Fig. 6.12 it is clear that power deviations in the system with the H_2 controller has performance that is more stable and equal to zero pu in less than 20 seconds compared with the original controller. During injection of solar power, power in tie-lines has significant changes especially with the proposed controller and that

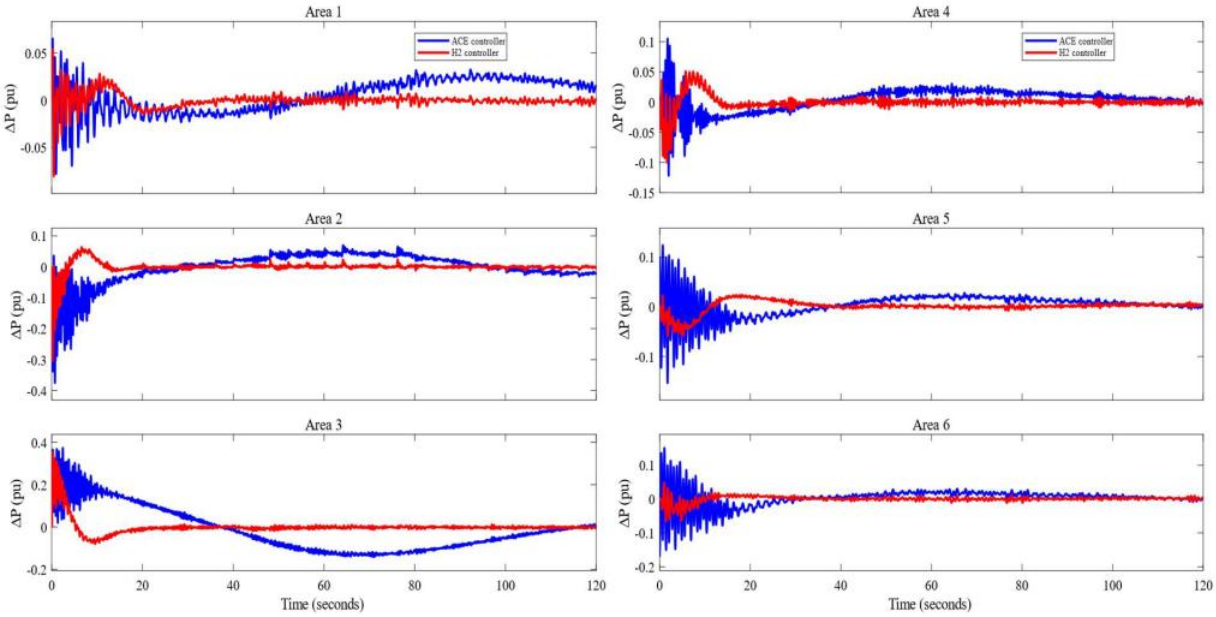

Fig. 6.12. Power deviation of INSGS with both ACE and H_2 controller.

reflects tries of the controller to mitigate any changes in these lines compared with the original system has large variation of power in tie-lines that can be seen in all areas.

6.4 INSGS and Three Countries Interconnection Tie-Lines

Plans are emerging for Iraq to connect its electrical network with neighboring countries, particularly Iran, Kuwait, and Turkey, to increase stability of the system and take advantage of differences in peak load time to compensate for load demand variability as shown in Fig. 6.13. This plan also will bring Iraq into power marketing and make it as a power hub for international electrical tie-lines.

To simulate this plan in the MATLAB environment in order to check the results, three scenarios are followed, and all countries areas are considered to be thermal power plants with non-reheat turbine. All ac tie-lines are assumed to have specific amount of power to run INSGS under expected power limits. The first scenario consists of connecting INSGS with neighboring countries through two ac tie-lines, with Iran and Turkey, while INSGS is connected with Kuwait

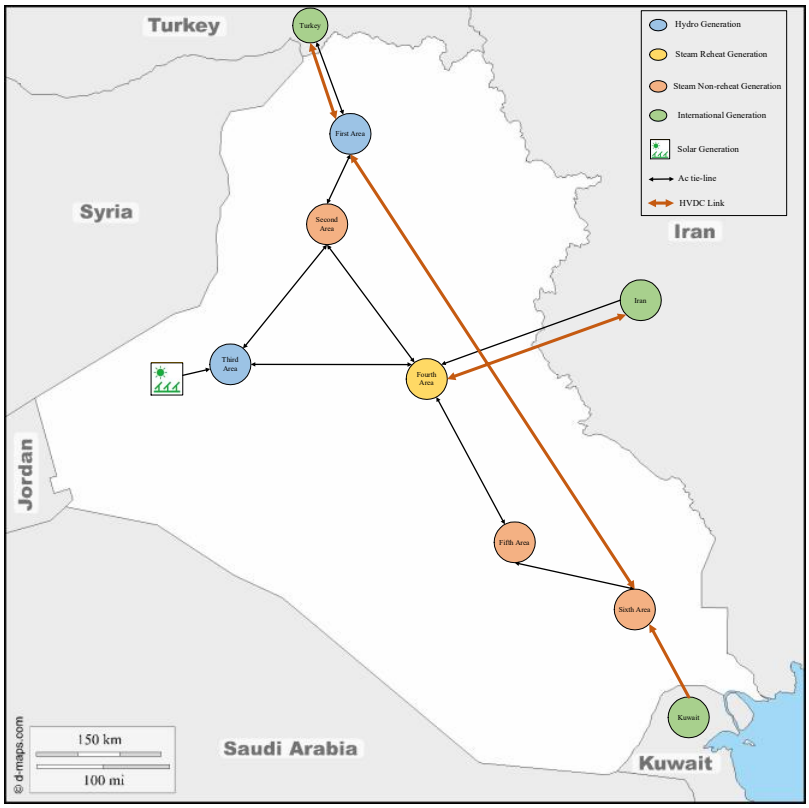

Fig. 6.13. Geographical map Of Iraq and its neighboring countries with the future tie-lines plan.

through a HVDC link, shown in Fig. 6.14. In this scenario, 20 transfer functions are added to the original system to mimic the interconnected network that consists of three governors, three

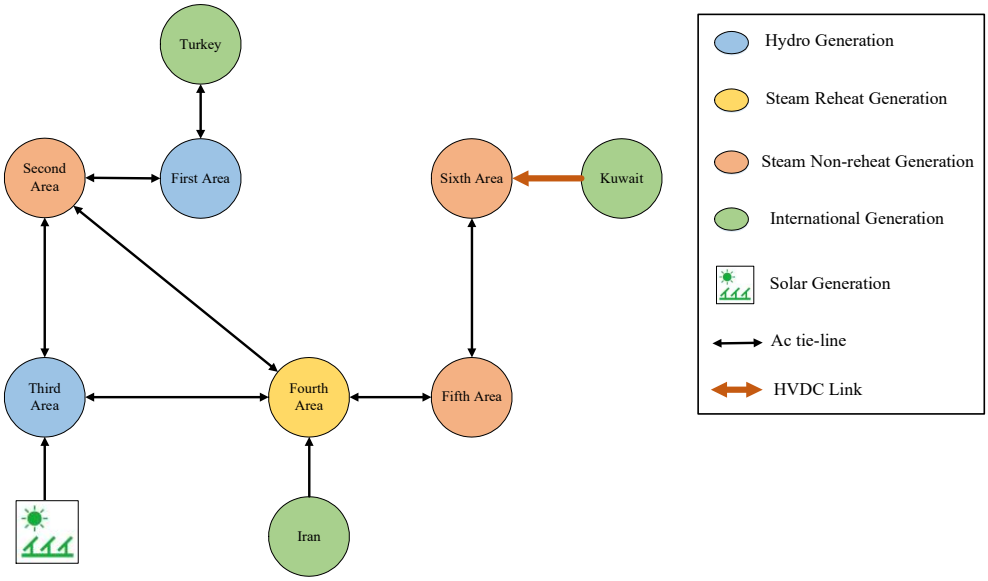

Fig. 6.14. INSGS with the three countries tie-lines.

turbines, three generators, three ACE controllers, two ac tie-lines, one dc tie-line, and five time-delay functions. Neighboring countries depend on ACE controllers due to the fact that H_2 control method is applied only on the INSGS as decentralized approach to monitor and set power flow. The added transfer functions can be given as:

For Turkey area:

$$\dot{x_{46}} = \frac{-1}{Tp_{tk}} x_{46} + \frac{Kg_{tk}}{Tp_{tk}} x_{47} - \frac{Kg_{tk}}{Tp_{tk}} x_{49}, \tag{6.58}$$

$$\dot{x_{47}} = \frac{-1}{Tt_{tk}} x_{47} + \frac{1}{Tt_{tk}} x_{48}, \tag{6.59}$$

$$\dot{x_{48}} = \frac{-1}{R_{tk} Tg_{tk}} x_{46} - \frac{1}{Tg_{tk}} x_{48} + \frac{1}{Tg_{tk}} x_{50}, \tag{6.60}$$

$$\dot{x_{49}} = -2\pi T_{tk-1} x_1 + 2\pi T_{tk-1} x_{49}, \tag{6.61}$$

$$\dot{x_{50}} = -Ki_{tk} x_{51} - Ki_{tk} x_{52}, \tag{6.62}$$

$$\dot{x_{51}} = \frac{B_{tk}}{T_d} x_{46} - \frac{1}{T_d} x_{51}, \tag{6.63}$$

$$\dot{x_{52}} = \frac{1}{T_d} x_{49} - \frac{1}{T_d} x_{52}, \tag{6.64}$$

For Kuwait Area

$$\dot{x_{53}} = \frac{-1}{Tp_{kw}} x_{53} + \frac{Kg_{kw}}{Tp_{kw}} x_{54} - \frac{Kg_{kw}}{Tp_{kw}} x_{56}, \tag{6.65}$$

$$\dot{x_{54}} = \frac{-1}{Tt_{tk}} x_{54} + \frac{1}{Tt_{tk}} x_{55}, \tag{6.66}$$

$$\dot{x_{55}} = \frac{-1}{R_{tk} Tg_{tk}} x_{53} - \frac{1}{Tg_{tk}} x_{55} + \frac{1}{Tg_{tk}} x_{57}, \tag{6.67}$$

$$\dot{x_{56}} = \frac{-1}{Tdc_{kw}} x_{56} + \frac{Kdc_{kw}}{Tdc_{kw}} x_{53} - \frac{Kdc_{kw}}{Tdc_{kw}} x_{29}, \tag{6.68}$$

$$\dot{x_{57}} = -Ki_{tk} x_{56} - Ki_{tk} x_{57}, \tag{6.69}$$

$$\dot{x_{58}} = \frac{B_{tk}}{T_d} x_{53} - \frac{1}{T_d} x_{58}, \tag{6.70}$$

For Iran area

$$\dot{x_{59}} = \frac{-1}{Tp_{ir}} x_{59} + \frac{Kg_{ir}}{Tp_{ir}} x_{60} - \frac{Kg_{ir}}{Tp_{ir}} x_{62}, \tag{6.71}$$

$$\dot{x_{60}} = \frac{-1}{Tt_{ir}} x_{60} + \frac{1}{Tt_{ir}} x_{61}, \tag{6.72}$$

$$\dot{x_{61}} = \frac{-1}{R_{tk}Tg_{ir}}x_{59} - \frac{1}{Tg_{ir}}x_{62} + \frac{1}{Tg_{ir}}x_{65}, \quad (6.73)$$

$$\dot{x_{62}} = -2\pi T_{ir-4}x_{18} + 2\pi T_{ir-4}x_{59}, \quad (6.74)$$

$$\dot{x_{63}} = \frac{B_{ir}}{T_d}x_{59} - \frac{1}{T_d}x_{63}, \quad (6.75)$$

$$\dot{x_{64}} = \frac{1}{T_d}x_{62} - \frac{1}{T_d}x_{64}, \quad (6.76)$$

$$\dot{x_{65}} = -Ki_{ir}x_{63} - Ki_{ir}x_{64}, , \quad (6.77)$$

where all variables with t_k are in the Turkey area, variables with *kw* are in the Kuwait area, and variables with i_r are in the Iran area. Then the modified INSGS system is simulated through applying the proposed method in Fig. 4.2 to calculate Kdc_{kw} and Tdc_{kw} values could produce optimal frequency deviation damping and low power deviation in tie-lines under H_2 controller condition. After running simulation for in MATALB environment, Kdc_{kw} and Tdc_{kw} are selected to be equal to 1.9pu and 0.45 seconds building on the modified H_2 control method that all results are illustrated in Table. 11. These values represent the fifth case can be considered the area without external impacts. In other words, there is not any disturbance or solar generation or international tie-lines or HVDC links located in this area. Therefore, the values of Kdc_{kw} and Tdc_{kw} remain within maximum allowed frequency deviations.

Table 11. Minimum frequency (Hz) and optimal cost values for the first scenario

Case No.	f_1	f_2	f_3	f_4	f_5	f_6	γ
1	50.0298	50.0477	50.0679	50.0410	50.0271	50.0278	2.0038
2	50.0314	50.0470	50.0678	50.0409	50.0290	50.0323	1.9741
3	50.0314	50.0471	50.0678	50.0410	50.0290	50.0323	1.9740
4	50.0306	50.0478	50.0680	50.0397	50.0210	50.0276	2.0083
5	50.0306	50.0478	50.0680	50.0398	50.0206	50.0279	2.0066
6	50.0304	50.0478	50.0680	50.0400	50.0245	50.0223	2.0080

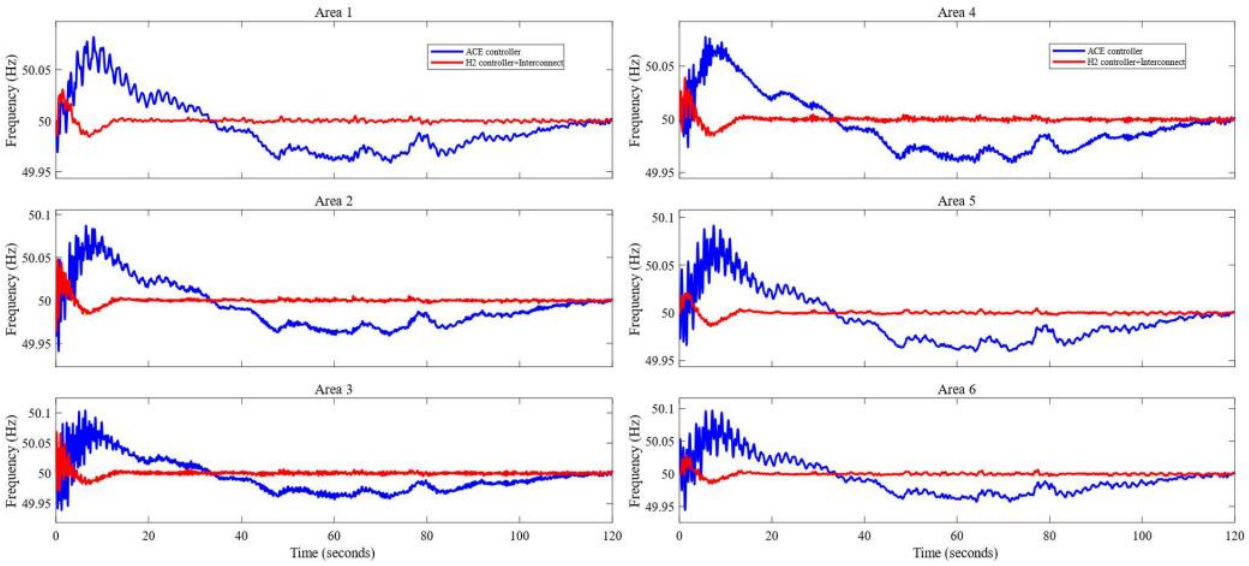

Fig. 6.15. Frequency deviation of INSGS with international connections.

Then these values are simulated to obtain a comparison between the original INSGS and the modified grid network. Results of the simulation are displayed in Fig. 6.15 and Fig. 6.16. In Fig. 6.15, frequency deviation of the system shows more stable performance under the H_2 controller even INSGS has been expanded to have more areas and all frequency deviation are within ±0.06Hz. However, the third area still has high frequency deviation, and this is because the solar generation injects power into INSGS through this area. The frequency oscillation has been damped to lower values compared with the original performance.

From the power view, ranges of power deviation in six areas of INSGS have been reduced from 0.6pu, highest range value in the third area, to be equal to 0.1pu in all cases after adopting H_2 controller and international connections, illustrated in Fig. 6.16. That means the suggested control method helps INSGS to have more stable condition with large size of network and renewable generation and keep power flow through tie-lines in constant variations.

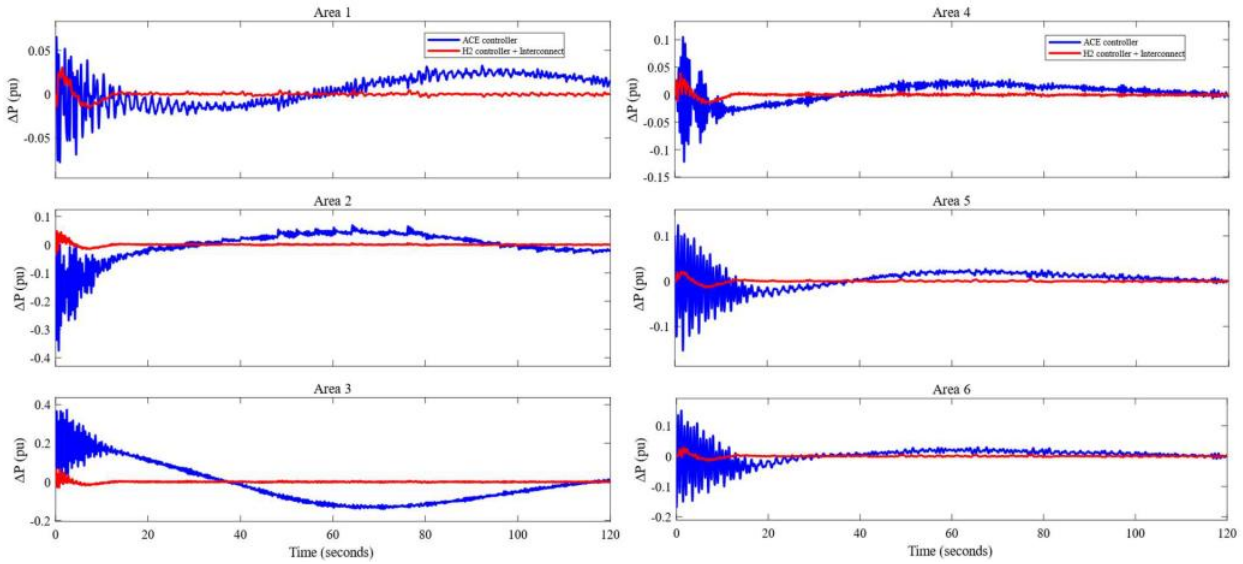

Fig. 6.16. Power deviation of INSGS with international connections.

6.5 INSGS and Three Countries Interconnection Tie- Lines with HVDC Links

The second and third scenarios analyzed in this section include setting HVDC links between different areas. The second scenario covers a case consists of placing a HVDC link between first and sixth areas, between Mosul in north of Iraq and Basra in south, and this link would have length equal to 780 km, 485 mi, shown in Fig. 6.17. This link will give benefits to INSGS through transferring power between these areas that have different demand load during seasons of the year and that would reduce power losses and line congestion or overload cases if power transfers through 400Kv and 132Kv. Moreover, this link would be a main flow-gate line carries power from Kuwait area to Turkey then to Europe via INSGS and this will make Iraq a hub node to transfer energy between Asia and Europe [113].

This scenario requires adding a transfer function between the first and sixth areas represents the HVDC link and that also will increase the number of variables to be equal to 66. The new variable could be given as

$$\dot{x_{66}} = \frac{-1}{Tdc_{16}} x_{66} + \frac{Kdc_{16}}{Tdc_{16}} x_1 - \frac{Kdc_{16}}{Tdc_{16}} x_{29} \,, \tag{6.78}$$

Fig. 6.17. INSGS configuration with international connections and HVDC link.

where values of Kdc_{16} and Tdc_{16} are obtained as K_X and T_X in the proposed method. The input of HVDC transfer function is frequency error between the first and sixth areas. After running a simulation of the suggested method, an optimal six cases are gathered in Table 12 that display lower frequency deviations for each area and the second case, which is similar to the fifth case, is selected to be the optimal case for two reasons; low optimal cost γ and low frequency deviation in the fifth area, which is the area without external influences. The optimal values of K_X and T_X, equal to parameters of HVDC link Kdc_{16} and Tdc_{16}, are 0.1pu and 0.95 seconds, respectively.

Table 12. Minimum frequency (Hz) and optimal cost values of the second scenario

Case No.	f_1	f_2	f_3	f_4	f_5	f_6	γ
1	50.0255	50.0492	50.0681	50.0404	50.0234	50.0327	2.1178
2	50.0308	50.0479	50.0692	50.0419	50.0211	50.0300	2.0074
3	50.0284	50.0486	50.0680	50.0409	50.0217	50.0304	2.0592
4	50.0458	50.0516	50.0690	50.0359	50.0294	50.0369	4.0330
5	50.0308	50.0479	50.0692	50.0419	50.0211	50.0300	2.0074
6	50.0297	50.0483	50.0684	50.0412	50.0211	50.0297	2.0080

Values of Kdc_{16} and Tdc_{16} are simulated to calculate frequency and power deviations and the results are shown Fig. 6.18 and Fig. 6.19. In these figures, frequency and power deviation are similar to results in the first scenario with slight differences due to increasing number of elements in INSGS.

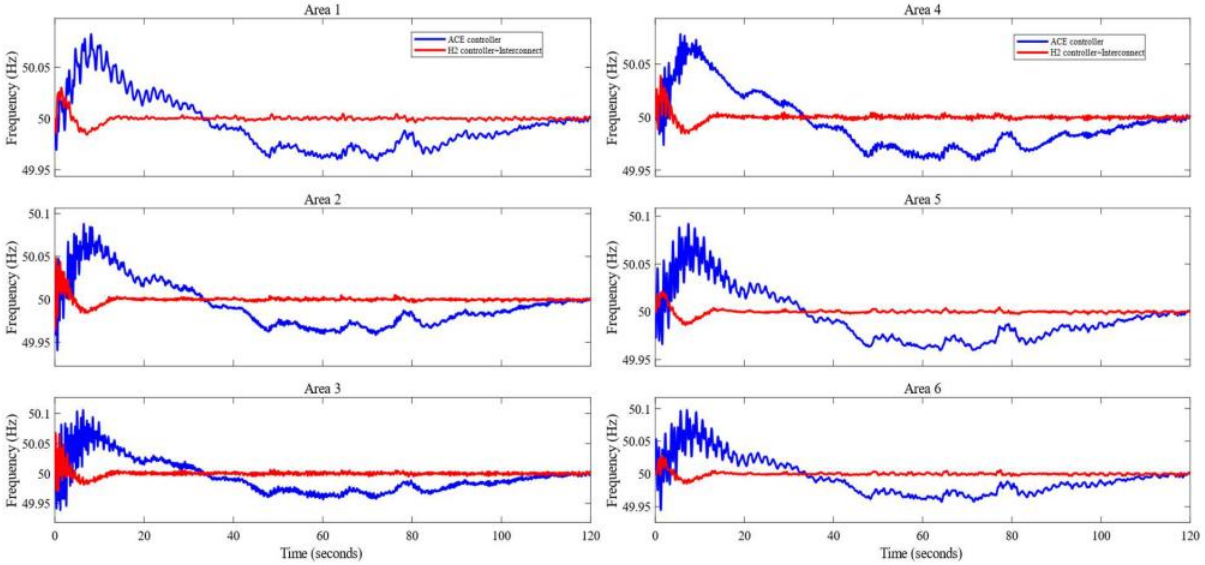

Fig. 6.18. Frequency deviation of INSGS with international connections with HVDC link.

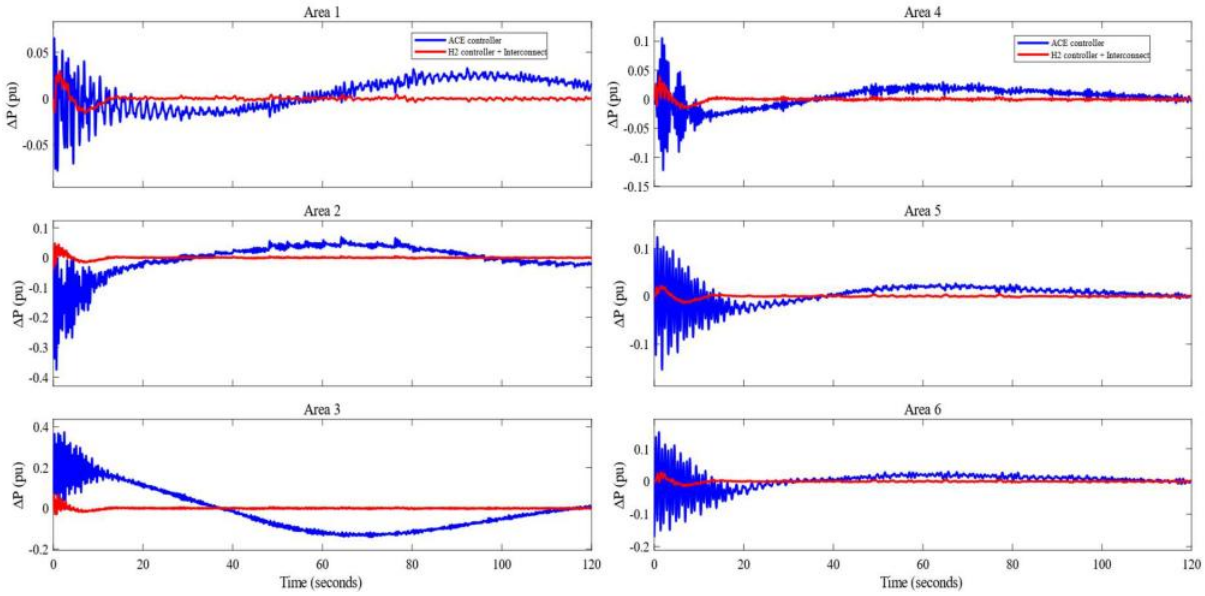

Fig. 6.19. Power deviation of INSGS with international connections with HVDC link.

In the third scenario, two HVDC links are placed as tie-lines connecting INSGS with both Iran and Turkey as shown in Fig. 6.20 as a new proposal in this research. The addition of these

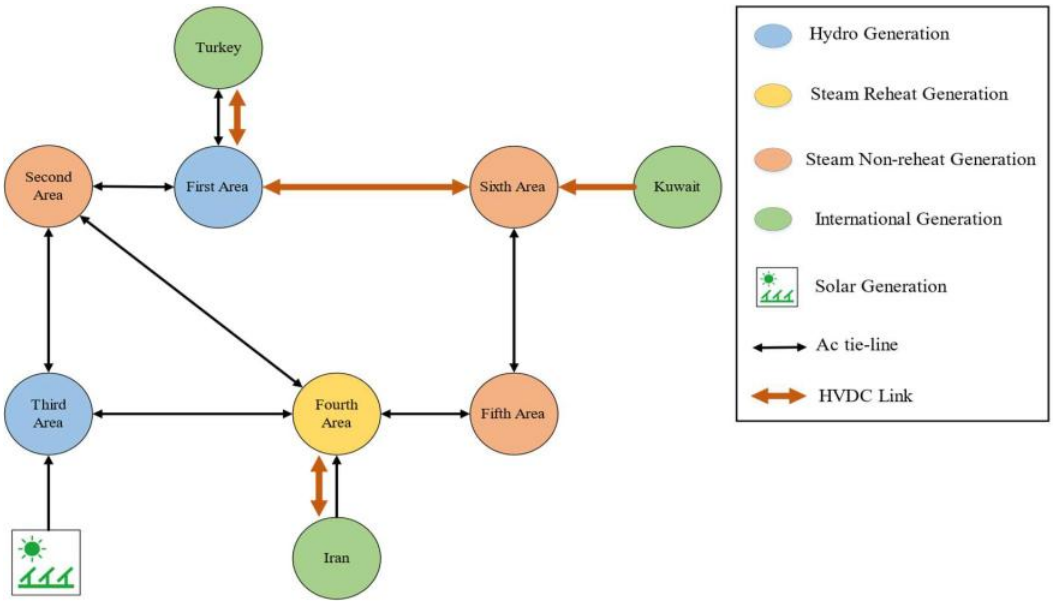

Fig. 6.20. INSGS configuration with international connections and four HVDC links.

AC/DC links with existence of an ac tie-line would help in increasing stability and reliability of INSGS and may help in raising power flow between the connected countries. Like in the second scenario, two HVDC transfer functions are added to define the H_2 controller and simulate the modified system in MATLAB environment. These transfer function produce two more variables which are written as

$$\dot{x_{67}} = \frac{-1}{Tdc_{tk}} x_{tk} + \frac{Kdc_{tk}}{Tdc_{tk}} x_1 - \frac{Kdc_{tk}}{Tdc_{tk}} x_{46} \,, \tag{6.79}$$

$$\dot{x_{68}} = \frac{-1}{Tdc_{ir}} x_{66} + \frac{Kdc_{ir}}{Tdc_{ir}} x_{18} - \frac{Kdc_{ir}}{Tdc_{ir}} x_{59} \,, \tag{6.80}$$

where variables with *tk* represent the HVDC link connected to Turkey area while variables with *ir* represent the HVDC link connected to Iran area. The optimal values of K_X and T_X in this scenario are calculated for the two HVDC links and they are Kdc_{ir}, Kdc_{tk}, Tdc_{ir} and Tdc_{tk}. After running the simulation for 2.5 hours, the optimal values of parameters for HVDC links are obtained for each area and listed in Table 13.

Table 13. Minimum frequency (Hz) and optimal cost values of the third scenario

Case No.	f_1	f_2	f_3	f_4	f_5	f_6	γ
1	50.0247	50.0442	50.0674	50.0319	50.0184	50.0212	2.3673
2	50.0247	50.0442	50.0674	50.0319	50.0184	50.0212	2.3673
3	50.0251	50.0445	50.0673	50.0371	50.0174	50.0216	2.3271
4	50.0287	50.0442	50.0674	50.0296	50.0197	50.0222	2.3837
5	50.0258	50.0442	50.0673	50.0353	50.0172	50.0214	2.3477
6	50.0247	50.0442	50.0674	50.0319	50.0184	50.0212	2.3673

Building on the same concepts used to select K_x and T_x in previous scenarios, the four variables have been chosen that represent the fifth case because this case shows low frequency deviation in the fifth area and this area is not damped by tie-lines or impacted by external disturbances. The obtained values, 3, 0.3, 0.1, and 0.2 which are Kdc_{ir}, Kdc_{tk}, Tdc_{ir} and Tdc_{tk}, respectively, assist INSGS with its new expansions to have a stable condition. These values have been simulated and compared with the original INSGS model in MATLAB environment and like previous conditions, the system runs normally, and its frequency and power changes have been reduced to minimum values and variations are kept within or near power standards, shown in Fig. 6.21 and Fig. 6.22.

6.6 INSGS with the H_2 controller under N-1-1 Contingencies

Similar to the three-area system analysis, INSGS is examined under N-1-1 contingency events through applying disturbances, power change with magnitude 0.1pu, 30 and 32.5 seconds in order to emphasize the system response with H_2 controller and two ac tie-lines and four HVDC links connect different areas. In Fig. 6.23, the frequency deviation for the system has been

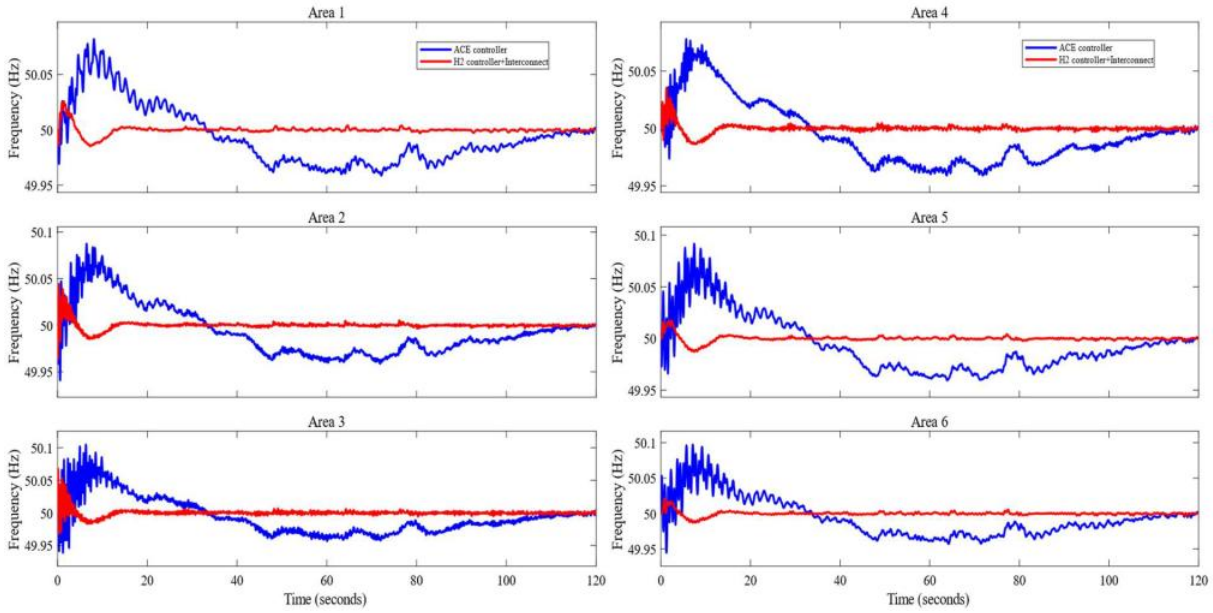

Fig. 6.21. Frequency deviation of INSGS model with two countries connections and four HVDC links.

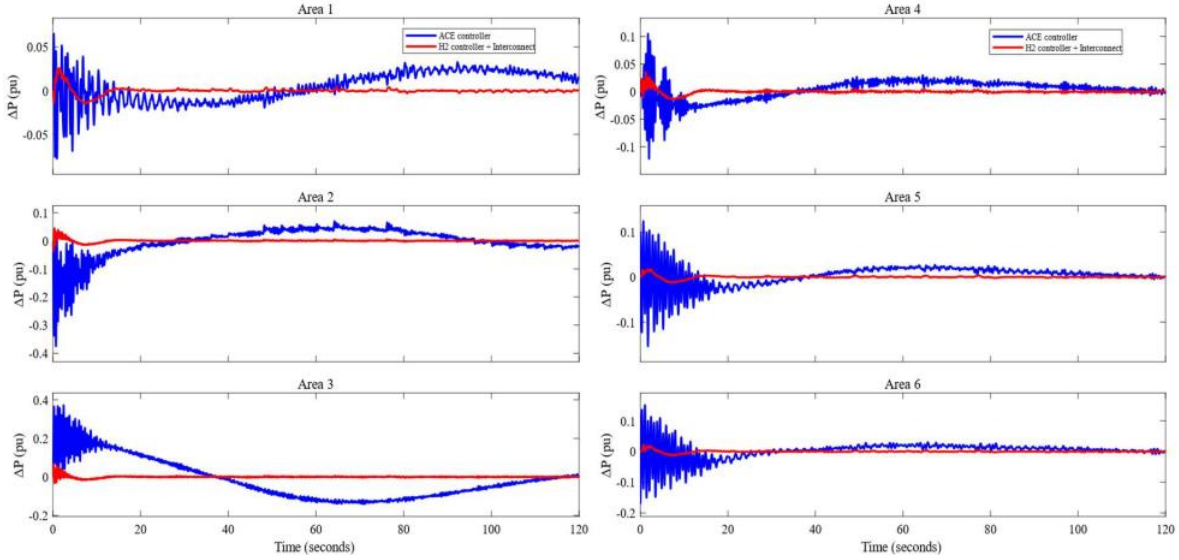

Fig. 6.22. Power deviation of INSGS model with two countries connections and four HVDC links.

improved with the H_2 controller and other added components compared with original system. The changes of frequency are maintained within ±0.05Hz for all areas and this does not violate the frequency standards, while deviations in the original model have ranges between 49.9 and 50.1Hz due to lack of any damping tools. Also, the shape of the response of systems to disturbances

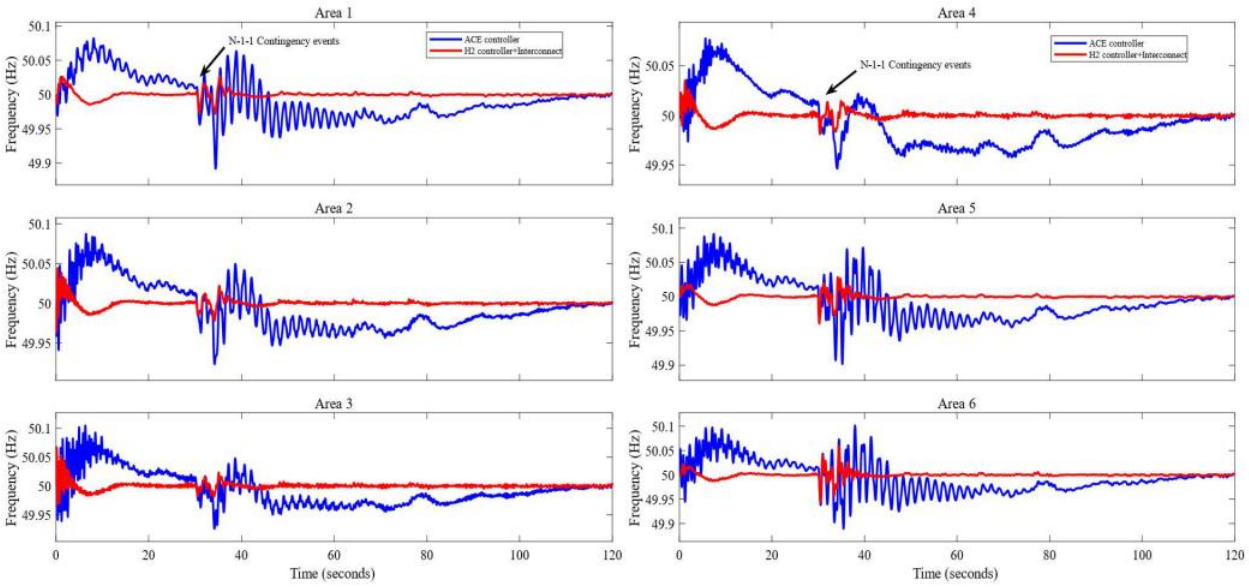

Fig. 6.23. Frequency deviation of INSGS under N-1-1 contingency events.

clearly is dependent on the type of turbines and governors, especially in the original model and this is highlighted in this exam. The second, fifth, and sixth areas, area with steam non-reheat turbines, show high responses with faults compared with other areas and this impact has been mitigated to lower values through the H_2 controller technique.

Another type of event is applied on the INSGS model and that occurs through setting disturbances on tie-lines 4-5 and 5-6 at 30 and 32.5 seconds, respectively, and that is simulated via multiplication of power synchronizing coefficients of these lines. This N-1-1 event is shown in Fig. 6.24 where the power deviation for all areas are present and it is clear that from the figure that the system gains some power oscillations on its tie-lines after having the disturbances, especially in the original model. However, the system experiences a stable manner with the final condition, with the H_2 control approach and other tie-lines connections and that means the system takes advantage having tie-lines with HVDC links to produce power with acceptable ranges under variable generation or large disturbances.

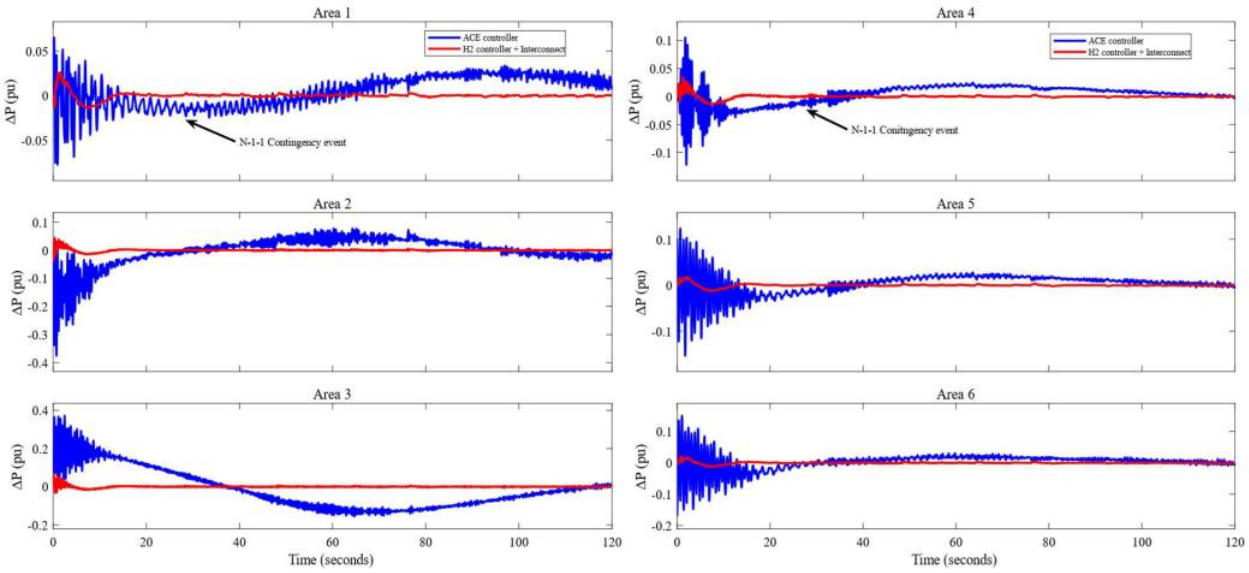

Fig. 6.24. Power deviation of INSGS under N-1-1 contingency events.

6.7 Eigenvalues Examination

The final case will exam INSGS under various circumstances to check its stability through positions of eigenvalues. In Fig. 6.25, the original system has eigenvalues that are near the imaginary axis, illustrated in Table 14, and these eigenvalues could be influenced by any disturbances and shifted to the right plane resulting in an unstable condition. Adoption of the suggested control method with extension the system with two ac tie-lines and four HVDC links helps INSGS to have more stable and firm response through moving these eigenvalues far from the imaginary axis and final eigenvalues after having the all extension are given in Table 15. All eigenvalues are tabulated in following tables have damping ratio below 1 or cos 0° and highlighting these eigenvalues are significant to show effects of the H_2 control approach with HVDC links.

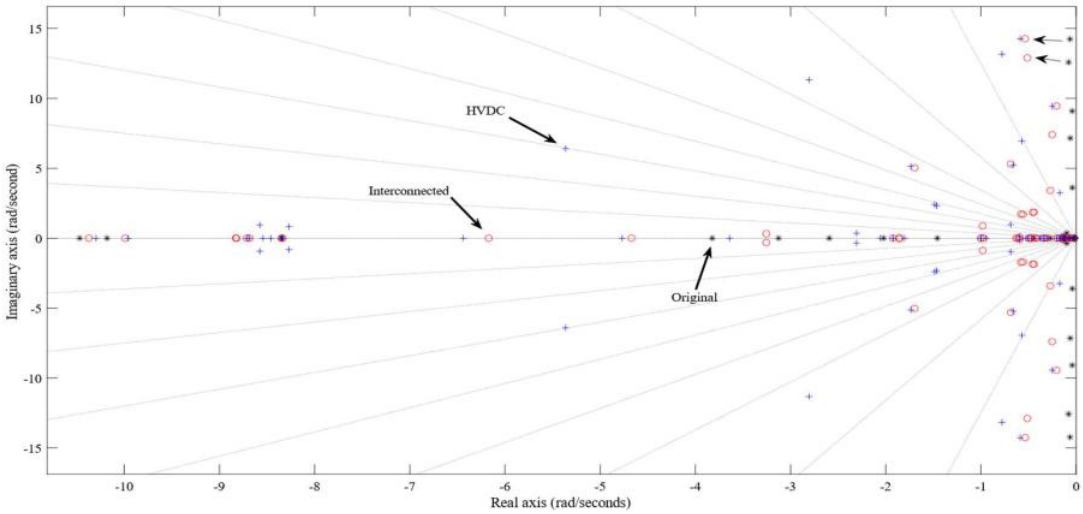

Fig. 6.25. Results of comparison between original system with ACE controller and system with H_2 controller two ac tie-lines and four HVDC links.

Table 14. Mode characteristics for INSGS (original model)

Eigenvalue	Damping	Freq.(rad/s)
-0.06.42+14.2i	0.00451	14.2
-0.0642-14.2i	0.00451	14.2
-0.0790+12.6i	0.00628	12.6
-0.0790-12.6i	0.00628	12.6
-0.0413+9.09i	0.00455	09.09
-0.0413-9.09i	0.00455	09.09
-0.0616+7.15i	0.00862	07.15
-0.0616-7.15i	0.00862	07.15
-0.0400+3.61i	0.01110	03.61
-0.0400-3.61i	0.01110	03.61
-0.0994+0.367i	0.26200	0.380
-0.0994-0.367i	0.26200	0.380
-0.130+0.174i	0.59900	0.217
-0.130-0.174i	0.59900	0.217
-0.0126+0.0441i	0.27500	0.0458
-0.0126-0.0441i	0.27500	0.0458
-0.0204+0.0486i	0.38700	0.0527
-0.0204-0.0486i	0.38700	0.0527
-0.0810+0.0616i	0.79600	0.1020
-0.0810-0.0616i	0.79600	0.1020

Table 15. Mode characteristics for INSGS with interconnections and HVDC links

Pole	Damping	Freq. (rad/s)
-0.252+9.43i	0.0267	9.44
-0.252-9.43i	0.0267	9.44
-0.570+6.95i	0.0818	6.97
-0.570-6.95i	0.0818	6.97
-0.663+5.21i	0.1260	5.25
-0.663-5.21i	0.1260	5.25
-1.74+5.13i	0.3210	5.42
-1.74-5.13i	0.3210	5.42
-8.58+0.938i	0.9940	8.63
-8.58-0.938i	0.9940	8.63
-8.27+0.817i	0.9950	8.31
-8.27-0.817i	0.9950	8.31
-0.171+3.24i	0.0527	3.25
-0.171-3.24i	0.0527	3.25
-1.49+2.41i	0.5250	2.83
-1.49-2.41i	0.5250	2.83
-1.46+2.31i	0.5350	2.74
-1.46-2.31i	0.5350	2.74
-2.31+0.350i	0.9890	2.33
-2.31-0.350i	0.9890	2.33
-0.688+0.977i	0.5760	1.19
-0.688-0.977i	0.5760	1.19
-0.594+0.110i	0.9830	0.605
-0.594-0.110i	0.9830	0.605

7 Conclusions and Future Work

7.1 Conclusion

This section briefly explains the main findings and corresponding improvements made by this research assessing and mitigating N-1-1 contingency events and employing a wide area control approach to increase reliability of power systems. First, previous work with N-1-1 contingency was often made with an assumption that all transmission faults could be cleared quickly by circuit breakers and therefore limit the spread of power outages. However, this kind of assumption does not consider critical load lines or susceptible points for instability that power systems could experience with cascading outages. Therefore, developing the risk-based reliability method for N-1-1 contingency analysis was necessary to highlight outcomes that could be appear under this type of disturbance.

The RBRM studied the reliability of transmission systems through checking each line case and comparing its condition under after an N-1 event. This allows for assessing each line's impact would have for a subsequent N-1-1 event. This approach utilized two main factors: age of lines (which could be modified after maintenance or conductor replacement) and power flow though the respective lines. The simulation results presented the effects of the sequence order of line faults.

To treat these types of faults using real power system networks as benchmarks, the research considered systems with high penetration of renewable resources. PMU data provided a mean for developing a synchrophasor validation method (SVM). Application of SVM with using Model Validation Working Group (MVWG) of NERC recommends as reference for results helped in producing a new benchmark model of power system with high penetration of wind generation. Results of the model validation processes showed that SVM gives planners and researchers an opportunity to build or develop power models extracted from real networks with low percentage

of errors and meet standards of regulatory agencies. This benchmark was reduced in size from 456 buses to 21 buses under load frequency control analysis in order to examine the suggested wide area control method.

A wide control area control using H_2 control approach was developed to increase the reliability of LFC power system with variable generation and stochastic disturbances. The proposed method was developed in this dissertation to help planners in power system to obtain parameters of power system compensators such as SSSC devices and HVDC links that could be installed to achieve optimal stability results. Validation methods were utilized to determine the effectiveness of the proposed method based on frequency and tie-line power deviations and eigenvalue analysis. This analysis is checked through setting two types of N-1-1 contingency events were assumed to place in LFC model. The first were disturbances of losing generation with 0.05pu of the net generation. The second was a circuit breaker trip and the associated loss of a transmission line.

These events took place in the 21 bus three-area system with a sequence of contingencies (N-1-1). The results showed that the system has an improved response under the abnormal conditions and stayed within NERC standards compared with the original system controlled by ACE technique. In the other hand, the second validation offered results that the critical eigenvalues located near the imaginary axis of s-plane had been shifted to the stable region after adoption the suggested control method. Moreover, both results helped in distinguish which technique of SSSC device and HVDC link could be most useful. Lower frequency and reduced power flow deviations with more stable eigenvalue locations were displayed by installation of an HVDC link between two areas in the 21 buses three-area system.

Another power model was employed to ensure the proper function of the proposed control method. The system examined was the Iraqi national electrical network (INSGS) and its LFC model included large amounts of solar PV generation. The suggested method was designed in this research to obtain optimal variables in order to make INSGS have cross-national tie-lines with neighboring countries and these tie-lines represent the future plan for the Ministry of Electricity in Iraq. Two ac tie-lines and four HVDC links were added and eight parameters of the HVDC technique were obtained. After selection of the optimal values of the HVDC parameters, two validation conditions were analyzed for the Iraqi model. The results showed that the Iraqi system with the proposed H_2 control method and new tie-lines could withstand random generation and N-1-1 disturbances and have reduced frequency deviations that stay within regulatory requirements. Also, the eigenvalue locations had been improved and shifted from critical regions to more stable positions and that helped to support the INSGS model for facing abnormal states.

7.2 Future Work

For future work, the suggested control method would be applied on models of the load frequency systems as a decentralized control framework with stochastic time delays with inclusion of inverter-based generation devices and dynamic conditions to reduce time response and increase reliability.

8 References

[1] Measurment Practices for Reliability and Power Quality. A toolkit of reliability measurments practices. Retrieved from http://www.science.smith.edu/~jcardell/Courses/EGR325/Readings.

[2] Standards Authorization Request Revision to BAL-003-1.1:Frequency Response and Frequency Bias Setting. Retrieved from https://www.nerc.com/pa/Stand/Project201701ModificationstoBAL00311/2017-01_BAL_003_Technical_Document_NWPP_Nov2017.pdf

[3] North American Electric Reliability Corporation, Reliability Assessment Guidebook, version 3.1, Aug. 2012.

[4] M. Alsarray, M. Saadeh, R. McCann, "A Risk-Based Planning Method for N-1-1 Contingency Analysis of Transmission Systems," *North American Power Symp*., Charlotte, NC, Oct 4-6 2015, pp. 1-6.

[5] K. A. Loparo, and F. Abdel-Malek, E. Ciapessoni, D. Cirio, A. Pitto, and G. Gross, "A Probabilistic Approach to Dynamic Power System Security," *IEEE Trans. on Circuits and Syst*., vol. 37, no. 6, pp. 787–798, June 1990.

[6] J. McCallely, S. Asgarpoor, L. Bertling, R. Billinton, H. Chao, J. Chen, C. Singh, "Probabilistic Security Assessment for Power System Operations," Task Force on Probabilistic Aspects of Reliability Criteria of IEEE PES Reliability, Risk, and Probability Applications Subcommittee.

[7] D. D. Le, A. Berizzi, C. Bovo, E. Ciapessoni, D. Cirio, A. Pitto, and G. Gross, "A Probabilistic Approach to Power System Security Assessment under Uncertainty," *IREP Symposium-Bulk Power System Dynamics and Control-IX*, Rethymnon, Greece, Aug. 2013.

[8] K. W. Wang, C. Y. Chung, C. T. Tse and K. M. Tsang, "Improved Probabilistic Method for Power System Dynamic Stability Studies," *IEE Proc-Gener*. Transm. Distrib, vol. 147, no. I, January 2000.

[9] S. Henry, E. Breda-Seyes, H. Lefebvre, V. Sermanson and M. Bena, "Probabilistic study of the collapse modes of an area of the French network," *9th International Conference on Probabilistic Methods Applied to Power Systems*, Stockholm, Sweden, June, 2006.

[10] H. Dong, M. Jin, and H. Renmu, "Effect of Uncertainties in Parameters of Load Model on Dynamic Stability Based on Probabilistic Collocation Method," *IEEE Lausanne* Power Tech, pp. 1100 - 1104, July 2007.

[11] D. R. Romero, and H. M.Mere1, "Probabilistic Transient Stability Utilizing a Transformation," *IEEE Int. Symp. on* Circuits and Systs., pp. 152 – 155, vol.1, May 1990.

[12] R. C. BURCHETT, and G. T. HEYDT, "Probabilistic Methods for Power System Dynamic Stability Studies," *IEEE Trans. on Power App. and Syst.,* Vol. PAS-97, no. 3, May/June 1978.

[13] Z. Bao-hui, W. Li-yong, Z. Wen-hao, and Z. De-cai, "Implementation of Power System Security and Seliability Considerieng Risk under Environment of Electriciy Market," *IEEE/PES Transmission and Distrib. Conf. and Exhibition*, Dalian, China, 2005, pp.1-6.

[14] M. P. Ehavaraju, R. Eillinton, N. D. Reppen,"Requirements for Composite System Reliablity Evaluation Models", *IEEE Trans. on Power Syst.,* vol. 3, no.1, pp. 149 – 157, 1988.

[15] Y. Sun, L. Cheng, H. Liu, S. He, "Power System Operational reliability evaluation Based on Real-time Operating State," *7th Inter. Power Eng. Conf.* , Singapore, Singapore, Vol. 2, Nov. 29-Dec. 2, 2005.

[16] A. G. Phadke, J. S. Thorp, "Expose Hidden Failures to Prevent Cascading Outages," *IEEE Comput. Applicat. in Power*, Vol. 9, No. 3, pp.20-23, 1996.

[17] F. Yang, A. P.Sakis Meliopoulos, G. J. Cokkinides, Q. B. Dam, "Effects of Protection System Hidden Failures on Bulk Power System Reliability," *38th North American Power Symp*., Carbondale, IL, Sept 17-19, 2006.

[18] F. Yang, A. P.Sakis Meliopoulos, G. J. Cokkinides, Q. B. Dam, "Bulk Power System Reliability Assessment Considering Protection System Hidden Failures," *Bulk Power System Dynamics and Control - VII, Revitalizing Operational Reliability Symp.,* Charleston, SC, August 19-24, 2007.

[19] M. Al-Sarray, H. Mhiesan, R. McCann and H. Liao, "A risk-based reliability method for N-1-1 contingency analysis," *North American Power Symp. (NAPS)*, Denver, CO, Sept. 18-20, 2016.

[20] C. T. Su, J. J. Wong, C. J. Fan, "System and Load Points Reliability Evaluation for Electric Power Systems," 1st Annu. IEEE Syst. Conf., Waikiki Beach, Honolulu, Hawaii, April 9-12, 2007.

[21] R.N. Allan, R. Billinton, A. Gawad, "The IEEE Reliability Test System - Extensions to and Evaluation of the Generating System", *IEEE Trans. on Power Syst*., vol. PWRS-1, no. 4, pp. 1-7, Nov. 1986.

[22] R. Billinton, W. Wangdee, "Delivery Point Reliability Indices of a Bulk Electric System Using Sequential Monte Carlo Simulation", *IEEE Trans. on Power Del*., vol. 21, no. 1, pp.345-352, Jan. 2006.

[23] R. Billinton, D. Huang, "Aleatory and Epistemic Uncertainty Considerations in Power System Reliability Evaluation," Proc. of *the 10th Int. Conf. on Probabilistic Methods App. to Power Syst.,* Rincón, Puerto Rico, May 25-29, 2008.

[24] M. Garmroodi, D. J. Hill, G. Verbič, and J. Ma, "Impact of tie-line power on inter-area modes with increased penetration of wind power," *IEEE Trans. Power Syst*., vol. 31, no. 4, pp. 3051-3059, Jul. 2016.

[25] N. Nguyen, and J. Mitra, "Reliability of power system with high wind penetration under frequency stability constraint," *IEEE Trans. Power Syst.,* vol. 33, Issue. 1, pp. 985-994, Jan. 2018.

[26] D. B. Payne and J. R. Stern, “Performance analysis of static network reduction methods commonly used in power systems,” presented at *the 18th Nat. Power Syst. Conf.*, Guwahati, India, Dec. 18–20, 2014.

[27] H. Oh, “A New Network Reduction Methodology for Power System Planning Studies,” *IEEE Trans. Power Syst*., vol. 9, no. 1, pp. 677-684, Feb. 1994.

[28] K. L. Lo, L.J. Peng, J. F. Macqueen, A. O. Ekwue, and N. H. Dandachi, “Extended Ward equivalent of external system for on-line security analysis,” presented at *the 2nd Int. Conf. on Advances in Power Syst. Control, Operation and Manage*., Hong Kong, Dec. 7-10, 1993.

[29] R. A. M. van Amerongen, and H. P. van Meeteren, “A generalized Ward equivalent for security analysis,” *IEEE Trans. Power App. Syst*., vol. PAS-101, no. 6, pp. 1519-1526, Jun. 1982.

[30] Z. W. Liu, and M. B. Liu, “Distributed reactive power optimization computing in multi-area power systems using Ward equivalent,” presented at *the Int. Conf. on Elect. and Control Eng*., Wuhan, China, Jun. 25-27, 2010.

[31] H. Li, Z. Lu, Y. Qiao, and Z. Sun, “The fast reliability evaluation method in transmission grid expansion project based on power flow tracing and Ward equivalent method,” presented at *the Int. Conf. on Power Syst. Technol.*, Chengdu, China, Oct. 20-22, 2014.

[32] Y. Zhu, and D. Tylavsky, “An Optimization Based Network Reduction Method with Generator Placement,” presented at *the North American Power Symp*., Charlotte, NC, Oct. 4-6, 2015.

[33] A. Vahidnia, G. Ledwich and E. W. Palmer, "Transient Stability Improvement Through Wide-Area Controlled SVCs," in *IEEE Trans. on Power Syst.*, vol. 31, no. 4, pp. 3082-3089, July 2016.

[34] A. S. Musleh, S. M. Muyeen, A. Al-Durra, I. Kamwa, M. A. S. Masoum and S. Islam, "Time-Delay Analysis of Wide-Area Voltage Control Considering Smart Grid Contingences in a Real-Time Environment," in *IEEE Trans. on Ind. Informatics*, vol. 14, no. 3, pp. 1242-1252, March 2018.

[35] R. Yousefian, R. Bhattarai and S. Kamalasadan, "Transient Stability Enhancement of Power Grid With Integrated Wide Area Control of Wind Farms and Synchronous Generators," in *IEEE Trans. on Power Syst*, vol. 32, no. 6, pp. 4818-4831, Nov. 2017.

[36] S. Sterpu, W. Lu, Y. Besanger and N. HadjSaid, "Power systems security analysis," *IEEE Power Eng. Soc. General Meeting*, Montreal, Que., Jun 18-22, 2006.

[37] J. Kang, I. Joo and D. Choi, "False Data Injection Attacks on Contingency Analysis: Attack Strategies and Impact Assessment," in *IEEE Access*, vol. 6, pp. 8841-8851, 2018.

[38] Ems-Lecture 6: Power System Security, Nptel. Retrieved from https://nptel.ac.in/courses/108106022/LECTURE%206.pdf.

[39] P. Kundur, Power System Stability and Control. New York City, NY: McGraw-Hill Education, 1994.

[40] B. S. Abdulraheem, and C. K. Gan, " Power System Frequency Stability and Control: Survey," in *Int. J. of Appl. Eng. Research*, vol. 11, no. 8, pp. 5688-5695, 2016.

[41] D. P. Wadduwage, U. D. Annakkage, and C. Q. Wu, "Hybrid algorithm for rotor angle security assessment in power systems," in *The J. of Eng.*, vol. 2015, no. 8, pp. 241-251, Aug 2015.

[42] A. J. Wood and B. F. Wollenberg, Power Generation, Operation and Control. New York: Wiley, 1996.

[43] Y. Sun and T. J. Overbye, "Visualizations for power system contingency analysis data," in *IEEE Trans. on Power Syst.*, vol. 19, no. 4, pp. 1859-1866, Nov. 2004.

[44] M. Sahraei-Ardakani, X. Li, P. Balasubramanian, K. W. Hedman and M. Abdi-Khorsand, "Real-Time Contingency Analysis with Transmission Switching on Real Power System Data," in *IEEE Trans. on Power Syst.*, vol. 31, no. 3, pp. 2501-2502, May 2016.

[45] P. Kaplunovich and K. Turitsyn, "Fast and Reliable Screening of N-2 Contingencies," in *IEEE Trans. on Power Syst.*, vol. 31, no. 6, pp. 4243-4252, Nov. 2016.

[46] W. Li, Probabilistic Transmission System Planning. Hoboken, NJ, University Science, 2011.

[47] C. M. Machado Ferreira, J. A. Dias Pinto, and F. P. Maciel Barbosa, "Dynamic Security Analysis of an Electric Power System using a Combined Monte Carlo-Hybrid Transient Stability Approach," Proc. of *the IEEE Porto Power Tech. Conf.*, Porto, Portugal, Sept. 2001.

[48] J. Choi, T. Mount and R. Thomas, "Transmission System Expansion Plans in View Point of Deterministic, Probabilistic and Security Reliability Criteria," *Proc. of the 39th Annu. Hawaii Int. Conf. on* Syst. Sci., 247b, vol.10, Jan. 2006.

[49] R. Billion, W. Wangdee, "Reliability-Based Transmission Reinforcement Planning Associated With Large-Scale Wind Farms," *IEEE Trans. on Power systs.,* vol. 22, no. 1, pp.34-41, Feb. 2007.

[50] X. Han, M. Mu, W. Qin, "Reliability Assessment of Power System Containing Wind Farm Based on Steady-state Power Flow," *IEEE 11th Int. Conf. on Probabilistic Methods Appl. to Power Systs*., Singapore, Singapore, 14-17 June 2010, pp.756-760.

[51] Y. Damchi, J. Sadeh, "Effect of Combined Transmission Line (Overhead Line/Cable) on Power System Reliability Indices," *4th Int. Power Eng. and Optimization Conf.*, Shah Alam, Selangor, MALAYSIA: 23-24 June 2010, pp.59-63.

[52] X. Du, W. Liu, "Evaluation of power system reliability based on the maintenance state," *4th Int. Conf. on Electric Utility Deregulation and Restructuring and Power Technologies*, Weihai, Shandong, China, 6-9 July 2011, pp. 1016-1020.

[53] M. Bourguignon, R. B. Silva, G. M. Cordeiro, "The Weibull-G Family of Probability Distributions," *J. of Data Sci*., vol. 12, pp. 53-68, 2014.

[54] P. Jiang, Y. Xing, X. Jia, B. Guo, "Weibull Failure Probability Estimation Based on Zero-Failure Data," *Math. Problems in Eng*., vol. 2015, no. 681232, pp. 1-8, 2015.

[55] G. Huang, W. Lin, Q. Niu, "Risk Analysis Model of Automobile Defect Based on Weibull," *Int. J. of Hybrid Inform. Technol*., vol.9, no. 1, pp. 353-366, 2016.

[56] M. S. Khan, R. King, "Transmuted Modified Weibull Distribution: A Generalization of the Modified Weibull Probability Distribution," *European J. of Pure and Appl. Math*., vol. 6, no. 1, pp. 66-88, 2013.

[57] B. C. Pal, and A. K. Singh, "IEEE PES Task Force on Benchmark Systems for Stability Controls Report on the 68-Bus, 16- Machine, 5-Area System," Version 2.0, Jul 2013.

[58] M. Al-Sarray, M. Saadeh and R. McCann, "Analyzing variable time between N-1-1 contingencies in assessing NERC TPL-001-4 multiple events reliability," *2016 IEEE/PES Transmission and Distrib. Conf. and Expo. (T&D)*, Dallas, TX, : May 3-5, 2016.

[59] Z. Y. Dong, C. K. Pang, and P. Zhang, "Power System Sensitivity Analysis for Probabilistic Small Signal Stability Assessment in a Deregulated Environment," *Int. J. of Control, Autom. and Syst*., vol. 3, no. 2 (special edition), pp. 355-362, Jun 2005.

[60] H. M. Wadsworth, The Handbook of Statistical Methods for Engineers and Scientists, 2n, New York City, NY: McGraw-Hill Professional, 1997. [E-book] Available: https://www.itl.nist.gov/div898/handbook/index.htm.

[61] Renewable Electricity Production Tax Credit (PTC). Energy Gov., Washington DC. [Online]. Available: https://energy.gov/savings/renewable-electricity-production-tax-credit-ptc, Accessed on: Mar. 12, 2017.

[62] T. Beckford. (2017, May). Wind Turbines Provide 8% of U.S. Generating Capacity, more than Any Other Renewable Source. The U.S. Energy Information Administration (EIA), Washington DC. [Online]. Available: https://www.eia.gov/todayinenergy/detail.php?id=31032, Accessed on: Feb. 15, 2017.

[63] S. Q. Bu, W. Du, H. F. Wang, Z. Chen, L. Y. Xiao, and H. F. Li, "Probabilistic analysis of small-signal Stability of large-scale power systems as affected by penetration of wind generation," *IEEE Trans. Power Syst*., vol. 22, no. 2, pp. 762-770, May. 2012.

[64] A. P. S. Meliopoulos, G. J. Cokkinides, O. Wasynczuk, E. Coyle, M. Bell, C. Hoffmann, C. Nita-Rotaru, T. Downar, L. Tsoukalas, and R. Gao, "PMU Data Characterization and Application to Stability Monitoring," presented on *the IEEE PES Power Syst. Conf. and Expo*., Atlanta, GA, Oct. 29 -Nov. 1, 2006.

[65] B. S. Munir, and A. Trisetyarso, "Field data accuracy analysis of phasor measurement unit application," presented at *8th Int. Conf. on Information Tech. and Elect. Eng*., Yogyakarta, Indonesia, Oct. 5-6, 2016.

[66] N. Nayak, H. Chen, W. Schmus, and R. Quint, “Generator parameter validation and calibration process based on PMU data,” presented at *IEEE/PES Transmission and Distribution Conf. and Expos.*, Dallas, TX, May 3-5, 2016.

[67] T. L. Baldwin, L. Mili, and A. G. Phadke, “Dynamic Ward equivalents for transient stability analysis,” *IEEE Trans. Power Syst*., vol. 25, no. 2, pp. 59-67, May. 2010.

[68] Yuchen Zhang, Y. Xu, and Z. Y. Dong, “Robust Ensemble Data Analytics for Incomplete PMU Measurements-Based Power System Stability Assessment,” *IEEE Trans. Power Syst*., vol. 33, no. 1, pp. 1124-1126, Jan. 2018.

[69] “Power System Equivalents,” PowerWorld Corporation. Champaign, IL, 2008. [Online] Available: https://www.powerworld.com/files/TrainingI14Equivalents.pdf, Accessed on: Jan. 5, 2017.

[70] J. B. Ward, “Equivalent circuits for power-flow studies,” Trans. of the American Inst. of Elect. Eng., vol. 68, issue. 1, pp. 373-382, Jul. 1949.

[71] M. S. Saadeh, “Model Development and Validation for Wind Generation Transmission Systems,” Ph.D. dissertation, Dept. Elect. Eng., Univ. of Arkansas, Fayetteville, AR, 2015.

[72] The NERC Model Validation Task Force of the Transmission Issues subcommittee. (2010, Dec.). White Paper on Power System Model Validation. North American Electric Reliability Corp., NJ. [Online]. Available: http://www.nerc.com/docs/pc/mvwg/MV%20White%20Paper_Final.pdf, Accessed on: Mar. 10, 2017.

[73] M. Shen, S. K. Nguang, C. K. Ahn and Q. Wang, "Robust H_2 Control of Linear Systems with Mismatched Quantization," in *IEEE Trans. on Autom. Control*. Early Access, pp. 1-8, Jul. 2018.

[74] Asli Soyiç Leblebici and Semiha Turkay, “Controller design for flexible and rigid bodied railway vehicles,” presented at *14th IEEE Int. Conf. Control and Autom*., Anchorage, Alaska, USA, Jun. 12-15, 2018.

[75] B. Zhenga and G. Yangb, " H_2 control of linear uncertain systems considering input quantization with encoder/decoder mismatch," in *ISA Trans.* vol 52, Issue 5, Sept. 2013, Pages 577-582.

[76] Peter M. Thompson, "Classical /H_2 Solution for a Robust Control Design Benchmark Problem", *J. of Guidance, Control, and Dynamics*, vol. 18, No. 1 (1995), pp. 160-169.

[77] G. Wang, B. Liang, and G. Duan, "H_2-optimal Control with Regional Pole Assignment via State Feedback", *Int. J. of Control, Automa. and Syst*., vol. 4, No. 5, Oct 2006, pp. 653-659.

[78] A. C. Zolotas, P. Korba, B. Chaudhuri, and I. M. Jaimoukha, “H_2 LMI-based Robust Control for Damping Oscillations in Power Systems,” presented at *IEEE Int. Conf. on Syst. of Syst. Eng.,* San Antonio, TX, USA, Apr. 16-18, 2007.

[79] M. Sojoodi and V. Johari Majd, "A technical approach to H_2 and H_∞ control of a flexible transmission system," *2010 IEEE Conf. on Robot., Autom. and Mechatron.*, Singapore, 2010, pp. 124-128.

[80] L. Sedghi and A. Fakharian, "Robust voltage regulation in islanded microgrids: A LMI based mixed H2/H∞control approach," *24th Mediterranean Conf. on Control and Autom. (MED)*, Athens, Greece, Jun. 21-24, 2016.

[81] P. Shukla, D. Ghodki, N. S. Manjarekar and P. M. Singru, " A Study of H_∞ and H_2 synthesis for Active Vibration Control", *IFAC-PapersOnLine*, vol 49, Issue 1, 2016, Pages 623-628.

[82] J. Zhou, C. Wang and H. Qian, "Gain-scheduled H_2-performance control of individual synchronous generators with static VAR compensator controllers," *2017 11th Asian Control Conf.*, Gold Coast, QLD, Australia, Dec. 17-20, 2017.

[83] F. K. Abo-Elyousr, "Load frequency controller design for two area interconnected power system with DFIG based wind turbine via ant colony algorithm," presented at *18th Int. Middle East Power Syst. Conf.*, Cairo, Egypt, Dec. 27-29, 2016.

[84] L. S. Levine, "The control handbook," CRC Press, Boca Raton, FL, 1996.

[85] Multivariable control systems, A. Megretski, Boston, MA, USA: MIT, 2004. [Online]. Available: https://ocw.mit.edu/courses/electrical-engineering-and-computer-science/6-245-multivariable-control-systems-spring-2004/lecture-notes/lec1_6245_2004.pdf

[86] S. W. Yun, Y. J. Choi, and P. Park, "H_2 control of continuous-time uncertain linear systems with input quantization and matched disturbances," *Automatica, Elsevier*, vol. 45, issue. 10, pp. 2435-2439, 2009.

[87] S. T. Mathewl, and Mija S.J, "Design of H_2 Controller for Stabilization of Two Wheled Inverted Pendulum," presented at *IEEE Int. Conf. on Advanced Commun Cont. and Computing Technol*., Ramanathapuram, India, May. 8-10, 2014.

[88] T. Nagado, "H_2/H_∞ controller reduction using the Riccati equations and the block balanced truncation," *2015 10th Asian Control Conf.*, Kota Kinabalu, Malaysia, May 31-Jun 3, 2015.

[89] Chapter Five, Standard LTI Feedback Optimization Setup. [Online]. Available: web.mit.edu/6.245/www/images/ch6.pdf

[90] Radek Matušů, Roman Prokop, and Libor Pekař, "Parametric and unstructured approach to uncertainty modelling and robust stability analysis," *Int. J. Math. Models and methods in Appl. Sci.,* vol. 5, issue. 6, pp. 1011-1018, 2011.

[91] B. C. Zheng, and G. H. Yang, "H_2 control of linear uncertain systems consideringinput quantization with encoder/decoder misatch," *ISA Trans., Elsevier*, vol. 52, pp. 577-582, 2013.

[92] M. Al-Sarray, R. McCann, "Consensus Damping of Inter-Area Oscillations using Utility-Scale Solar-Battery Generaio," *IEEE Elect. Power Grid 2018*, Charleston, SC, Nov 1-14, 2018.

[93] J. Morsali, K. Zare and M. T. Hagh, "S. W. Yun, Y. J. Choi, and P. Park, "Performance comparison of TCSC with TCPS and SSSC controllers in AGC of realistic interconnected multi-source power system," *Ain Shams Eng. J.*, vol 7, Issue 1, Mar. 2016, Pages 143-158.

[94] I. Ngamroo, "Application of static synchronous series compensator (SSSC) to stabilization of frequency oscillations in an interconnected power system," *The 2001 IEEE Int. Sympo. on Circuits and Syst.*, Sydney, NSW, Australia, May 6-9, 2001.

[95] P. Bhatt, S. P. Ghoshal and R. Roy, "Optimized Automatic Generation Control by SSSC and TCPS in Coordination with SMES for Two-Area Hydro-hydro Power System," *Int. Conf. on Advances in Computing, Control, and Telecom. Technol.*, Trivandrum, Kerala, India, Dec. 28-29, 2009.

[96] G. Zareiegovar, H. Shayeghi, A. Sakhavati and V. Nabaei, "A new scheme to control SSSC in interconnected power systems," *9th Int. Conf. on Environment and Elect. Eng.*, Prague, Czech Republic, May 16-19, 2010.

[97] D. Lastomo, Widodo, H. Setiadi and M. R. Djalal, "Enabling PID and SSSC for load frequency control using Particle Swarm Optimization," *2017 3rd Int. Conf. on Sci. in Inform. Technol.*, Bandung, Indonesia, Oct. 25-26, 2017.

[98] T. Mahto and V. Mukherjee, "Frequency stabilization of a hybrid two-area power system by a novel quasi-oppositional harmony search algorithm," in *IET Generation, Transmission & Distrib.*, vol. 9, no. 15, pp. 2167-2179, Nov. 2015.

[99] R. Shankar, M. K. Babu, R. Bhushan and K. Chatterjee, "Load frequency control for interconnected power system in-coordination with SSSC and RFB through AC/DC link," *2015 IEEE Power, Commun. and Inform. Technol. Conf.*, Bhubaneswar, India, Oct 15-17, 2015.

[100] A. D. Falehi and A. Mosallanejad, "Neoteric HANFISC–SSSC based on MOPSO technique aimed at oscillation suppression of interconnected multi-source power systems," in *IET Generation, Transmission & Distrib.*, vol. 10, no. 7, pp. 1728-1740, May 2016.

[101] S. Selvakumaran, S. Parthasarathy, Karthigaivel R., and V. Rajasekaran, " Optimal Decentralized Load Frequency Control in a Parallel AC-DC Interconnected Power System Through HVDC Link Using PSO Algorithm," in *Energy Procedia*, vol. 14, pp. 1849-1854, Dec. 2012.

[102] R. Rajbongshi and L. C. Saikia, "Combined voltage and frequency control of a multi-area multisource system incorporating dish-Stirling solar thermal and HVDC link," in *IET Renewable Power Generation*, vol. 12, no. 3, pp. 323-334, Feb. 2018.

[103] N. Pathak, A. Verma, T. S. Bhatti and I. Nasiruddin, "Modeling of HVDC Tie Links and Their Utilization in AGC/LFC Operations of Multiarea Power Systems," in *IEEE Trans. on Ind. Electrons.*, vol. 66, no. 3, pp. 2185-2197, Mar. 2019.

[104] G. Fujita, G. Shirai and R. Yokoyama, "Automatic generation control for DC-link power system," *IEEE/PES Transmission and Distrib. Conf. and Exhibition*, Yokohama, Japan, Oct. 6-10, 2002.

[105] X. M. Mao, Y. Zhang, L. Guan, X. C. Wu and N. Zhang, "Improving power system dynamic performance using wide-area high-voltage direct current damping control," in *IET Generation, Transmission & Distrib.*, vol. 2, no. 2, pp. 245-251, Mar. 2008.

[106] Z. Miao, L. Fan, D. Osborn and S. Yuvarajan, "Wind Farms with HVDC Delivery in Inertial Response and Primary Frequency Control," in *IEEE Trans. on Energy Conversion*, vol. 25, no. 4, pp. 1171-1178, Dec. 2010.

[107] R. Preece, J. V. Milanović, A. M. Almutairi and O. Marjanovic, "Damping of inter-area oscillations in mixed AC/DC networks using WAMS based supplementary controller," in *IEEE Trans. on Power Syst.*, vol. 28, no. 2, pp. 1160-1169, May 2013.

[108] K. N. Mackey and R. A. McCann, "Improved inter-area stability using an LQG controller incorporating synchrophasor data," *2013 IEEE Power and Energy Conf. at Illinois*, Champaign, IL, Feb 22-23, 2013.

[109] A. Alkhazraji, "Iraqi National Grid Restoration Strategy Based on Modified Depth First Search Algorithm," Advances in Natural and Appl. Sci., vol. 10, no. 15, pp. 1-12, Sep. 2018.

[110] R. H. Al-Rubayi, and L. H. Hassan Al-Sharafany, "Robust-Load Frequency Controller Design for Iraqi National Super Grid System," *Eng. and Tech. J.*, vol. 26, no. 3, pp. 305-305, 2008.

[111] A. Al-Khazragy, and M. Al-Sarray, "The Application of Neural Network on The Contingency Analysis of Iraqi Super Grid Network," *Eng. and Tech. J.,* vol. 28, no. 1, pp. 199-213, 2010.

[112] H. A. F. Mohamed, L. H. Hassan, M. Moghavvemi and S. S. Yang, "Load frequency controller design for Iraqi National Super Grid System using fuzzy logic controller," *2008 SICE Annu. Conf.*, Tokyo, Japan, Aug 20-22, 2008.

[113] "Iraqi Electrical Network- 2020 Plan," National Dispatch and Control Center, Ministry of Electricity, Baghdad, Iraq, 21 May 2017.

9 Appendix

A. 21 Buses Three-Area System Data

B=1, R=3

Kp_1=100, Tg_1=0.12, Tt_1=0.5, Tp_1=18;

Kp_2=90, Tg_2=0.10, Tt_2=0.52, Tp_2=20;

Kp_3=105, Tg_3=0.19, Tt_3=0.48, Tp_3=21;

Ki=0.09;

T_{12}=0.0145, T_{13}=0.002, T_{23}=0.024, T_{21}=0.0145, T_{31}=0.002, T_{32}=0.024;

R_{blade}=23.5, W_{blade}=3.14, p=1.25, A_r=1735, β=1.74533, T_W=1.5,

K_{W1}=0.3, K_{W2}=0.5, K_{W3}=0.4.

B. Iraqi National Super Grid System (INSGS) Data

Tp_1= 32.376, Tp_2= 5.211, Tp_3= 6.911, Tp_4= 3.333, Tp_5= 18.598, Tp_6= 7.664;

Kp_1=84.134, Kp_2=16.286, Kp_3=36.764, Kp_4=12.820, Kp_5=48.945, Kp_6=20.169;

R = 2.4;

B_1 = 0.5059, B_2 = 0.530, B_3 = 0.5136, B_4 = 0.539, B_5 = 0.5102, B_6 = 0.5247;

a_{12} = -1.218, a_{23} = -1.1491, a_{24} = -0.9576, a_{34} = -0.833, a_{45} = -0.923, a_{56} = -1.71;

Tr = 6.0; Kr = 0.333;

T_{12}=2.1135, T_{23}=2.0814, T_{24}=1.4918, T_{34}=1.9819, T_{45}=1.4641, T_{56}=1.5820.

Table 16. Iraqi Turbine-Governor Parameters

Area No.	T1 (sec)	T2 (sec)	T3 (sec)	TR (sec)	Tw (sec)	Tt (sec)	Tr (sec)
1	48.7	0.51	-	5	1	-	-
2	0.2	0	0.1	-	-	0.25	-
3	48.7	0.51	-	5	1	-	-
4	0	0	0.1	-	-	0.25	6
5	0.1	0	0.12	-	-	7	-
6	0.1	0	0.12	-	-	7	-